UNDERSTANDING THE ROLE OF RECEPTOR FOR ADVANCED GLYCATION ENDPRODUCTS (RAGE) IN PANCREATIC CANCER AND MELANOMA

A Dissertation
Submitted to the Graduate Faculty
of the
North Dakota State University
of Agriculture and Applied Science

By

Sakshi Taneja

In Partial Fulfillment of the Requirements
for the Degree of
DOCTOR OF PHILOSOPHY

Major Department:
Pharmaceutical Sciences

June 2021

Fargo, North Dakota

North Dakota State University
Graduate School

Title

UNDERSTANDING THE ROLE OF RECEPTOR FOR ADVANCED GLYCATION ENDPRODUCTS (RAGE) IN PANCREATIC CANCER AND MELANOMA

By

Sakshi Taneja

The Supervisory Committee certifies that this ***disquisition*** complies with North Dakota State University's regulations and meets the accepted standards for the degree of

DOCTOR OF PHILOSOPHY

SUPERVISORY COMMITTEE:

Dr. Estelle Leclerc
Chair

Dr. Jagdish Singh

Dr. Sathish Venkatachalem

Dr. Katie Reindl

Approved:

10/13/2021
Date

Dr. Jagdish Singh
Department Chair

ABSTRACT

In this project we study the role of RAGE in the melanoma and pancreatic cancer progression. Based on published studies, we hypothesized that RAGE localization in melanoma varies with different cellular architectures. To test this hypothesis, we utilized an *in vitro* spheroid model and a lung colonization mice model to compare the RAGE localization in 3D architecture vs 2D monolayer culture. RAGE was found at the cell surface in WM115 and B16F10 spheroids, whereas RAGE is mostly distributed intracellularly in WM266. We also observed that RAGE is present at the surface of B16F10 melanoma cells within tumor nodules in the lungs of mice colonized with B16F10 cells.

Previously, our group has demonstrated that RAGE promotes pancreatic tumor cell survival under normoxic conditions, upon gemcitabine administration. Hypoxia is also associated with increased tumor aggressiveness. Based on published reports, we hypothesized that RAGE upregulation under hypoxic conditions contributes to autophagy and migration in pancreatic cancer cells. We observed that autophagy decreases after RAGE inhibition by FPSZM1. Moreover, we observed decreased cell migration after RAGE blockage, indicating that RAGE also mediates migration under hypoxia.

We also investigated Advanced Glycation Endproducts (AGEs) on proliferation and migration of pancreatic cancer cells. Based on published reports, we hypothesized that RAGE activation by AGEs contributes to the proliferation and migration in pancreatic cancer cells. We employed ribose modified BSA to activate RAGE in the murine KPC 5517 pancreatic cancer cell line. We observed that AGE-treated samples showed significant increase in migration but no change in proliferation.

As RAGE is involved in the progression of melanoma and pancreatic cancer, our results will help researchers to better understand the biology of RAGE. Our research can help to design RAGE-specific antibodies and inhibitors that could target RAGE more effectively. Moreover, our findings on AGE-RAGE interactions, and on the role of RAGE in pancreatic cancer progression under hypoxia, may contribute to reduce the progression of pancreatic cancer. Our results showing that a RAGE inhibitor can reduce autophagy and migration of pancreatic tumor cells, suggest that FPS-ZM1 could be utilized as a potential therapeutic aid for the treatment of pancreatic cancer.

ACKNOWLEDGMENTS

There are many people who supported me personally and professionally. I am very grateful to them and want to acknowledge their efforts to help me stand where I am today. First and foremost, I want to thank my advisor, Dr. Estelle Leclerc, who continuously motivated me during my research work. I am thankful that she was always there to give me her precious feedback and advice. My PhD journey would not have been possible without her endless support and inspiration. I also want to thank Dr. Stefan Vetter for his suggestions to troubleshoot the problems during my experiments. I want to express my sincere gratitude to my committee members – Dr. Jagdish Singh, Dr. Sathish Venkatachalem and Dr. Katie Reindl for their valuable suggestions on my project. I want to acknowledge Dr. Yagna Jarajapu for allowing me to use hypoxia chamber in his lab. I am thankful to Saimon Mia, Dr. Nilesh Ambhore and Dr. Jiyan Mohammad for helping me with the mice studies. I want to acknowledge my past lab mates – Dr. Priyanka Swami and Dr. Sultan Kadasah for teaching me techniques and give their inputs to improve my experiments. I am so glad that I have Swetha Thiyagarajan as a friend and lab mate. She is a huge support and a true motivator. I am thankful to our office staff – Janet Krom, Diana Kowalski and Tiffany Olson for their enormous support in helping graduate students like me.

I want to thank my mother, who has been always an inspiration to achieve smallest and the biggest milestones in my life. Since childhood she taught me to be confident and fearless. I am grateful to my father who helped me to make wise choices and my brother who encouraged me to pursue my dreams. I am so thankful to my husband, Haneesh Jasuja, who has supported my decisions and was beside me when I needed him the most. I am blessed to have Arav as my son.

I am grateful to all of you and to the greatest God.

DEDICATION

Dedicated to Almighty,

my loving parents, Subhash Taneja and Asha Taneja

my supportive parent-in-laws, Arvind Jasuja and Indu Bala

my husband, Haneesh Jasuja and

my son, Arav Jasuja.

TABLE OF CONTENTS

LIST OF TABLES

LIST OF FIGURES

LIST OF ABBREVIATIONS

AGE	Advanced Glycation Endproducts
BCA	Bicinchoninic acid assay
BSA	Bovine serum albumin
ECL	Enhanced chemiluminescence
EDTA	Ethylenediaminetetraacetic acid
ELISA	Enzyme linked immunosorbent assay
EMT	Epithelial to mesenchymal transition
ERK	Extracellular signal-regulated kinases
FBS	Fetal bovine serum
FITC	Fluorescein isothiocyanate
HEK 293	Human embryonic kidney 293 cells
HMGB-1	High-mobility group protein B1
HRP	Horseradish peroxidase
IACUC	Institutional animal care and use committee
IgG	Immunoglobulin
KRAS	Kirsten rat sarcoma
MAPK	Mitogen activated protein kinase
MMP	Matrix metalloproteinases
NF-κB	Nuclear factor kappa-light-chain-enhancer of activated B
RAGE	Receptor for advanced glycation end products
SEER	Surveillance, Epidemiology, and End Results Program
sRAGE	Soluble receptor for advanced glycation end products

TBS .....Tris buffered saline

TBS-T .....Tris buffered saline tween

1. GENERAL INTRODUCTION

The American Cancer Society has estimated that about 60,430 people will be diagnosed with, and about 48,220 people will die of Pancreatic Cancer (PC) in the United States this year, while 106,110 new cases will be diagnosed with, and about 7,180 people are expected to die from Melanoma. Cancer treatment with drugs comes with a limitation of chemoresistance. Despite the fact that surgical resection is considered as first line of treatment in cancer, complete removal of tumor is always challenging which may result in cancer relapses. It is therefore necessary to design new treatment strategies and to study in-depth the pathogenesis of cancer. The Receptor for Advanced Glycation Endproducts (RAGE) plays critical roles in tumor proliferation, migration and invasion. Antagonists of RAGE can prove beneficial as anticancer therapies. To design RAGE targeted therapeutics, we need to better understand the biology of this receptor. This was the purpose of the studies described in this disquisition. In chapter 1, we discuss the structure and functional role of RAGE. Moreover, we discuss RAGE mediated signaling pathways involved in cancer progression. RAGE has been found to be overexpressed in cancers including brain, breast, colon, colorectal, prostate, oral squamous cell, ovarian cancer, and melanoma [1]. It has been suggested that RAGE knockdown can reduce pancreatic cancer survival [2]. Thus, antagonists of RAGE can prove beneficial as anticancer therapies. However, to design RAGE targeted therapeutics, we need to better understand the biology of this receptor. It is reported that RAGE participates in melanoma progression. However, RAGE localization in melanoma cells is still not clearly understood and this knowledge is important to target RAGE more effectively. Based on published reports we hypothesized that RAGE localization varies with different cellular architectures. In chapter 2, we have investigated the localization of RAGE in Melanoma cells in different growth conditions (2D, 3D and within the tumor microenvironment). It has also been

demonstrated that RAGE is upregulated in cancer tumors under hypoxia. In these pancreatic tumors, hypoxic conditions promote autophagy and cell migration, resulting in poor patient outcome. In Chapter 3, we have investigated the contributing role of RAGE in mediating autophagy and migration under hypoxia, in pancreatic cancer cells. This study could lead to new therapeutic options to attenuate the aggressive behavior of pancreatic cancer under hypoxia. Advanced Glycation Endproducts (AGEs) are well known ligands for RAGE, but their role in cancer is still not fully understood. In chapter 4, we have evaluated the effect of AGE/RAGE interaction to better understand the effect of RAGE activation on the proliferation and migration of pancreatic cancer cells.

1.1. Receptor for Advanced Glycation Endproducts (RAGE)

RAGE was first identified as a 35 kDa polypeptide in the endothelial cells of bovine lungs as a binding partner for advanced glycation endproducts (AGEs) [3]. Since RAGE is able to recognize common patterns within its different ligands, RAGE has been described as a pattern-recognition receptor [4]. Similar to RAGE, other pattern recognized receptors (PRRs) such as Toll-like and mannose receptors recognize conserved molecular structures (patterns) shared by a large group of pathogens/ligands [5]. Such PRRs exhibit common features such as the presence of multidomain structures, the ability to recognize different classes of ligands, and the presence of repeated structurally similar domains [6]. RAGE belongs to the immunoglobulin superfamily, and its gene is located close to the class III Major Histocompatibility Complex (MHC) region on chromosome 6 [7]. This MHC locus embodies several genes involved in inflammation [8]. The gene of RAGE about 1.4 kb long and the full length form of RAGE contains 404 amino acid residues chains with a molecular weight of 55 kDa [3]. RAGE is constitutively expressed at high levels during embryonic development, however in later developmental stages, RAGE expression

is reduced. Most differentiated cells of an adult, such as neurons, lymphocytes, monocytes, cardiomyocytes, dendritic cells and vascular endothelial cells, express low levels of RAGE with the exception of cells in lung where high levels of RAGE are expressed constitutively [9-12]. RAGE is highly expressed during embryogenesis, suggesting an important role in this process. However, its physiological function in adult cells is still poorly understood. Several studies have suggested a role of RAGE in the nervous system development. For example, a study using an in *vivo* unilateral sciatic nerve crush model has shown that blockade of RAGE reduced functional regeneration of the peripheral nerve [13]. Another study showed that RAGE knockout in mice resulted in behavior abnormalities such as higher sensitivity to auditory signals and higher activity in darkness, indicating a potential role of RAGE in neuronal signaling [14]. RAGE has also been reported in other physiological functions. Zhou et al. observed that an increase in bone mineral density and decreased bone resorptive activity in RAGE knockout mice, suggesting the role of RAGE in osteoclast maturation [15].

RAGE activation has also been implicated in several chronic diseases including diabetes, neurodegenerative disorders, and cancer [16, 17]. Kang et al. have demonstrated the unique role of RAGE in pancreatic tumorigenesis and drug resistance [21, 22]. Several studies suggest that there is a direct link between RAGE activation and proliferation, survival, migration, and invasion of tumor cells [23, 24]. Thus, targeting RAGE represents a novel approach for pancreatic cancer therapy because blockade of the RAGE signaling pathway suppresses tumor growth, angiogenesis, and metastases [19, 20]. Some studies have reported that RAGE-deficient mice are resistant to chemically induced skin carcinogenesis, colitis-associated cancer induction, as well as pancreatic tumorigenesis [21-23].

1.1.1. RAGE structure

The full-length human RAGE is a transmembrane protein that encompasses three domains - an extracellular domain (amino acid residues 23-342), a transmembrane domain (amino acid residues 343–363), and a cytoplasmic domain (amino acid residues 364-404) [29]. The extracellular domain is further comprised of a variable (V) and two constant (C1 and C2) subdomains. The V subdomain is the principal site of binding of a large number of extracellular ligands [30]. Moreover, since V and C1 subdomains contain positive charges on their surfaces, owing to these characteristics, they interact together with negatively charged (acidic) ligands such as high mobility group box 1 (HMGB1) [31, 32]. The V and C1 domains also contain domains that provide ligand-based dimerization of RAGE via V-V or C1-C1 domain interactions. In contrast, the C2 subdomain is mainly negatively charged surface and linked to C1 subdomain via a 12-residue-long linker [33]. The transmembrane domain is characterized by a helical structure containing a GxxxG motif involved in the homodimerization of the helix-helix interface. This small amino acid motif allows the two helices to come in proximity and promotes their interaction via hydrogen bonding of Cα–H donors present on one helix and backbone carbonyl oxygen (O=C) acceptors of another helix [34]. A short cytoplasmic tail participates in the activation of downstream effector molecules such as diaphanous-1 and NF-κB required for cellular migration and neurite growth of neuroblastoma cells, respectively [35, 36]. Moreover, it has been shown that cytoplasmic tail interacts with TIRAP (Toll interleukin 1 receptor domain containing adaptor protein) and MyD88 (Myeloid differentiation primary response gene), that are adaptor proteins for TLR2 and TLR4 respectively, suggesting the involvement of cytoplasmic tail in immune-mediated signaling [37]. Thus, deletion of this domain may block various RAGE-mediated pathological effects [35, 36]. The extracellular and cytoplasmic domains of human RAGE share sequence

identity with rodents (79.2% and 70.7% for the extracellular and cytoplasmic domains respectively) and with primates (96.5% and 92% for the extracellular and cytoplasmic domains respectively) [33].

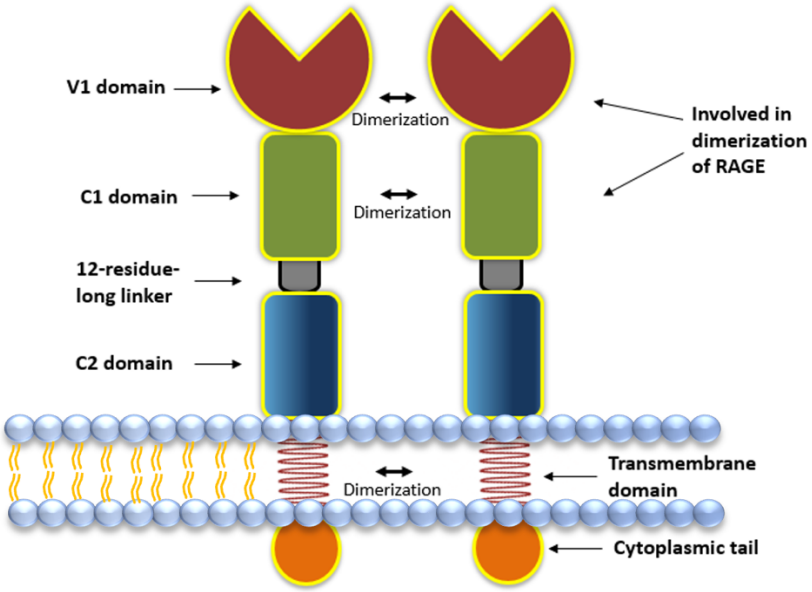

Figure 1.1. Structure of full-length human RAGE and regions involved in dimerization. The extracellular domain is comprised of a variable (V) and two constant (C1 and C2) subdomains. The C2 subdomain is linked to C1 subdomain via a 12-residue-long linker [33]. The transmembrane domain is characterized by a helical structure which is involved in homodimerization [34]. The intracellular domain of RAGE is a short cytoplasmic tail that participates in the activation of downstream signaling [35, 36].

1.1.2. RAGE isoforms

The main RAGE isoforms are soluble RAGE (amino acid residue 23-342), dominant negative RAGE (amino acid residue 23-363), and N-truncated RAGE (amino acid residues 124-404) [30, 38]. Soluble RAGE (sRAGE) contains an extracellular domain but lacks both transmembrane and cytoplasmic domains (figure 1.2) [39]. sRAGE is generated from either pre-mRNA alternative splicing or cleavage of the extracellular domain of membrane-bound RAGE by an enzyme called A Disintegrin and Metalloproteinase 10 (ADAM10) [40]. The dominant negative RAGE (DN-RAGE) isoform lacks the cytoplasmic domain, producing a "dominant negative"

effect - an atypical cellular response not shown by full-length RAGE. For instance, a recent study demonstrated the effect of RAGE ligand-HMGB1 on fibrosarcoma cell proliferation via overexpressing human full-length RAGE and DN-RAGE. The results showed that HMGB1 mediated signaling through full-length RAGE accelerated cell proliferation and invasion while signaling through DN-RAGE attenuated cell proliferation and invasion of these cells [41]. The N-truncated RAGE (N-RAGE) isoform is deficient of N-terminal V-domain, and hence does not bind with most RAGE ligands [42] The N-RAGE isoform is expressed on the cell membrane, however its biological role still needs to be elucidated [43].

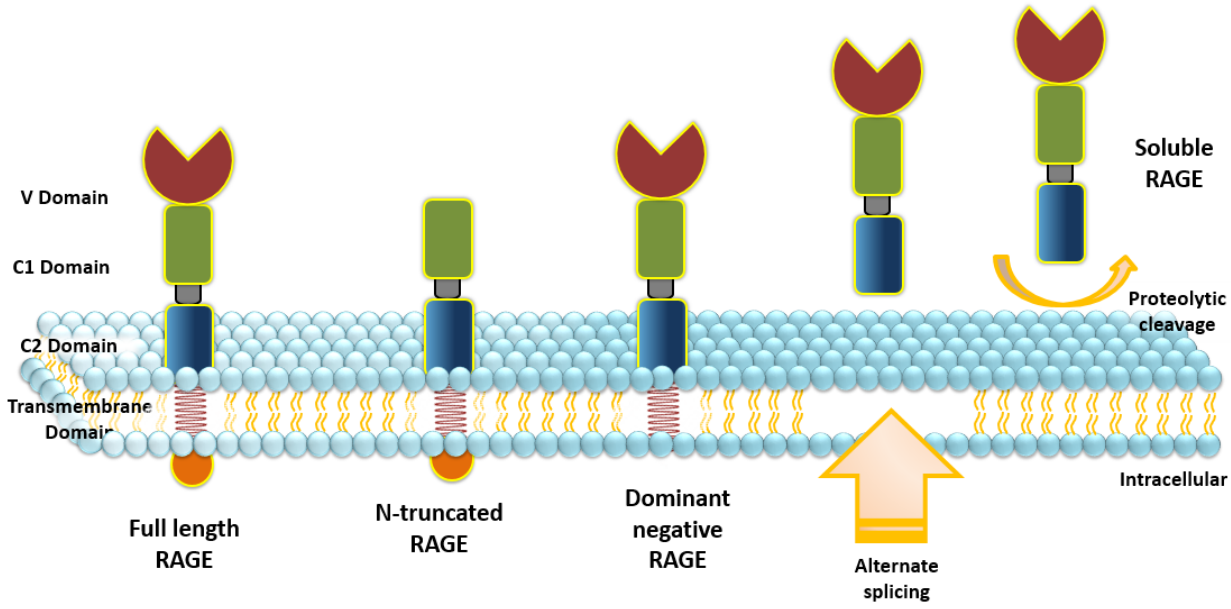

Figure 1.2. RAGE isoforms - The full-length human RAGE encompasses an extracellular domain containing one variable (V) and two constant (C1 and C2) subdomains, a transmembrane domain, and a cytoplasmic domain. The N-truncated RAGE (N-RAGE) is deficient of the V-domain while the dominant negative RAGE (DN-RAGE) lacks the cytoplasmic domain. The soluble RAGE (sRAGE) contains an extracellular domain but lacks both transmembrane and cytoplasmic domains.

1.1.3. RAGE ligands

Advanced Glycation End Product (AGEs) were the first identified ligand of RAGE. The level of AGEs increases in pathological conditions such as oxidative stress, vascular complications

and diabetes and alter cellular properties after interacting with RAGE [43-45]. Other RAGE ligands are Damage Associate Molecular Patterns (DAMPs) such as HMGB1, S100 proteins [16, 46, 47]. DAMPs can be released from cells either actively or passively and induce their responses majorly during stress conditions such as hypoxia, nutrient deprivation, and chemotherapy. Due to their homology to pathogen-associated molecular patterns (PAMPs), DAMPs may induce inflammatory response even in the absence of any infection [48].

1.1.3.1. Advanced glycation end-products (AGEs)

AGEs form a heterogeneous class of compounds that can be generated from Maillard's reaction, polyol pathway and peroxidation of lipids. Maillard's reaction is a nonspecific and non-enzymatic reaction that occurs between amino groups of amino acid residues and aldehyde groups of sugar moieties [49]. This type of reaction initially produces amadori products that subsequently rearrange and are oxidized to form complex AGEs. Through the polyol pathway, glucose undergoes the conversion into sorbitol and fructose. Fructose is subsequently metabolized and produces α-oxaldehydes compounds. These compounds act as glycating agents by reacting with monoacids to form AGEs [50]. Biochemical processes occurring inside the body like autoxidation of glucose and the peroxidation of lipids are also the causes of production of AGEs [51]. These processes result into the generation of dicarbonyl derivatives under increased oxidative stress.

The interaction of AGE-RAGE has been studied in various cancers including melanoma [52], breast cancer [53], pancreatic cancer [54], prostate cancer [55] and renal carcinoma [56]. AGEs have been reported to promote cell proliferation in HEL cells via MAP kinase and PI3K pathway [57], to participate in angiogenesis by inducing VEGF production in MCF-7 breast cancer cells [53], to mediate ROS generation via activation of NADPH oxidase [45], and to promote migration, invasion and metastasis in melanoma cells and in oral cancer cells [58, 59]. The authors

who showed that AGEs promote cell invasion and migration did not discuss the mechanisms associated with these cellular changes. However, a mechanism has been proposed for the induction of angiogenesis by AGEs. In this study, the authors showed that AGEs significantly increased RAGE and VEGF mRNA levels in MCF-7 cells. The study showed that in these cells, metformin at 0.01 mM completely blocked the AGE-dependent RAGE and VEGF gene upregulation. However, an inhibitor of AMP-activated protein kinase, compound C, reversed the inhibitory effects of metformin on AGEs-exposed MCF-7 cells. Indeed, co-treatment of AGE exposed MCF-7 cells with Metformin and compound C, resulted in upregulation of the RAGE and VEGF mRNA levels. Thus, the data shows that metformin inhibits RAGE and VEGF gene expression levels in MCF-7 breast cancer cells via AMP-activated protein kinase.

1.1.3.2. HMGB1

HMGB1 is a nuclear protein that contains two DNA-binding domains – the HMG box A and B, and a long acidic tail that facilitates the binding of HMGB1 to the linker DNA between adjacent nucleosomes [60, 61]. HMGB1 is released by cells into the extracellular space via either an active process involving the hyperacetylation and packaging of HMGB1 into secretory vesicles or via a passive process during necrosis [62]. Recently, HMGB1 in the cytosol has been shown to participate in autophagy by competitively binding to Beclin1 and disrupting the interaction between Beclin1 and Bcl-2. Inhibition of HMGB1 translocation to the cytosol by an inhibitor, ethyl pyruvate, blocked autophagy [63]. Activation of RAGE by HMGB1 has been implicated in many cancers including colon carcinoma [64], prostate cancer [65], and colorectal cancer [66]. A clinical study on colorectal carcinoma demonstrated that the co-expression of RAGE and HMGB1 is linked with increased invasion and metastasis [66]. Another study also showed increased tumor

growth and metastasis of C6 glioma cells in immunocompromised mice due to HMGB1-RAGE interaction [20].

1.1.3.3. S100 proteins

S100 proteins are small dimeric calcium-binding proteins, each subunit comprising two helix-loop-helix EF-hand motifs. These EF-hand motifs form calcium-binding domains that result in conformational rearrangements required for target binding [67]. S100 proteins are encoding by 24 genes and among them 19 are located within chromosome 1q21 [68]. S100 proteins exhibit both intracellular and extracellular functions where extracellular S100 proteins regulate the activity of target cells via activation of cell surface receptors in a paracrine and autocrine manner. The functions regulated by extracellular S100 proteins include cell proliferation, differentiation, migration and inflammation. Intracellular S100 proteins activate several metabolic enzymes after interacting with target proteins [69]. There are twenty-four different S100 proteins identified in the human body [70]. In this chapter, we will particularly discuss S100 proteins that are involved in cancer progression. S100 proteins interact with RAGE [71] to promote cancer cell growth [72], survival [73] angiogenesis [74] and invasion [75]. S100B proteins play a critical role in carcinogenesis [76]. S100B binds to the V and C1 domain of RAGE and modulates cell survival that involves formation of reactive oxygen species, activation of PI3K-AKT and activation of NF-κB signaling pathways in a RAGE-dependent manner [46]. S100P protein bind to the V domain of RAGE and is involved in promoting cell proliferation, survival [73, 77] and migration [78]. Interaction of RAGE with calcium bound S100P homodimer results in RAGE homodimerization [79]. S100A4 protein plays an essential role in metastasis of tumor cells by inducing angiogenesis [80], promoting aggressive behavior of tumor cells [81], and stimulating metalloproteinase activity to trigger pro-metastatic cascades [82]. S100A4 is overexpressed in tumors such as pancreatic

cancer [83], colon cancer [84], ovarian cancer [85], thyroid, and gall bladder cancer [86]. S100A4 has also been examined as a prognostic marker for colorectal cancer [87]. Binding of S100A4 to RAGE led to increased migration and invasion of colorectal cancer cells [88]. S100A6 is overexpressed in many cancers such as hepato-cellular carcinoma [89], melanoma [90], colorectal carcinoma [91] gastric cancer and pancreatic cancer [92]. Moreover, S100A6 has been shown to correlate with poor prognosis in gastric cancer [93] and pancreatic cancer [94]. It has been observed that S100A6 triggered apoptosis in neuroblastoma cells [46]. S100A8 and S100A9 form heterodimers and act via intracellular or extracellular signaling [95]. Although S100A8/A9 is constitutively expressed in myeloid cells [96], yet under diseased conditions like cancer, they act as ligands for RAGE to further aggravate cancer [97, 98]. S100A8/A9 proteins are markedly expressed in prostate [99], renal cell carcinoma [100], thyroid [101], colorectal cancer [102] skin cancer [72, 103], colitis-associated colon cancer [104], hepatocellular carcinoma, gastric cancer [105], and squamous cervical cancer [106]. Ghavami et al. observed that S100A8/A9 promotes breast cancer cell growth via RAGE-dependent signaling. RAGE activation results in MAPK and NF-κB activation [97]. Similarly, in prostate cancer cells, S100A8/A9 induces MAPK and NF-κB signaling via RAGE to promote migration [98]. Increased expression of S100A10 has been found in gallbladder cancer [107], renal cell carcinoma [108], colorectal cancer [109], breast cancer [110], melanoma [111] and gastric cancer [105]. Our group previously showed that S100A10 levels were found to be upregulated in RAGE overexpressed tumors, suggesting RAGE overexpression is responsible for the upregulation of S100A10 in melanoma [112].

1.1.4. RAGE signaling in cancer

Increased RAGE signaling has been observed in various cancers, including brain, breast, colon, colorectal, prostate, oral squamous cell, ovarian cancer, and melanoma [1]. The most well-

known signaling pathways activated by RAGE in cancer progression are MAPK/ERK, PI3K/Akt, and Jak/STAT.

In the MAPK/ERK pathway, RAGE triggers phosphorylation of ERK that upregulates NF-κB mediated transcription of genes involved in cellular proliferation, apoptosis [2], and migration [97] [98]. A study demonstrated that RAGE inhibition using a pharmacological agent (FPS-ZM1) or RAGE-specific antibody reduced ERK activation, suggesting the critical role of RAGE-mediated upregulation of MAPK/ERK pathway in the growth of pancreatic cancer [113]. Another study by Sharaf et al. showed that incubation of MDA-MB-231breast cancer cells, with RAGE ligand methylglyoxal-derived bovine serum albumin (MG-BSA) increased RAGE-mediated phosphorylation of ERK. It was also observed that these breast cancer cells, when pre-treated with RAGE neutralizing antibody, didn't show ERK phosphorylation after MG-BSA treatment, suggesting that RAGE blockade hinders ERK activation [114]. Additionally, RAGE activates ERK phosphorylation and subsequent activation of NF-κB, promoting proliferation and migration of breast cancer and prostate cancer cells, respectively [97, 98].

RAGE signaling through PI3K/Akt pathway has been investigated in prostate cancer and cervical squamous cancer. In PC3 prostate cancer cells, RAGE activation promotes retinoblastoma (Rb) phosphorylation and E2F release via PI3K/Akt signaling. Rb and E2F are crucial regulators of cell cycle progression and prevent cell proliferation by inhibiting the G1 to S phase transition of the cell cycle. Rb forms a complex with E2F inside the nucleus and is degraded after its phosphorylation, resulting in the release of E2F from the E2F-Rb complex that promotes cancer cell proliferation by allowing cell cycle progression from the G1 to the S-phase [55]. Similarly, in cervical squamous cancer cells (SiHa) RAGE overexpression activates PI3K/Akt signaling that further promotes cancer cell proliferation via proliferating cell nuclear antigen (PCNA)

upregulation. PCNA is a nuclear protein that participates in DNA replication; thus, overexpression of PCNA leads to abnormal cell proliferation [115].

Another important signaling mechanism responsible for cancer cell proliferation is the JAK/STAT pathway [18]. JAK phosphorylates STAT3 in response to cytokines like IL-6. STAT3 further translocates to the nucleus and promotes cell proliferation [116]. A study reported by Kang et al. showed that RAGE plays an essential role in amplifying IL-6 mediated JAK/STAT3 signaling in pancreatic cancer. The study demonstrated that STAT3 translocated to the mitochondria and increased ATP production, serving as the energy source for increased tumor cell proliferation. Additionally, RAGE knockdown in a mice model showed decreased mitochondrial p-STAT3; thus, a decrease in pancreatic cancer cell proliferation [18]. All these pathways are shown in Figure 1.3.

In addition to these signaling pathways, it is also suggested that RAGE can be internalized upon stimulation by its ligands. RAGE expressed at the cell surface participates into various signaling pathways leading to cancer cell proliferation and migration, however, little is known about the functional role of intracellular RAGE. In a study, HMGB1 was shown to interact with RAGE and cause its internalization through a regulated endocytosis of HMGB1 [117, 118]. It is also reported that RAGE internalizes upon binding to AGEs in wild type Chinese Hamster Ovary (CHO-k1) and Neuro-2a (N2a) cells in which RAGE internalization leads to the activation of ERK1/2 signaling, necessary for the generation of intracellular responses such as increased binding affinity of NF-κB with DNA [120]. In another study, RAGE stimulation with S100B resulted in its internalization in Schwan cells. Endocytosed RAGE then promoted Src-mediated fusion of endosomes with secretory vesicles. Inhibition of Src further blocked RAGE recycling to the cell

membrane, S100B secretion, and morphological changes, suggesting that RAGE transmits signal when present intracellularly [121].

It is also reported that RAGE can interact with endogenous HMGB1. A study showed that endogenous HMGB1 increases mitochondrial RAGE expression in pancreatic cancer cells, which is associated with tumor cell ATP production via MEK-ERK-MAPK pathway. In-addition, lack of RAGE or inhibition of HMGB1 reduces ATP production resulting in decrease in pancreatic cancer cell growth [119].

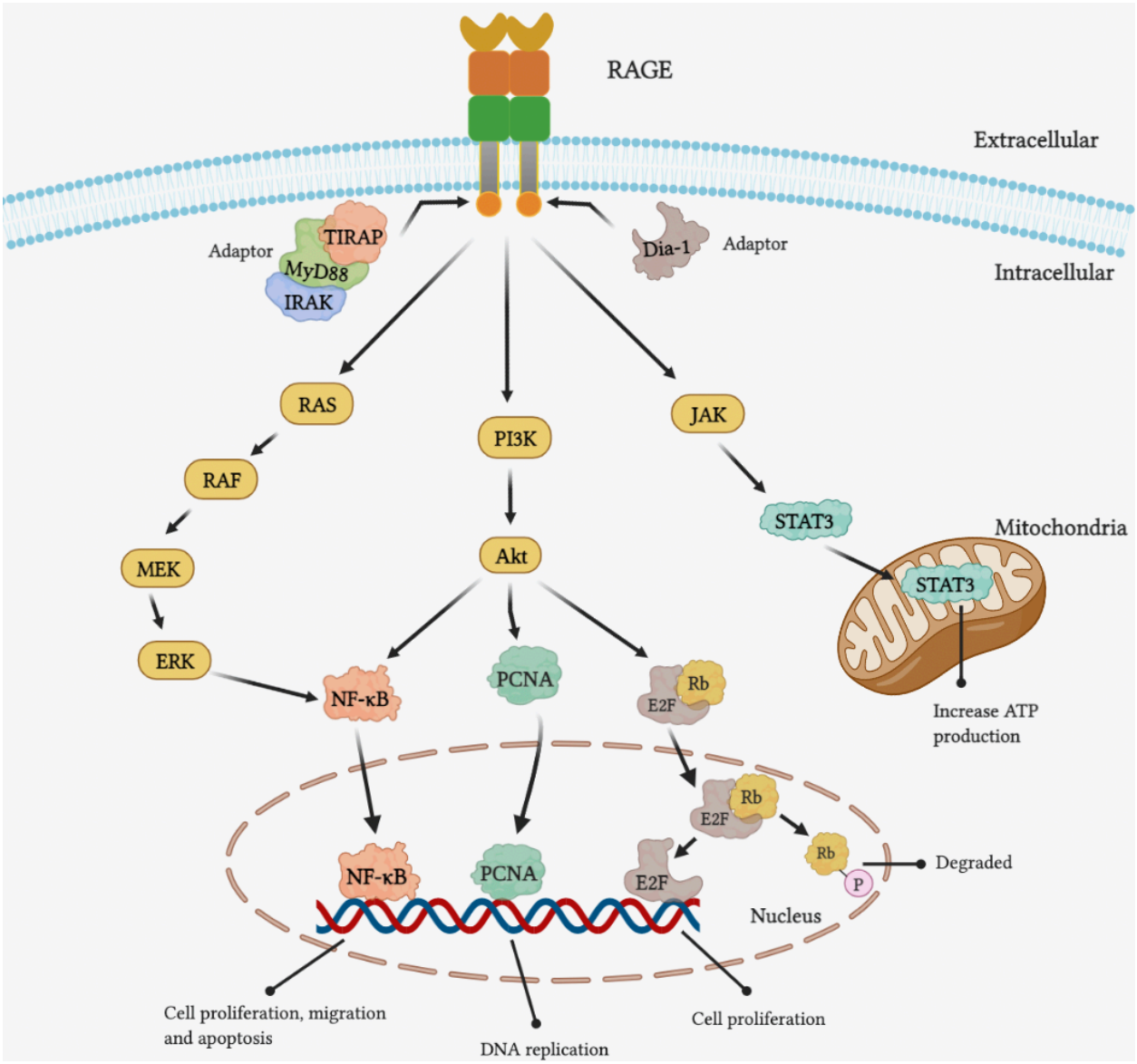

Figure 1.3. RAGE signaling pathways in cancer. RAGE activation results in the activation of MEK/ERK, PI3K/AKT, and JAK/STAT3 pathways. RAGE leads to the activation of ERK that upregulates NF-κB mediated transcription of genes involved in cellular proliferation, migration and apoptosis [113]. RAGE signaling through PI3K/Akt causes phosphorylation of retinoblastoma (Rb) [55] and activation of proliferating cell nuclear antigen (PCNA) [115], leading to enhanced cancer cell proliferation. RAGE-mediated activation of Janus kinase (JAK) leads to the phosphorylation of STAT3 that further translocates to the nucleus and promotes cell proliferation [116].

1.2. Hypoxia

1.2.1. Definition, role in physiological and pathological conditions

A persistent oxygen supply is needed to fulfil the energy demands of the body. The balance between oxygen demand and supply is necessary to maintain the appropriate cellular functions. The ambient atmospheric air contains 21% oxygen. When the air is inhaled, the percentage of oxygen that reaches alveoli drops to 14%. As the oxygen molecules further travel from the lungs to the tissues, the concentration significantly lowers to 4-7%. However, the condition where tissues receive oxygen lesser than 1% is termed hypoxia [122].

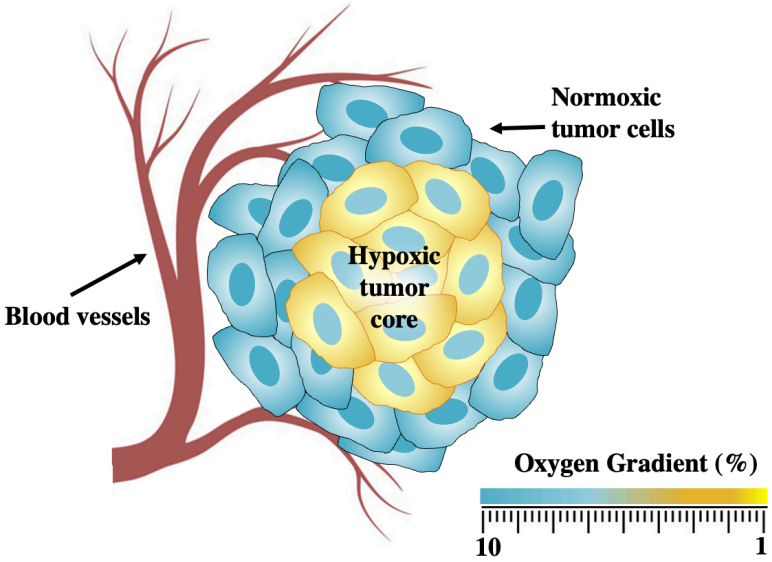

Figure 1.4. Representation of hypoxia in the core of tumor and normoxia at the periphery of the tumor that is sufficiently vascularized.

Hypoxia is found in nearly all solid tumors. Uncontrolled proliferating cancer cells promote increased expression of neo-angiogenesis factors such as vascular endothelial factor (VEGF) that stimulate the development of aberrant vasculature, not found in normal tissues. The poorly developed tumor vasculature limits oxygen supply to the cancer cells, dropping the oxygen levels to less than 1% [123]. Most current anticancer drug therapies can target the cancer cells located in vascularized areas, however, it is challenging to target cancer cells located in the poor vascularized

hypoxic regions [124]. In another study it was suggested that the under hypoxic environment cancer cells (MCF-10A) undergo epithelial to mesenchymal transition (EMT) by reducing the expression of E-cadherin and β-catenin, and upregulating vimentin [125]. An hypoxic microenvironment stabilizes Hypoxia Inducible Factor-1α (HIF-1α), a critical biomarker of hypoxia. The subsequent section will discuss the structure and the functional role of HIF-1α.

1.2.2. Hypoxia-inducible factor: Structure, function, and regulation

Hypoxia-inducible factor-1 (HIF-1) was first discovered in 1991 by Semenza and co-workers during the identification of a DNA sequence (-RCGTG-) of erythropoietin (EPO) gene that was upregulated under hypoxic environment [126]. Later many other hypoxia-inducible genes that contain a promoter region for HIF were identified. These genes include genes coding for glucose transporter type 1 (GLUT 1), interleukin-6, carbonic anhydrase XII and vascular endothelial factor A (VEGF A) [127, 128]. Thus, DNA sequences responsible for gene activation in response to hypoxia were named hypoxia-responsive elements (HRE).

HIF entails an oxygen-sensitive α-subunit and an oxygen-independent β-subunit (also known as the aryl hydrocarbon receptor nuclear translocator (ARNT1)). The α-subunit is further classified into three isoforms - HIF-1α, HIF-2α, and HIF-3α [129]. All three HIF-α isoforms can heterodimerize with HIF-1β, and such complexes subsequently bind to the HRE of HIF-targeted genes, modulating their expressions and promoting cellular adaptation to hypoxia [130-132]. HIF-1α has been considered as the master regulator of hypoxia for a long time; however, after the discovery of HIF-2α [133] and HIF-3α [134], a better understanding of hypoxia-responsive factors has been developed. Intriguingly, HIF-1α is expressed ubiquitously inside the body, HIF-2α expression is restricted to specific tissues including lung, brain, heart, liver, pancreas, kidney, and

intestine [135] while HIF-3α is present in the heart, brain, lung, liver, skeletal muscle, kidney, and pancreas [136].

Structurally, all HIF-α isoforms and HIF-1β contain identical basic-helix-loop-helix (bHLH) and Per-ARNT-Sim (PAS) domains that aid in α-β heterodimerization and in their binding to HREs [137, 138]. Moreover, HIF α isoforms are oxygen-sensitive due to the presence of an oxygen-dependent degradation domain (ODDD) that is responsible for their stability under hypoxic conditions [139]. HIF-1α and HIF-2α are structurally more similar with each other (almost 48% identical amino acid sequence) than with HIF-3α [140, 141]. All three isoforms contain two transactivation domains: the N-terminal transactivation domain (N-TAD) and C- terminal transactivation domain (C-TAD). In association with the Coactivator Binding Protein (CBP)/p300, C-TAD controls the transcription of HIF-1α and HIF-2α dependent genes while N- TAD stabilizes these α subunits against oxygen degradation [140, 142]. In contrast, HIF-3α encompasses the Leucine Zipper (LZIP) domain instead of the C-TAD domain that participates in protein-protein interactions [143]. However, HIF-1β lacks both ODDD and N-TAD domains but embodies the C-TAD domain [143].

HIF-1α is regulated by proline-hydroxylases (PHDs). Under physiological oxygen levels (normoxia), two proline residues (human: Pro402 and Pro564) in ODDD become susceptible to be hydroxylated by PHDs [144]. These hydroxylated residues are subsequently recognized by the von Hippel-Lindau protein (pVHL - a tumor suppressor protein), leading to proteasomal degradation of HIF-1α and HIF-2α subunits under oxygenated conditions [144-146]. However, under hypoxic conditions, PHDs lose their activity and cannot hydroxylate proline residues, resulting in the stabilization of HIF-1α [129, 146]. Subsequently, accumulated HIF-1α translocates

to the nucleus and heterodimerizes with HIF-1β. The dimer then binds to HREs of target genes to activate a variety of hypoxia-responsive genes [147].

Interestingly, under normoxic conditions, the activity of HIF-1α is also abrogated due to the hydroxylation of asparagine residue (human: Asn803) present on the C-TAD domain. Hydroxylation of this asparagine causes hindrance in the binding of HIF-1α with the Coactivator Binding Protein/p300 [144]. On the other hand, an hypoxic microenvironment prevents hydroxylation of this asparagine, leading to the transcription of HIF-1α dependent genes [144, 148]. As previously mentioned, the HIF-1β subunit does not contain ODDD; and possesses a C-TAD without asparagine residue; thus, the activity of HIF-1β is not affected by the presence of oxygen [149].

HIF-1α is also regulated by oxygen-independent mechanisms. For instance, transcription of HIF-1α has been demonstrated to be regulated via the ERK signaling pathway [150]. ERK pathway may affect HIF activity by promoting the formation of the HIF-p300/CBP complex and by modulating the transactivation activity of p300/CBP [151].

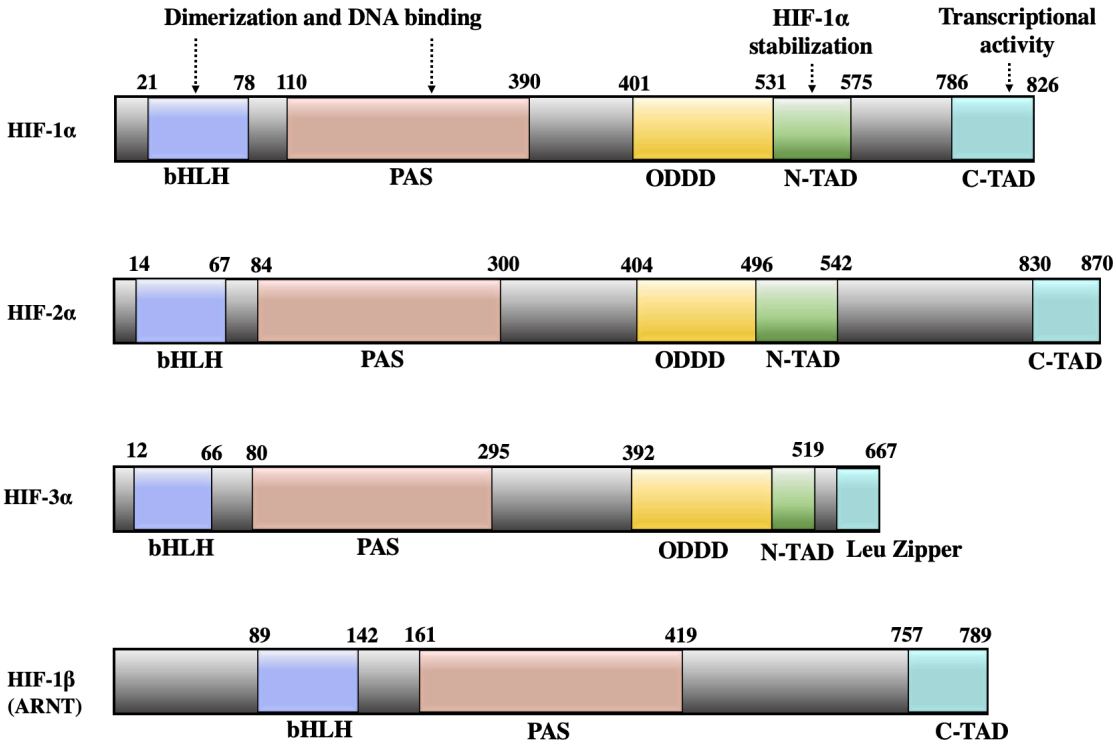

Figure 1.5. Domain structures of the four isoforms of hypoxia-inducible factor (HIF). All isoforms contain a basic-helix-loop-helix (bHLH) and PAS sequences (PER (Period) ARNT (aryl hydrocarbon receptor nuclear translocator) SIM (single-minded)). The bHLH and PAS domains, located at the amino terminus, contain DNA binding sites and dimerization sites. In comparison, the carboxy terminus holds the oxygen-dependent degradation domain (ODDD) and two transactivation domains (N-TAD and C-TAD). N-TAD is responsible for stabilizing HIF-α during hypoxic conditions, while C-TAD controls the transcription of HIF-α target genes. HIF- 3α encompasses the Leucine Zipper (LZIP) domain instead of the C-TAD domain. HIF-1β lacks both ODDD and N-TAD domains but contains the C-TAD domain.

1.2.2.1. Role of HIF-1α in cancer angiogenesis

HIF-1α participates in developing new blood vessels in solid tumors. HIF-1α regulates the motility of endothelial cells by controlling autocrine production of VEGF that results in capillary sprouting and new vessel formation. HIF-1α depleted endothelial cells showed disruption of VEGF mediated autocrine loop in endothelial cells [152]. HIF-1α participates in the transcription of VEGF and leads to increased angiogenesis. *In vivo* studies showed that VEGF deletion, in stem cells of mouse embryo, decreased tumor progression [153]. Another study showed that knockdown of HIF-1α by transfection with a dominant-negative HIF-1α or siRNA reduced VEGF secretion

and cell growth in glioma [154]. Furthermore, tumor cells lacking HIF- 1 produced tumors with impaired vascularization when injected into nude mice [155], whereas the transfection of colon cancer cells with a vector encoding HIF-1α resulted in increased expression of VEGF, angiogenesis and tumor growth [156].

1.2.2.2. Role of HIF-1α in epithelial to mesenchymal transition (EMT)

HIF-1α also plays a critical role in inducing epithelial to mesenchymal transition (EMT) of cancer cells, that further enhances the invasive and metastatic ability of tumors [157, 158]. EMT is a process in which epithelial cancer cells lose their cell-cell adhesion and cell polarity and acquire mesenchymal properties due to cytoskeleton changes required for their progression and dissemination to distant organ [159]. Increased expression of Snail, Twist-related protein 1 (TWIST), Zinc finger E-box-binding homeobox 1 (ZEB1) and the repression of E-Cadherin are the hallmarks of EMT [160]. Snail and TWIST are the transcription factors that activate the EMT program by causing disjunction of cellular adhesions [161]. Snail, TWIST and ZEB1 promote tumor progression and invasiveness by their ability to downregulate E-cadherin and upregulate Vimentin [162-164].

It is reported that HIF-1α binds directly to the HREs located in the proximal promoter of TWIST and ZEB1, thus promoting EMT in head and neck squamous cell carcinoma [143] and colorectal cancer [157], respectively. It has also been demonstrated that EMT induced the formation of finger-like protrusions called invadopodia, that are critical for extracellular matrix (ECM) degradation and facilitation of tumor cell invasion [165]. A recent study investigated the role of HIF-1α in mediating cysteine-rich protein 2 (CSRP2) upregulation in invadopodia in the MDA-MB-231 and MCF-7 breast cancer cell lines [166]. CSRP2 contains two HRE (HRE1 and HRE2) in the proximal promoter region and localizes along with the protrusive actin core of

invadopodium [167]. The results revealed that HIF-1α binds to both HREs of CSRP2 and promotes invadopodium formation, ECM degradation, and invasion of breast cancer cell lines [166]. Another study also established a link between HIF-1α and ECM degradation proteins such as matrix metalloproteinases (MMPs). The study reported that hypoxia activates Ras that participates to the stabilization of HIF-1α. HIF-1α subsequently upregulates MMP9 gene expression and promotes the invasion of breast cancer cells [168].

1.2.2.3. Role of HIF-1α in glucose metabolism

Under hypoxic conditions, rapidly growing tumor cells shift their glucose metabolism from a more efficient oxygen-dependent mitochondrial oxidative phosphorylation to a less efficient oxygen-independent glycolytic pathway, to meet their energy requirements. HIF-1α mediates the transcription of glucose transporters (GLUTs) and glycolytic enzymes to govern this metabolic conversion [169, 170]. HIF-1α upregulates the expressions of GLUT1 and GLUT3 to increase glucose uptake, and promotes gene expressions of glycolytic enzymes such as aldolase (ALDA), PFK-liver type (PFKL), lactate dehydrogenase-A (LDHA), phosphoglycerate kinase-1 (PGK1), and enolase (ENOL), to increase glucose metabolism and generate ATP production under reduced oxidative conditions [169].

1.2.3. RAGE signaling in cancer under hypoxia

Previously, we have discussed studies related to RAGE-mediated signaling pathways involved in cancer progression; however, in this section, we will discuss studies on signaling pathways that illustrate the significance of hypoxia on RAGE upregulation.

A recent study demonstrated that under hypoxia, HIF-1α induces increased RAGE expression that further increases migration and invasion of breast cancer cells, suggesting the prominent role of RAGE in promoting tumor malignancy. The signaling involves translocation of

HIF-1α to the nucleus and initiation of RAGE transcription resulting in an overall increase in RAGE expression under a hypoxic environment. Subsequently, upregulated RAGE activates NF-κB that further increases the transcription of MMP-2 and MMP-9 [171].

RAGE activation under hypoxia also contributes to the activation of the RAF-MEK-ERK and the PI3K-AKT signaling pathways. A recent study suggested that RAGE preferentially binds to KRAS under hypoxia and activates two different pathways in pancreatic cancer: the RAF-MEK-ERK and the PI3K-AKT pathways that further activate HIF-1α Activation of these pathways further promoted the survival of pancreatic tumor cells by increasing their autophagy. Moreover, knockdown of RAGE in pancreatic cancer cells inhibited mutant KRAS activation and subsequent HIF1α stabilization and transactivation. The study also showed that knockdown of both RAGE and HIF1α in Panc02 cells inhibited hypoxia-induced autophagy and increased hypoxia-induced apoptosis that was confirmed by increased levels of the LC3 autophagy markers and decreased levels of the cleaved PARP apoptosis marker [2].

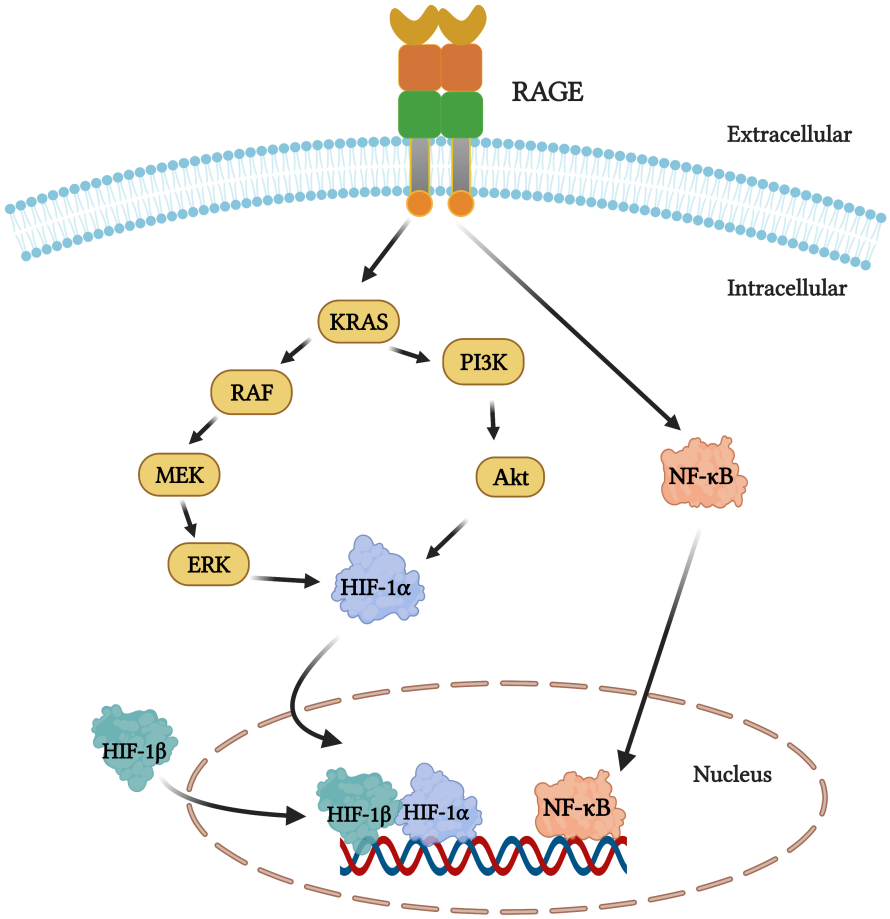

Figure 1.6. RAGE signaling in cancer under hypoxic conditions. Under hypoxic conditions, upregulation of RAGE activates NF-κB. RAGE-mediated KRAS activation under hypoxia further activates two different pathways: the RAF-MEK-ERK-HIF-1α and the PI3K-Akt-HIF-1α pathway. HIF-1α translocates to the nucleus resulting in the transcription of genes responsible for cell survival [2].

1.2.4. Role of RAGE ligands in cancer progression under hypoxia

1.2.4.1. HMGB1

Some cancer cells adapt to low oxygen environment during hypoxia, while others undergo necrosis due to nutrient and oxygen starvation. Necrotic cells release HMGB1 that acts as a ligand for RAGE stimulation in cancer cells [172-174]. Many studies have demonstrated increased HMGB1 under hypoxic conditions [175, 176]. Yao et al. observed hypoxia-mediated upregulation of HMGB1 in hepatocellular carcinoma cells (HCC) promotes tumor proliferation [175].

Similarly, Jiang et al. have reported increased transcriptional levels of HMGB1 under low-level oxygen concentration (1%) in HCC. Activation of HMGB1 under hypoxia can lead to increased cancer cell proliferation [177], metastasis [172], and epithelial to mesenchymal transition (EMT) [178].

It has been demonstrated that HTLA-230 neuroblastoma cells incubated in hypoxic condition (1% O2) undergo EMT. The study showed that the generation of hypoxia upregulates HMGB1 that further promotes EMT by increasing the expression of EMT-related markers such as Twist-1 and N-cadherin [178].

Another study demonstrated that increased HMGB1 released under hypoxic conditions facilitates melanoma growth and metastasis. The study demonstrated that metastatic melanoma tumor sections that were positive for HIF-1α showed high expressions of HMGB1 in the cytoplasm, confirming nucleus to cytoplasmic localization of HMGB1 before active or passive HMGB1 release [172].

A recent study also reported an increase in cancer cell proliferation with increasing concentration of HMGB1 in GBM glioblastoma cells under hypoxia. The conditioned medium of U118 and U251 GBM cell lines under hypoxic conditions showed a significant increase in HMGB1 concentration (600 to 1600 pg/ml) than the conditioned medium of GBM cells under normoxic conditions (10 to 30 pg/ml). Moreover, increased activation of AKT and ERK by HMGB1 under hypoxia confirmed an increase in the proliferation of GBM cells via AKT-ERK signaling [177].

1.2.4.2. S100 proteins

There are 24 genes coding for S100 proteins in the human body [67]; however, among them only five S100 family members (S100B, S100P, S100A4, S100A8, and S100A9) have been studied in the context of hypoxia in tumors.

A recent study on human colon adenocarcinoma reported increased proliferation and invasiveness of Caco-2 cells with increased HIF-1α expression after S100B protein treatment. Treatment of Caco-2 cells with exogenously S100B resulted in the activation of the RAGE-mediated p38 MAPK and pAkt-mTOR pathways. The activation of these pathways subsequently upregulated HIF-1α expression, leading to the release of pro-angiogenic factors VEGF and nitric oxide (NO). Moreover, the authors also demonstrated that treatment of CaCo-2 cells with a monoclonal anti-S100B antibody resulted in decreased pro-angiogenic and proliferative effects [76].

Another study showed increased expression of S100P under hypoxia that promoted migration and invasiveness of hepatocellular carcinoma (HCC) via activation of the NF-κB pathway. Moreover, stable knockdown of S100P by RNA interference significantly abrogated invasive and metastatic potential of HCC cells under hypoxia [179].

Upon exposure to a hypoxic environment, it was reported that transcript levels of S100A4 were upregulated in BGC 823 gastric cancer cells compared to normoxic conditions. The expressions of S100A4 were increased because the first intron of the S100A4 gene contains an HRE sequence (TACGTG) that served as a HIF-1 binding site under hypoxic conditions [180]. Intriguingly, a recent study has also reported epigenetic transformation of ovarian cancer cells into a more invasive phenotype due to the upregulation of S100A4 under hypoxia. The study showed that HRE containing CpG dinucleotides in the S100A4 intron changed its methylation status in a

time-dependent manner under hypoxic conditions. The methylation status can be determined by evaluating the ratio of cytosine (methylated) to thymidine (unmethylated) at each CpG site. A decreased ratio of cytosine (methylated) to thymidine (unmethylated) under hypoxia resulted in increased binding of HIF-1α and subsequent S100A4 upregulation [181]. Similarly, increased migration and invasion of esophageal squamous cancer cells (ESCC) were observed due to increased S100A4 expression under hypoxia. Xuan et al. showed that both mRNA and protein expressions of S100A4 were upregulated after exposure of ESCC cell lines EC-1 and EC-9706 to hypoxia-mimetic agent, cobalt chloride (CoCl2) for 48 hours [182]. It was also shown that HIF-1α activity increased upon RAGE stimulation with human recombinant S100A4 (rS100A4) in CRC colorectal cancer cells [88]. In CRC cells, HIF-1α activity has been reported to enhance cellular motility and increased resistance to apoptosis and chemotherapy [183-185].

Interestingly, hypoxia has also been shown to promote the expression of S100A8/A9 in prostate cancer [186]. The study showed that mRNA and protein levels of S100A8/A9 in prostate cancer cells were upregulated via direct binding of HIF-1α to HRE within the promoter regions of S100A8 and S100A9 [186]. In table 1.1 we summarized the involvement of several RAGE ligands in cancer progression under hypoxic conditions.

Table 1.1. Role of RAGE ligands in initiating pathophysiological responses during hypoxic conditions in cancer.

RAGE ligands	**Cancer type**	**Pathological response**	**Method of hypoxia generation**	**Reference**
HMGB1	Hepatocellular carcinoma	Hypoxia-mediated upregulation of HMGB1 in HCC cells promotes tumor proliferation	1% O_2	[175]
HMGB1	Hepatocellular carcinoma	m-RNA levels of HMGB1 increase under hypoxia	1% O_2	[176]
HMGB1	Neuroblastoma	Hypoxia upregulates HMGB1 that further promotes EMT of HTLA-230 cells	1% O_2	[178]
HMGB1	Melanoma	Hypoxic tumor cells release HMGB1, which promotes melanoma growth and metastasis	1% O_2 and DMOG	[172]
HMGB1	Glioblastoma	GBM cell lines U118 and U251 under hypoxic conditions showed a significant increase in HMGB1 concentration than in normoxia	1% O_2	[177]
S100B	Colon adenocarcinoma	Expression of RAGE and HIF-1α were upregulated when Caco-2 cells were treated with exogenous S100B	-	[76]
S100P	Hepatocellular carcinoma	Hypoxia upregulates S100P and further promotes migration and invasion of HCC cells	1% O_2	[179]
S100A4	Colorectal cancer	HIF-1α activity and expression increases upon RAGE stimulation with human recombinant S100A4 in CRC cells	-	[88]
S100A4	Gastric cancer	Exposure to a hypoxic environment increased transcript levels of S100A4 in gastric cancer cells compared to normoxic conditions	2.5% O_2	[180]
S100A4	Ovarian cancer	S100A4 increased the invasiveness of ovarian cancer cells under hypoxia	1% O_2	[181]
S100A4	Esophageal squamous cancer cells (ESCC)	mRNA and protein expressions of S100A4 were upregulated after exposure of ESCC cell lines to hypoxia	$CoCl_2$	[182]
S100A8/A9	Prostate cancer	Hypoxia treatment resulted in induction of S100A8/A9 protein and mRNA expression in prostate epithelial cells	1% O_2	[186]

1.3. Pancreatic cancer

1.3.1. Statistical facts

According to the American Cancer Society, in year 2021, about 60,430 people (31,950 men and 28,480 women) will be diagnosed with Pancreatic Cancer (PC) and about 48,220 people (25,270 men and 22,950 women) will die because of PC in the United States [187]. Though PC accounts for about 3 % of all cancers in the US, it is one of the deadliest cancers owing to its late diagnosis [187, 188]. Pancreatic cancer is most frequently diagnosed among people aged 65-74. Overall survival rate of PC patients is poor because the tumor is difficult to detect in early stages. The most common type of pancreatic cancer is pancreatic ductal adenocarcinoma in which the exocrine cells in the pancreas start to proliferate at an uncontrolled rate [189]. Table 1 summarizes the five-year relative survival rate of patients suffering from pancreatic cancer.

Table 1.2. 5-year relative survival rates of people diagnosed with pancreatic cancer between 2010 and 2016 [187, 188].

Stage	5-year Relative Survival Rate
Localized	39%
Regional	13%
Distant	3%
All SEER stages combined	10%

1.3.2. Stages of PC

American Joint Committee on Cancer (AJCC) defines PC stages based on three key pieces of information - the size of the tumor, the spread to nearby lymph nodes, and the metastasis at distant sites such as liver, lungs, and peritoneum. The earliest stage of pancreatic cancer is stage 0, and the later stages range from stages I through IV [190].

Table 1.3. Stages of PC [190].

AJCC Stage	Description
0	The cancer is confined to the top layers of pancreatic duct cells and has not invaded to the tissues.
IA	The cancer is confined to the pancreas and is no bigger than 2 cm
IB	The cancer is confined to the pancreas and is larger than 2 cm
IIA	The cancer is confined to the pancreas and is bigger than 4 cm
IIB	The cancer is confined to the pancreas and is no bigger than 2 cm and has spread to less than 3 nearby lymph nodes OR The cancer is confined to the pancreas and is larger than 2 cm but no more than 4 cm and has spread to less than 3 nearby lymph nodes
III	The cancer is growing outside the pancreas and into nearby major blood vessels
IV	The cancer has spread to distant sites such as the liver, peritoneum (the lining of the abdominal cavity), lungs or bones

1.3.3. Genetic mutations of PC

PC is characterized by the genetic abnormality in mainly four genes – KRAS, p16/CDKN2A, TP53, and SMAD4/DPC4. The most common mutation is found in KRAS, present in about 90-95% of patients suffering from pancreatic cancer [191]. RAS guanine nucleotide exchange factors (RASGEFs) activates KRAS by facilitating KRAS- guanosine triphosphate (GTP) binding. Activated KRAS is further responsible for cell proliferation, cell survival, and migration. However, guanosine-triphosphatase-activating proteins (GAPs) promotes the inactivation of KRAS via GTP hydrolysis to GDP. The switching of the active to inactive state further attenuates KRAS signaling. Mutation in G12, G13, and Q61 amino acid residues results in alteration of GTPase activity of KRAS. This causes KRAS to be constitutively active, resulting in the stimulation of signaling pathways such as RAF–mitogen-activated protein kinase (RAF-MAPK) and phosphatidylinositol 3 kinase (PI3K) [192], leading to uncontrolled cancer cell proliferation [193].

Inactivation of a tumor suppressor gene known as p16/CDKN2A, or INK4A is seen in approximately 90% of pancreatic cancer patients. This gene encodes a protein that belongs to the cyclin-dependent kinase (CDK) inhibitor family. The normal function of the p16/CDKN2A gene is to inhibit cell cycle progression through the G1-S cell cycle checkpoint. Deletion or mutation of the p16/CDKN2A gene may increase the activity of cyclin-dependent kinase 4, resulting in hyperphosphorylation of the Rb protein, progression of the cell cycle from G1 to S, and hence, enhancement of cell proliferation [194, 195].

Inactivation of TP53 gene occurs in about 50-75% of pancreatic cancers. p53 protein is responsible for regulating cell cycle, maintenance of G2-M arrest, and the induction of apoptosis. Thus, inactivation of TP53 gene results in increased cancer cell survival and cell division [196]. A gene known as 'deleted in pancreatic carcinoma 4 gene' or DPC4 (also known as SMAD4) is inactivated in approximately in 55% of pancreatic cancers. SMAD4 encodes the Smad4 protein, which in conjugation with Smad 2/3 carries out transcription of tumor suppressor genes. Thus, loss of SMAD4 leads to tumor progression [197].

1.3.4. Pathophysiology of PC

The changes in pancreatic ductal adenocarcinoma (PDA) are characterized by different grades of lesions based on extent of cytological and architectural changes [198]. Lesion formation initiates with low-grade dysplasia, also known as pancreatic intraepithelial neoplasia (PanIN) grade 1 that further progresses into low to moderate grade PanIN-2 and high grade PanIN-3 lesions. PanINs usually appear in smaller pancreatic ducts and are less than 0.5 cm in size. PanIN-1 lesions are further characterized as PanIN-1a lesions that comprises columnar epithelial cells with small round to oval nuclei, and PanIN-1b epithelial lesions, characterized by papillary or basally pseudostratified architecture [199, 200]. In PanIN2 lesions, papillary epithelial cells develop mild

abnormalities in their nucleus such as nuclear enlargement and crowding, loss of polarity and pseudo stratification. PanIN-3 lesions predominantly exhibit papillary or micropapillary structures with enlarged irregular nuclei. These lesions are also regarded as carcinoma *in situ* type lesions and characterized by increased atypical forms. The last stage of lesions is pancreatic ductal adenocarcinoma (PDA) which is the aggressive form of carcinoma having metastatic potential [189].

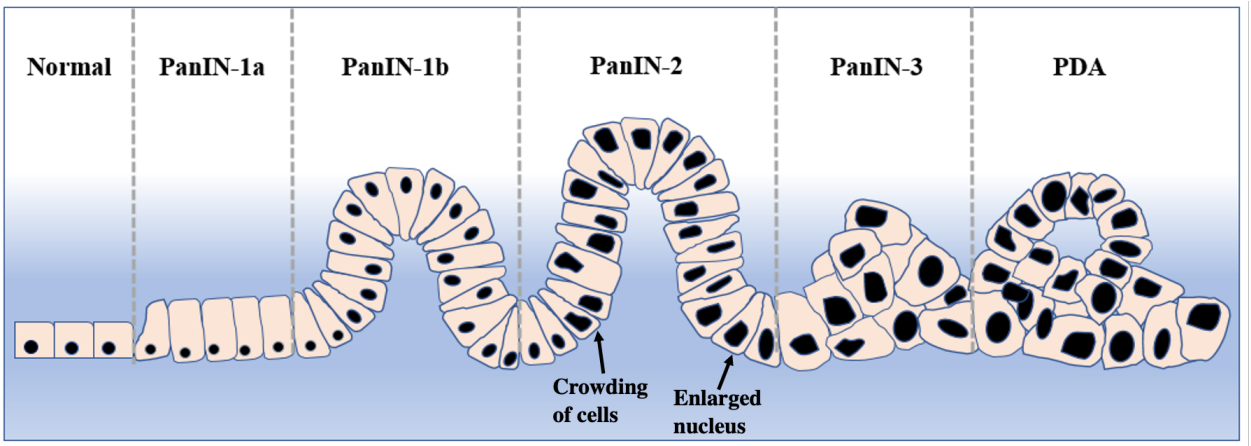

Figure 1.7. Schematic of the different stages of Pancreatic Ductal Adenocarcinoma (PDA). PDA arises from the multi-stage progression of precursor lesions known as pancreatic intraepithelial neoplasia (PanIN). Adapted from [201].

1.3.5. Treatment of PC

Surgical resection is always considered as first line of treatment in pancreatic cancer however, chemotherapy adjuvant to surgical resection has also been shown to improve overall survival rates of patients compared to surgery alone [202, 203]. Depending on the tumor's anatomical location, different surgical options are available such as Pancreatico-duodenectomy (also known as Whipple's procedure), distal or total pancreatectomy. The Whipple's procedure is the most common type of surgery performed in pancreatic cancer patients and involves removal of pancreas head, duodenum, gall bladder and bile duct [204]. A meta-analysis has shown that leakage from pancreatic anastomosis and development of pancreatic fistula after Whipple's

procedure is a possible cause of morbidity in some cases [205, 206]. The ultimate goal of surgery is to improve survival rate of patients by completely removing the tumor [207]. Gemcitabine is the standard chemotherapeutic agent for pancreatic cancer that acts by inhibiting DNA synthesis [208]. As a prodrug, gemcitabine or dFdC (2′,2′-difluoro-2′-deoxycytidine) is metabolized to the active triphosphate form of gemcitabine or dFdCTP (2′,2′-difluoro-2′-deoxycytidine triphosphate). When dFdCTP is incorporated into DNA, it inhibits DNA polymerases thus preventing DNA synthesis [209]. A randomized study of gemcitabine as adjuvant therapy to surgery showed a significant improvement in median disease-free survival rate from 6.7 months to 13.4 months and a five-year survival rate from 10.4% to 20.7%. The overall survival rate was also improved from 20 months to 23 months [210]. In another trial, gemcitabine and 5- Fluorouracil (5-FU) were compared for pancreatic cancer treatment and found that both drugs are equally potent for improving the overall survival rate of patient (25.5 months). However, it was also noticed that 5-FU was less tolerated by patients. Additionally, a dual therapy of capecitabine and gemcitabine showed promising results with an overall survival of 28 months as compared to gemcitabine alone [211]. Recently, a randomized clinical trial was conducted to compare the outcomes of gemcitabine and FOLFIRONOX as adjuvant therapies in pancreatic adenocarcinoma patients. FOLFIRONOX is a combination of fluorouracil, oxaliplatin, leucovorin (or folinic acid) and irinotecan drugs that showed a significant improvement in overall survival of 54.4 months compared to gemcitabine (35 months) [212]. FOLFIRONOX and gemcitabine have also been tested in patients with metastasized pancreatic cancer and the results revealed that the group treated with FOLFIRONOX showed promising outcomes with overall median survival of 11.1 months compared to 6.8 months in the gemcitabine treated group [213].

1.4. Melanoma

1.4.1. Statistical facts

Melanoma, a type of skin cancer, is lethal upon metastasis to distant organs. The American Cancer Society's estimates that about 106,110 new melanomas will be diagnosed (about 62,260 in men and 43,850 in women) and about 7,180 people are expected to die of melanoma (about 4,600 men and 2,580 women) in the United States by the end of 2021 [214]. 5-year relative survival rate for distant melanoma is just 27%. Melanoma develops when melanocytes (the cells that give the skin its tan or brown color) start to proliferate at an uncontrolled rate [215]. It is one of the most lethal type of skin cancer as it has a great potential to metastasize to other organs.

Table 1.4. 5-year relative survival rates for melanoma skin cancer from 2010 and 2016.

Stage	5-year Relative Survival Rate
Localized	99%
Regional	66%
Distant	27%
All SEER stages combined	93%

1.4.2. Stages of melanoma

Melanoma can be classified into four clinical subtypes: superficial spreading melanoma (SSMM), lentigo maligna melanoma, nodular melanoma and acral lentiginous melanoma (figure 1.8). Around 70% of the total melanoma cases belong to SSMM subtype. Lentigo maligna melanoma is a premalignant lesion form present in the skin with different shapes and colors. Nodular melanoma is characterized as an inflammatory nodule that does not possess brown or black pigment and is present on the exposed body parts. Acral lentiginous melanoma is a type of melanoma that starts as a slowly growing patch of discolored skin and is characterized by the site of origin- palm, sole or subungual [216].

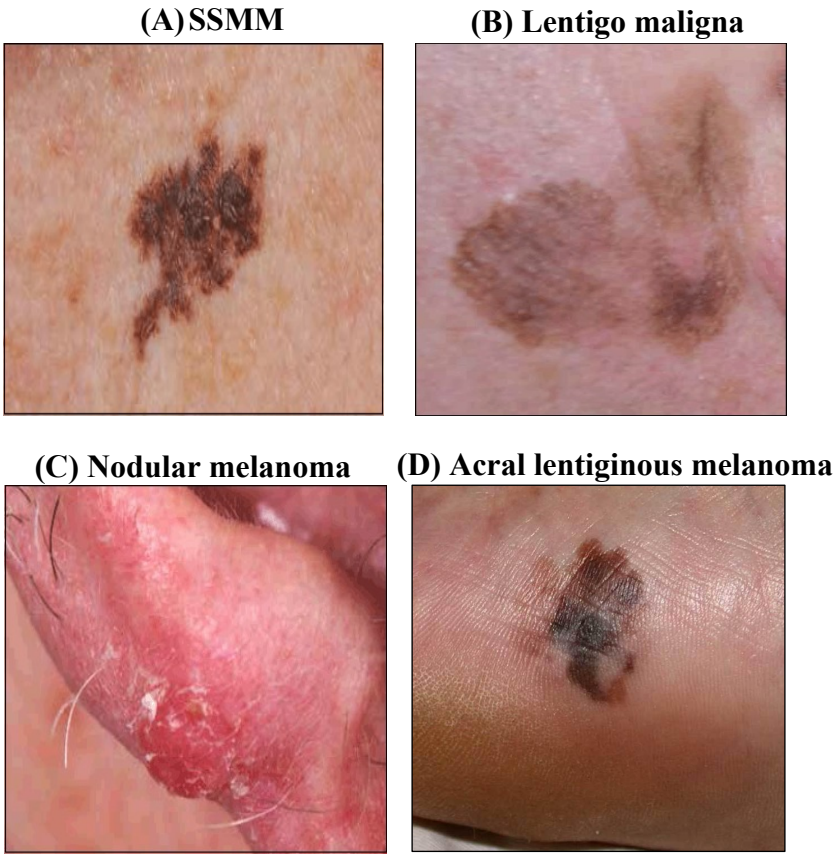

Figure 1.8. Different types of melanomas (A) SSMM, (B) Lentigo maligna, (C) Nodular melanoma, and (D) Acral lentiginous melanoma. Figure taken from [216].

1.4.3. Genetic alterations in melanoma

Mutations of BRAF, NRAS, and KIT genes have been correlated to the development of melanoma [217]. BRAF gene encodes a serine-threonine protein kinase of the RAF (rapidly accelerated fibrosarcoma) family. This protein plays an important role in the regulation of MAPK pathways signaling, causing changes in cell cycle, differentiation, and apoptosis [218]. The most common BRAF mutation is V600E that is in the activation site of the kinase. This mutation represents 60 to 80% of all mutations BRAF [219]. Neuroblastoma-RAS or NRAS oncogene belongs to p21 GTPase protein superfamily [220]. These proteins exist in equilibrium between GTP- and GDP-bound forms. The GTP-bound conformation of RAS is the active form that shows high-affinity interactions with effector proteins, subsequently propagating downstream signaling [220]. They participate in the activation of MAPK/PI3K pathway, during cellular proliferation and

survival. The most common NRAS gene mutations are Q61R and Q61K and represent around 25% of mutations for biopsies of patients with melanoma [221]. KIT encodes for a tyrosine-protein kinase that acts as a cell surface receptor and participates in the normal growth of melanocytes and intervenes in the activation of MAPK/PI3K pathways [217]. KIT gene mutations are present in 39% of mucosal melanomas (MM), 36% of acral lentiginous melanomas (ALM), and in 28% of skin with chronic solar damage [222, 223].

1.4.4. Pathophysiology of melanoma

The progression of melanoma involves a series of events based on the Clark model, originating from slow progression of benign melanocytic nevi to become metastatic melanoma [224] (figure 1.9). The benign nevus is characterized by controlled growth of normal melanocytes [225]. Subsequently, the benign nevus becomes dysplastic nevus due to abnormal growth of melanocytes resulting in the formation of pre-malignant lesions with random cytological atypia. These lesions are usually greater than 5 mm in size with variable pigmentation that further translates into a primary melanoma tumor. These primary melanocyte tumor cells gain the ability to proliferate horizontally in the epidermis that is termed as radial growth phase [226]. In the next phase, known as vertical growth phase, few of these cells invade into the papillary dermis. Subsequently, these invading cells undergo transition into a motile form due to increased expression of N-Cadherin that allows them to invade the basement membrane and starts proliferating vertically in the dermis as an expanding nodule. Due to acquired metastatic potential at this step these transformed cells further disseminate to other body parts such as lymph nodes, skin, subcutaneous soft tissue, lungs and the brain [227].

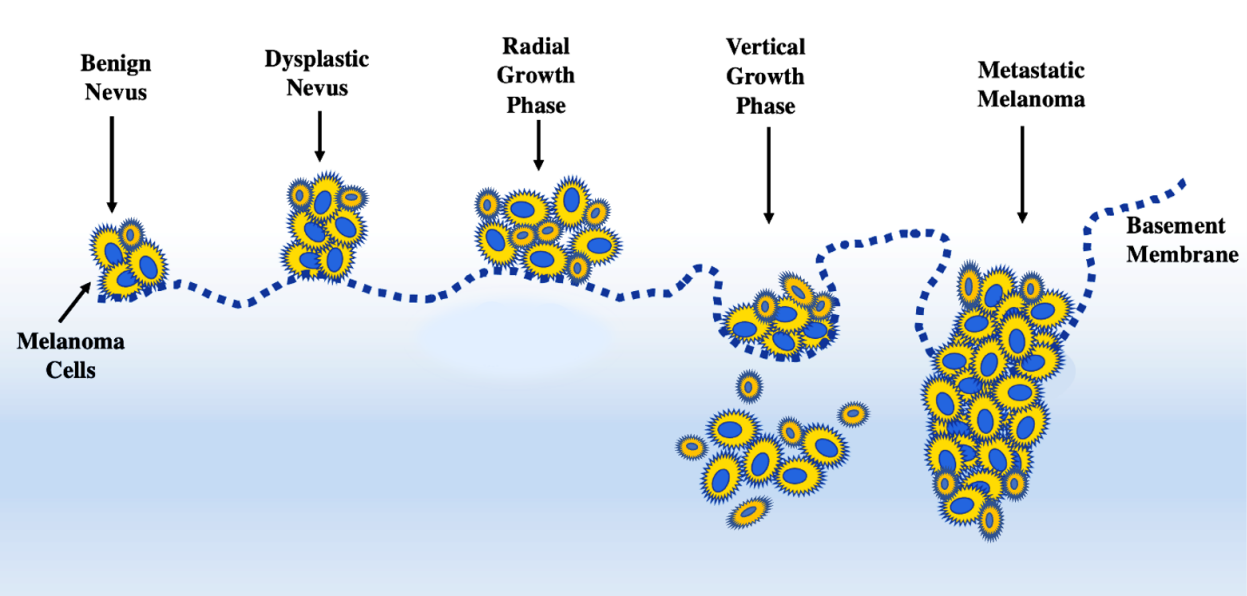

Figure 1.9. Pathophysiology of melanoma involves the formation of benign nevus after the proliferation of normal melanocytes. Subsequently, abnormal growth of melanocytes in a pre-existing nevus results in a pre-malignant lesion called dysplastic nevus. Next phase involves radial growth where melanocytes acquire the ability to proliferate horizontally in the epidermis. At this stage, presence of E-cadherin holds the tumor at the primary site. This stage is followed by a vertical growth phase that occurs after the loss of E-cadherin and expression of N-cadherin that allow cells to invade basement membrane and protrude vertically in the dermis. Metastasis is the last stage where malignant melanocytes spread first to lymph nodes, then to the lungs, brain and other organs [224, 226, 227].

1.4.5. Treatment of melanoma

Chemotherapy is an important treatment option for the treatment of refractory, progressive and relapsed melanoma [228]. Dacarbazine, an alkylating agent, was the first approved drug for metastatic melanoma in 1974. Dacarbazine alkylates nucleic acids, specifically guanine, leading to cell growth arrest [229]. Immunotherapy is another therapeutic approach that was developed based on the activation of immune responses against cancer cells. During an antitumoral response, T- cells that recognize tumor specific antigens at the surface of cancer cells become activated, proliferate and kill cancer cells [230]. Interferon (IFN) α-2b was the first immunomodulating agent approved by the FDA in 1995 as an adjuvant therapy for the treatment of stage IIB/III melanoma [231]. IFN α-2b inhibits the proliferation of melanoma cells by inducing the stimulatory effect of

class I MHC of melanoma and immune cells [232]. However, due to low patient responses, more efficient immunotherapies were discovered later. In 1998, high dose interleukin-2 (IL-2) was approved for the treatment of metastatic melanoma. IL- 2 is a cytokine that demonstrates an antitumor effect by expanding effector T-cells and showed overall response of 19.7% [233, 234]. In 2011, Polyethylene gycol (Peg) combined IFN α-2b, Peginterferon α-2b (Peg-IFN) was approved by the FDA for stage III melanomas as adjuvant therapy [235]. The advantage of Peg conjugation is to enhance the therapeutic effect of IFN α-2b by improving its half-life in the bloodstream [236]. However, due to increased adverse effects of IL-2 and Peg-IFN such as hypotension, cardiac arrhythmias, peripheral edema and multisystem organ failure, these agents were replaced by newer immunomodulatory therapies [237]. One of these new agents, ipilimumab, is an anti-cytotoxic T lymphocyte-associated antigen 4 (CTLA-4) that was approved by the FDA in 2011 for the treatment of advanced staged melanomas. CLTA- 4 is a factor expressed on T-cells that inhibits T-cell activation. Ipilimumab acts via blocking the inhibitory effect of CLTA-4 and increased clonal T-cell expansion [238]. A phase IB study of ipilimumab and Peg-IFN demonstrated an overall response rate of 40% and median progression free survival (PFS) of 5.9 months in patients with unresectable melanoma [239]. In 2014, an anti- Programmed cell death protein 1 (PD-1) monoclonal antibody, Nivolumab, was approved by the FDA for the treatment of metastatic melanoma. PD-1 receptors are expressed in tumor cells and suppress T-cell activation upon activation with PD-1 ligands [240]. Nivolumab blocks the interaction between PD-1 and its ligands to promote antitumor activity of activated T-cell [241]. The outcomes of Nivolumab trials showed a PFS of 6.9 months, however, a combination of nivolumab and ipilimumab showed a median PFS of 11.5 months [241, 242]. As a continuous development of new therapeutic agents

is required to treat melanoma effectively, a better understanding of the biology of melanoma is needed. Our next chapter aims at investigating the role of RAGE in melanoma.

2. CELLULAR LOCALIZATION OF RAGE IN MELANOMA CELLS WITH DIFFERENT CELLULAR ARCHITECTURES

2.1. Hypothesis

The goal of this study was to understand the role of RAGE in melanoma progression. Involvement of RAGE and its ligands in melanoma has been shown by several groups including ours [58, 243-245]. RAGE has been found to be upregulated in melanoma tumors both at transcriptional levels [243] as well as at protein levels [246]. Moreover our group has observed that overexpression of RAGE in human melanoma cells led to increased tumor growth in mice, and treatment with an in-house IgG 2A11 anti-RAGE antibody resulted in diminished tumor growth [112]. IgG 2A11 is a monoclonal anti-RAGE antibody that targets the V-domain of the receptor present on the cell surface suggesting that RAGE is expressed on cell surfaces within tumors [112]. However, in a study performed on melanoma cells in 2D monolayer culture, RAGE was localized in the cytoplasm as well as on cell membrane in melanoma cells (G361 and A375) [58]. A previous student in our group, Sultan Kadasah, also observed that cells grown in 2D monolayer express RAGE intracellularly (data not shown). Based on these studies, we thus hypothesized that RAGE is expressed on cell surface in 3D conditions and intracellularly in 2D monolayer cultures. To test our hypothesis, we employed 3D spheroid models of one murine melanoma cell line (B16F10) and two human melanoma cell lines (WM115 and WM266) to evaluate RAGE localization versus melanoma cells in 2D monolayer conditions. Furthermore, we used a lung colonization mice model to study RAGE localization in complex 3D *in vivo* tumor microenvironment. Overall, our understanding of RAGE localization in melanoma tumors might contribute to design therapeutic entities, such as anti-RAGE antibodies and small molecule inhibitors that could act as therapeutics for melanoma.

2.2. Abstract

The objective of this chapter was to investigate RAGE localization in melanoma cells with different cellular architectures. RAGE participates in melanoma progression; however, the clear understanding on RAGE localization in melanoma progression is still not conquered. Previously, our group observed that anti-RAGE antibody IgG 2A11 diminishes tumor growth in mice by targeting V-domain of RAGE indicating that RAGE is present on the surface of melanoma cells in tumors [112]. Further, our group and others showed that RAGE is located intracellularly in melanoma cells when cultured in 2D monolayer conditions. Thus, we hypothesized that RAGE localization in melanoma cells is influenced by the cellular 3D architecture. To test our hypothesis, we utilized spheroids of B16F10, WM115 and WM266, and a lung colonization mice model of melanoma to compare the RAGE localization in their 3D architecture vs 2D *in vitro* monolayer cultures using immunofluorescence.

In the present study, we observed green fluorescence distributed inside the melanoma cells cultured in 2D monolayer, indicating intracellular localization of RAGE in 2D monolayer conditions. However, in spheroids we noticed high fluorescence intensity of RAGE on the periphery of WM115 whereas in WM266 we observed mainly intracellular localization of RAGE with a few peripheral sites of RAGE expression. In B16F10 spheroids, we observed a green fluorescence at the cell surfaces and bright spots in the nucleus, suggesting RAGE localized both at cell surfaces and inside the nuclei. Moreover, we observed high intensity of green fluorescence at the surface of melanoma cells in tumors, indicating the presence of RAGE at the cell surface.

2.3. Introduction

Melanoma, a type of skin cancer, arises from the uncontrolled growth of melanocytes [247]. After formation of a primary tumor, melanoma cells disseminate through systemic

circulation to extravasate and proliferate to secondary distant sites [225]. The most common sites of distant metastases are - lung, brain, liver, bone, and intestine, however, lung is mostly the first clinically apparent site of metastasis in melanoma patients [248]. It has been previously described that RAGE participates in Melanoma progression [58, 112, 243, 249]. Various groups have used antibodies against RAGE to reduce melanoma tumor growth and metastasis in animal models. Abe et al. found that upon treatment with anti-RAGE antibody, tumor growth in athymic mice was decreased and their survival rate was increased [58]. Previous studies from our group showed five to ten-fold increase in RAGE mRNA levels in 40 melanoma tumor samples compared to non-tumor skin samples. Moreover, it was also observed that RAGE transcript levels were significantly higher ($p<0.05$) in stage IV melanoma patient samples than stage III samples [243]. Our group has also demonstrated that the overexpression of RAGE in WM115 human melanoma cells contributed to their migratory properties by promoting their mesenchymal characteristics that were reversed after RAGE silencing using a RAGE-specific siRNA [249]. Later, our group also observed that RAGE overexpressing melanoma cells (WM115-RAGE), when implanted subcutaneously into mice, generated tumors faster than control (WM115-MOCK) cells. In addition, upon treatment of WM115-RAGE tumors with the anti-RAGE antibody IgG 2A11, the tumor growth rate was significantly reduced. IgG 2A11 is a monoclonal anti-RAGE antibody that targets the V-domain of the receptor present on the cell surface suggesting that RAGE is expressed on cell surfaces within tumors [112]. However, Abe et. al. demonstrated that RAGE is expressed in the cytoplasm and at the membrane of melanoma cells (G361 and A375) grown in 2D conditions [58]. Moreover, a former member of our group, Dr. Sultan Kadasah has observed the presence of RAGE in the cytoplasm of WM115 melanoma cells when cultured in 2D conditions (data not shown). Based on these studies we hypothesize that RAGE localization may vary in melanoma cells with different

cellular architectures. In the present study, we utilized a tumor spheroid model and *in vivo* mice models to investigate RAGE localization in 3D cellular architecture.

Tumor spheroids are 3D structures that are generated *in vitro* [250]. In comparison to 2D monolayer culture system, 3D *in vitro* spheroid models have the advantages of replicating some of the complex features of *in vivo* tumors [251, 252]. 2D culture of cancer cells *in vitro* do not recapitulate the 3D architecture and heterogeneity of tumors [253].

In the present study, we hypothesized that RAGE is expressed on cell surface in 3D spheroids and in *in vivo* melanoma tumors compared to 2D monolayer cultures. To test our hypothesis, we used immunofluorescence to determine the localization of RAGE in WM115, WM266 and B16F10 spheroids, as well as in melanoma tumors generated from B16F10 cells.

2.4. Materials and methods

2.4.1. Cell lines

B16F10, WM115 and WM266 cancer cells were purchased from American Type Culture Collection (ATCC) (Manassas, VA, USA). Cells were cultured and maintained in Dulbecco's Modified Eagle's Medium (DMEM, ATCC) with high glucose, containing 10% fetal bovine serum (PEAK, Wellington, Colorado USA), penicillin (100 U/ml) and streptomycin (100 µg/ml) (ATCC) under standard culture conditions (5% CO_2, at 37ºC). B16F10 is a murine melanoma cell line originated from a C57BL/6J mouse. B16F10 cells have epithelial-like morphology and were derived from lung colonized tumor nodules. The WM115 cell line originates from the primary tumor in vertical growth phase from a melanoma patient and exhibits epithelial-like morphology while WM266 cells were derived from a lymph node metastatic site of the same patient and have mesenchymal-like morphology [254]. HEK-293 cells stably transfected with RAGE cells were a generous gift from Prof. Heizmann (University of Zürich, Zurich, Switzerland).

2.4.2. Spheroid formation

Multicellular spheroids can been generated via various techniques such as hanging drop, low attachment technique, spinner culture, and hydrogel cell aggregation [255]. We chose the ultra-low attachment technique because of its high reproducibility of results. Moreover, this technique allows for better analysis of cell viability and cell cytotoxicity assays because there is no need to transfer of spheroids during such assays [256]. Also, this technique has an advantage of producing 3D cellular aggregates using non-scaffold-based cell culture system [15]. For spheroid formation, first the melanoma cells were trypsinized using Gibco™ Trypsin-EDTA (0.05%) and centrifuged at 1100 rpm to obtain the cell pellet. The cells were resuspended in growth media and counted using a hematocytometer. Next, 2.5 x 10^3 cells were seeded onto each well of round bottom 96 well-plates (Falcon, BD NJ, USA) using 80% complete medium (DMEM+FBS) and 20% methyl cellulose (figure 2.1). Before seeding the cells, the plates were pre-treated with a poly-HEMA (hydroxyethyl methacrylate) solution in 95% ethanol and dried under sterile hood for 72 h as per manufacturer protocol [257]. Spheroids were grown under standard culture conditions (5% CO2, at 37ºC) and imaged at day 2 and day 4 using a microscope (Leica Microsystems Inc., Buffalo Grove, IL).

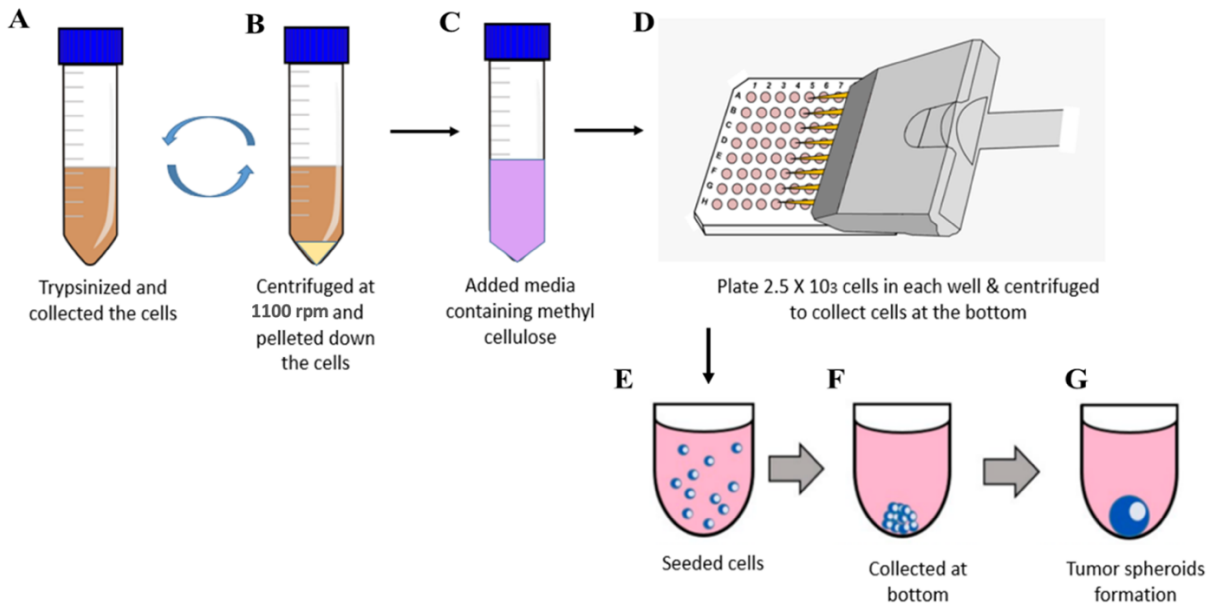

Figure 2.1. Schematic representation of preparation of spheroids. (A) Cells were trypsinized and collected in the centrifuge tube. (B) Cells were centrifuged at 1100 rpm to obtain a cell pellet. (C) Resuspension of the cells with the media containing DMEM containing methyl cellulose. (D) Cells were seeded in ultra low attachment plate and then centrifuged. (E - G) Represent tumor spheroid formation.

2.4.3. Immunofluorescence

2.4.3.1. Staining of 2D cultured cells

Cells (60% confluent) were trypsinized and counted using a hematocytometer. 2.5 x 10^3 cells were seeded in each well of 8-well chambered glass slides (Ibidi GmbH, Martinsried, Germany). Next, the cells were fixed with 4% paraformaldehyde (PFA), permeabilized for 5 minutes with 0.1% triton X-100 solution in PBS and finally blocked with 5% bovine serum albumin (BSA) for 1 hour. Next, the cells were incubated with primary RAGE polyclonal antibody (R&D systems, Minneapolis, MN) using 1:50 dilution in 5% BSA (Bovine serum albumin) in TBST at 4ºC overnight. The cells were washed three times with Tris-buffered saline (TBS) (50mM Tris pH 7.4, 150mM NaCl) containing 0.1% Tween 20 (TBS-T) for 5 minutes each and incubated with FITC conjugated donkey anti-goat secondary antibody (Jackson Immuno Research, West Grove, PA) using 1:100 dilution in 5% BSA (Bovine serum albumin) in TBST. Finally, the cells

were imaged using a confocal microscope (Zeiss LSM 900, Carl Zeiss Microscopy LLC, White Plains, NY) and images were processed using Zeiss Zen software (blue edition, version 3.1).

2.4.3.2. Formation and staining of spheroids

For the formation of spheroids, we utilized methylcellulose in the culture medium. Methylcellulose aids in the gathering of cells and facilitates to form multilayered aggregates [258, 259]. We also pre-coated the plates with poly-HEMA which is a biocompatible hydrogel that forms a non-adherent coating surface on plates and prevents cell adherence to plate surface [260]. At day 4 the spheroids were fixed with 4% PFA for 30 minutes and then dehydrated with a series of ethanol concentrations. First, PFA was replaced with 50% ethanol and kept at 4ºC overnight. Further the solution was replaced with 70% ethanol and kept at 4ºC for another 24 hours. Next, the spheroids were embedded into aluminum molds containing 3% agarose solution (figure 2.2) and kept in 70% ethanol at 4ºC. The agarose embedded spheroids were paraffinized and sectioned in 5µm thickness sections using a microtome. Following this, spheroid sections were heat treated for 1 hour at 55ºC in an oven (Thermo Scientific, Waltham, MA) to deparaffinize them. Next the sections were treated with three xylene (100 % concentration) washes to further remove the wax from slides and rehydrated in series of ethanol concentrations -100%, 90%, 70%, 50% (15 dips each) followed by deionized (DI) water for three minutes. Further, the slides were immersed in chamber containing citrate buffer (at pH 6.0) and placed inside Retriever 2100 (Diagnostic Technology) for 15 minutes at temperature 120ºC for antigen retrieval. Further, sections were washed with TBS-T for three minutes. The sections were then incubated with 5% BSA in TBS-T blocking buffer for 1h at room temperature. Next, the sections were incubated with affinity-purified polyclonal goat anti-human RAGE IgG (R&D Systems, Minneapolis, MN)) using 1:50 dilution in 5% BSA in TBST overnight at 4ºC. The sections were washed three times with TBS-T

and incubated with FITC conjugated affinipure donkey anti-goat IgG secondary antibody (Jackson Immuno Research, West Grove, PA) using 1:100 dilution in 5% BSA (Bovine serum albumin) in TBST for an hour at room temperature. The sections were then washed three times with TBS-T and stained with 4, 6-diamidino-2-phenylindole (DAPI) containing mounting media (Vector Laboratories, Burlingame, CA). The slides were imaged under confocal microscope (Zeiss LSM 900, Carl Zeiss Microscopy LLC, White Plains, NY) at 40X magnification.

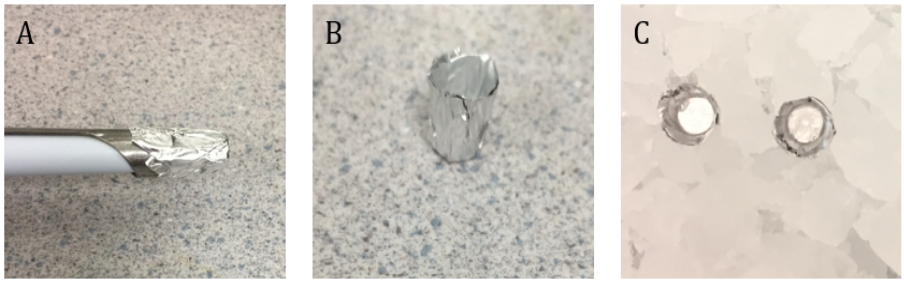

Figure 2.2. Formation of aluminium molds to embed spheroids in 3% agarose solution. (A) Mold formation using 1000 µl pipette aid. (B) Representation of formed mold. (C) Molds kept on the ice before adding molten agarose solution.

2.4.4. Animal models

For the lung colonization model, we chose murine melanoma - B16F10 cells that have tendency to localize into the lungs of mice due to its metastatic nature. Originally, Fidler et al. extracted cells from B16F1 parent tumor and reinjected them through mice tail vein to produce daughter B16F10 cells over ten generation of tumors. It was found that the B16F10 cells had a greater metastatic potential than their parent cell line. It was suggested that B16F10 metastasis model is one of the best characterized experimental metastasis model [261, 262]. For this model, C57BL/6 mice were maintained in ventilated cages, and all of the experiments were performed according to a protocol approved by the Institutional Animal Care and Use Committee (IACUC). We employed eight to ten-week-old mice (20-25 g) that were bred at the animal care facility at North Dakota State University, Fargo, ND. To assess RAGE localization, we used tumor colonized

lungs that were collected as a part of a different study that was planned to investigate the effectiveness of combination of RAGE antibody – IgG 2A11 and Dacarbazine.

However, we chose a subcutaneous model for investigating RAGE localization in human cell lines – WM115 and WM266 because there is a lack of evidence that these cell lines have a metastatic potential to colonize in the lungs upon tail vein injection. For this model, female Severe Combined Immunodeficiency (SCID) mice of age ten weeks were used. These mice were bred and carefully maintained in germ free conditions and kept in sterile cages in the animal facility of the Department of Pharmaceutical Sciences, at NDSU. All the experiments were performed according to protocols approved by the Institutional Animal Care and Use Committee (IACUC).

2.4.5. Cell suspension preparation for mice models

For the lung colonization model, a cell suspension of $2x10^6$ cells/ml was prepared in PBS and 100 µl of the suspension was injected to each mouse through the tail vein using 28 gauze needle syringes (BD insulin syringes). In control mice, 100 µl of PBS was injected via the tail vein (figure 2.3). 21 days after injection, the animals were euthanized, lung tissues were harvested and fixed in formalin to perform staining experiments.

For the subcutaneous model, a suspension of $4x10^6$ cells/ml was prepared in PBS and 100 µl of this suspension was injected subcutaneously in the flanks of each mouse using 27 gauze needle syringes (figure 2.3).

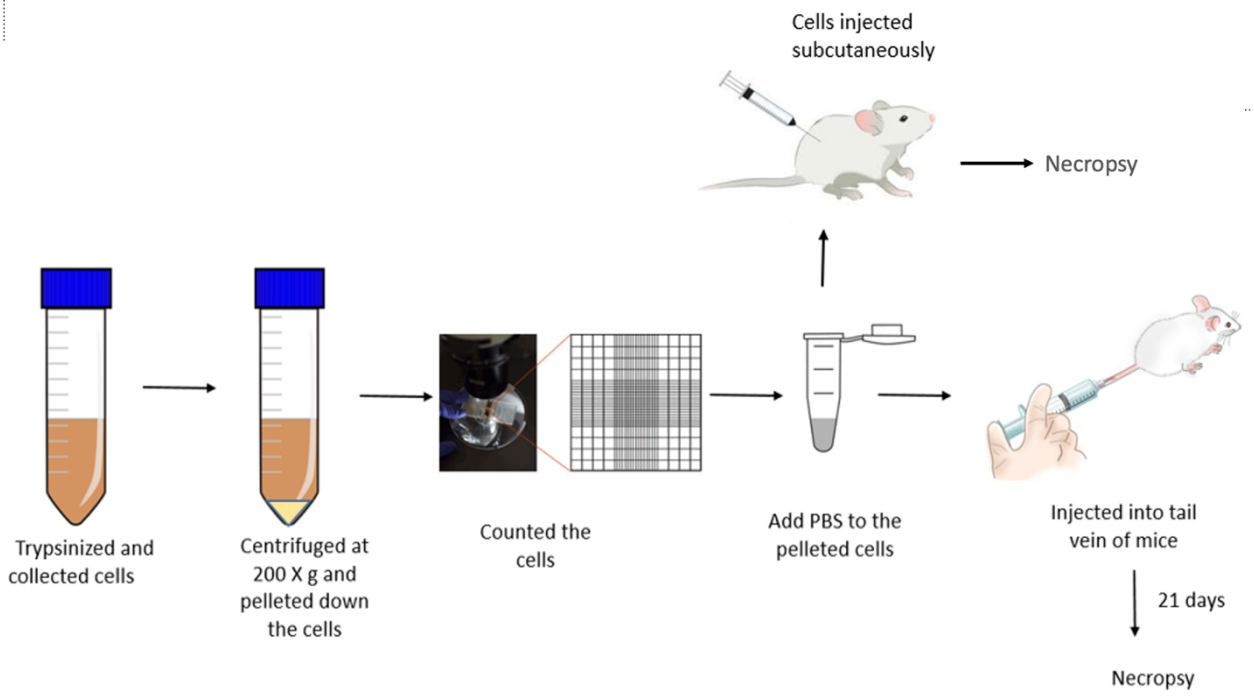

Figure 2.3. Schematic representation of cell suspension preparation for the lung colonization model and the subcutaneous model.

2.4.6. Tissue processing, staining and imaging

Tissues were embedded in paraffin using the autotechnicon tissue processor. Tissue sections of 5 µm thickness were sectioned by Jordan Flatten using a microtome at the Department of Animal Sciences, NDSU. Tissue sections were heat treated for 1 hour at 55ºC in oven to deparaffinize. Next the sections were treated with xylene (100% - three times) and rehydrated in series of ethanol concentrations -100%, 90%, 70%, 50% (15 dips each) followed by rehydration with DI water for three minutes. To identify tumor regions, the sections were stained with hematoxylin (Richard-Allan Scientific, Kalamazoo, MI) for 1 min 50 sec and eosin (Richard-Allan Scientific, Kalamazoo, MI) for 1 min 50 sec. The tissue sections were also processed, stained and imaged for RAGE with the same procedure as mentioned in section 2.4.3.2.

2.5. Results

2.5.1. Establishment of *in vitro* tumor spheroids

We observed spheroids formation under bright field microscopy on day 2 and day 4 after cell seeding. Next, we measured spheroid size from a representative image of each cell line by drawing the line (using the graphic scale tool) across the spheroid. The spheroid size of B16F10 was 225 μm, WM115 was 275 μm and WM266 was 280 μm on day 2. On day 4 we imaged the same spheroids and we found that the size of B16F10 spheroids grew to 375 μm while WM115 and WM266 spheroids on day 4 increased to 300 μm (figure 2.4). During our preliminary study, we observed that after day 4 the spheroids tend to break apart therefore, we chose day 4 to collect the spheroids.

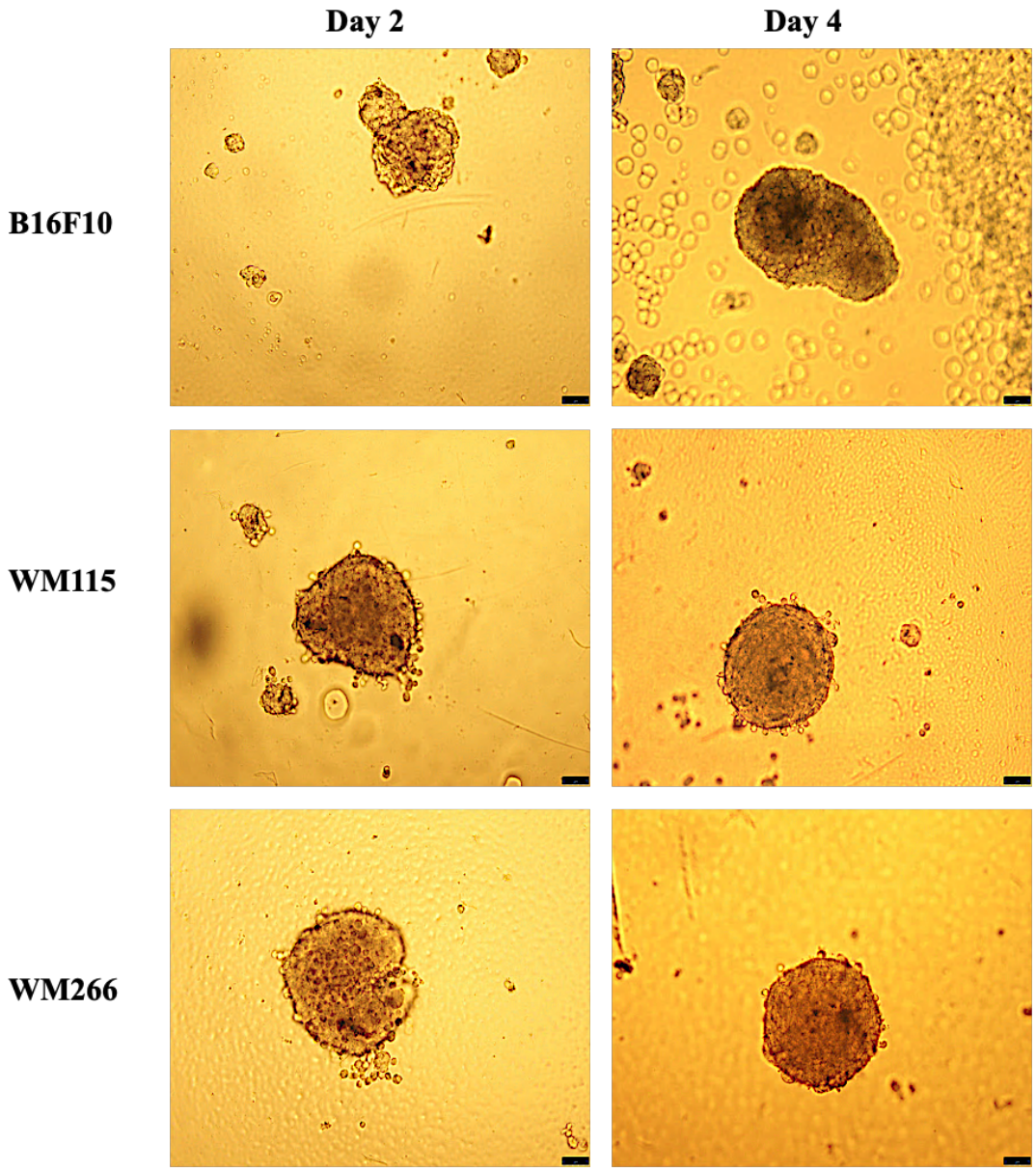

Figure 2.4. Bright field microscopic images of spheroids of melanoma cell lines- B16F10, WM115 and WM266 taken at day 2 and day 4 (n=1). Scale bar, 75 µm.

2.5.2. RAGE is distributed intracellularly in 2D monolayer cell culture

We performed the immunofluorescence imaging of the melanoma cell lines - B16F10, WM115, and WM266 cultured in 2D monolayer and observed that RAGE is mainly distributed intracellularly in all cell lines. RAGE also seemed to be polarized at the edges of some cells. We also evaluated RAGE expression in controlled cell lines- RAGE transfected human kidney cells -

HEK RAGE that contain 200 folds higher RAGE transcript levels than wild type human kidney cells - HEK 293 (data not shown). We observed a higher RAGE fluorescence in HEK RAGE cells and a lack of RAGE expression in HEK 293 cells (figure 2.5). Next, we investigate the distribution of RAGE in 3D tumor spheroids.

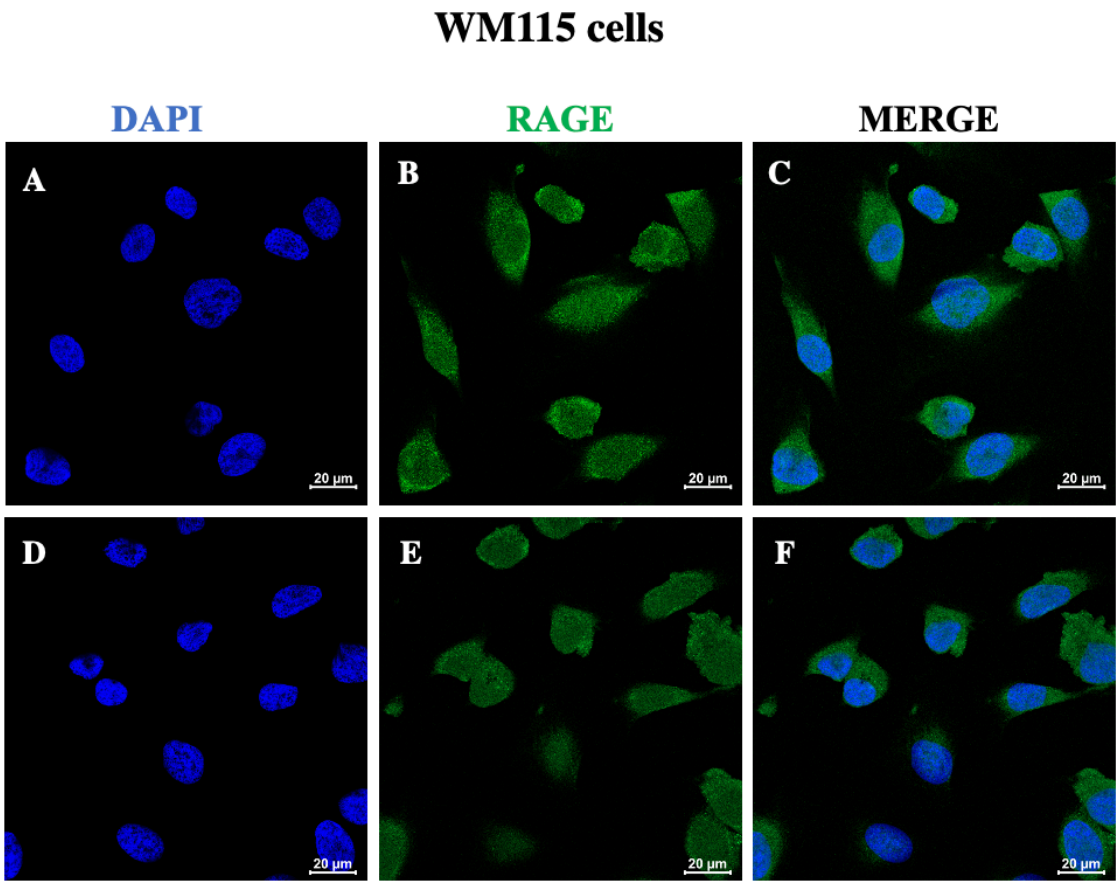

Figure 2.5. Localization of RAGE in 2D monoculture of B16F10 (n=3), WM115 (n=2), WM266 (n=3) cell lines – The green fluorescence of RAGE protein indicating that RAGE is localized intracellularly in B16F10, WM115, and WM266 cells. HEK RAGE cells (positive control) also showed green fluorescence of RAGE while HEK 293 (negative control) did not show any green fluorescence confirming specificity of the RAGE antibody used in the study. Green staining represents RAGE and blue staining represents cell nucleus.

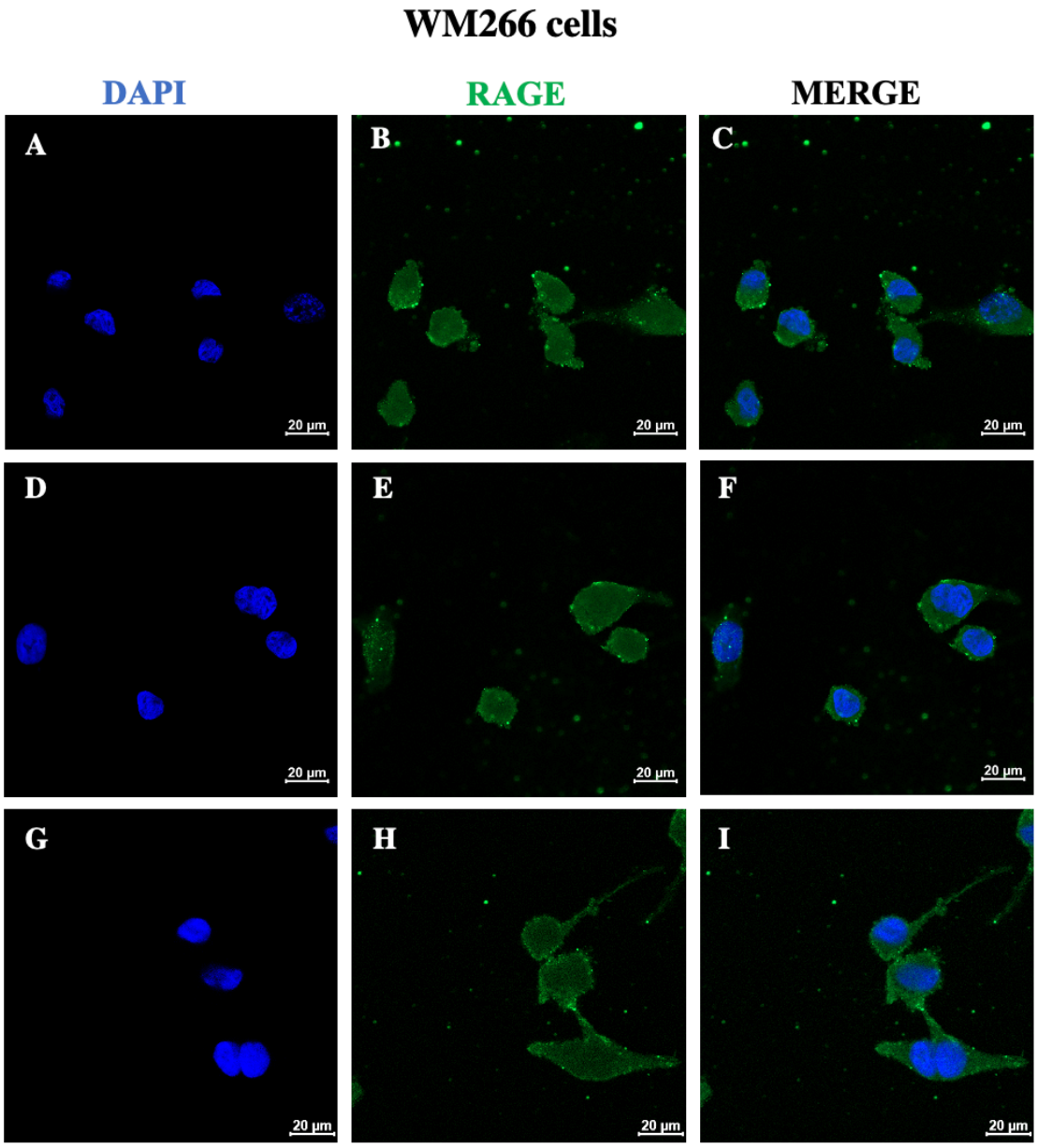

Figure 2.5. Localization of RAGE in 2D monoculture of B16F10 (n=3), WM115 (n=2), WM266 (n=3) cell lines – The green fluorescence of RAGE protein indicating that RAGE is localized intracellularly in B16F10, WM115, and WM266 cells. HEK RAGE cells (positive control) also showed green fluorescence of RAGE while HEK 293 (negative control) did not show any green fluorescence confirming specificity of the RAGE antibody used in the study. Green staining represents RAGE and blue staining represents cell nucleus (continued).

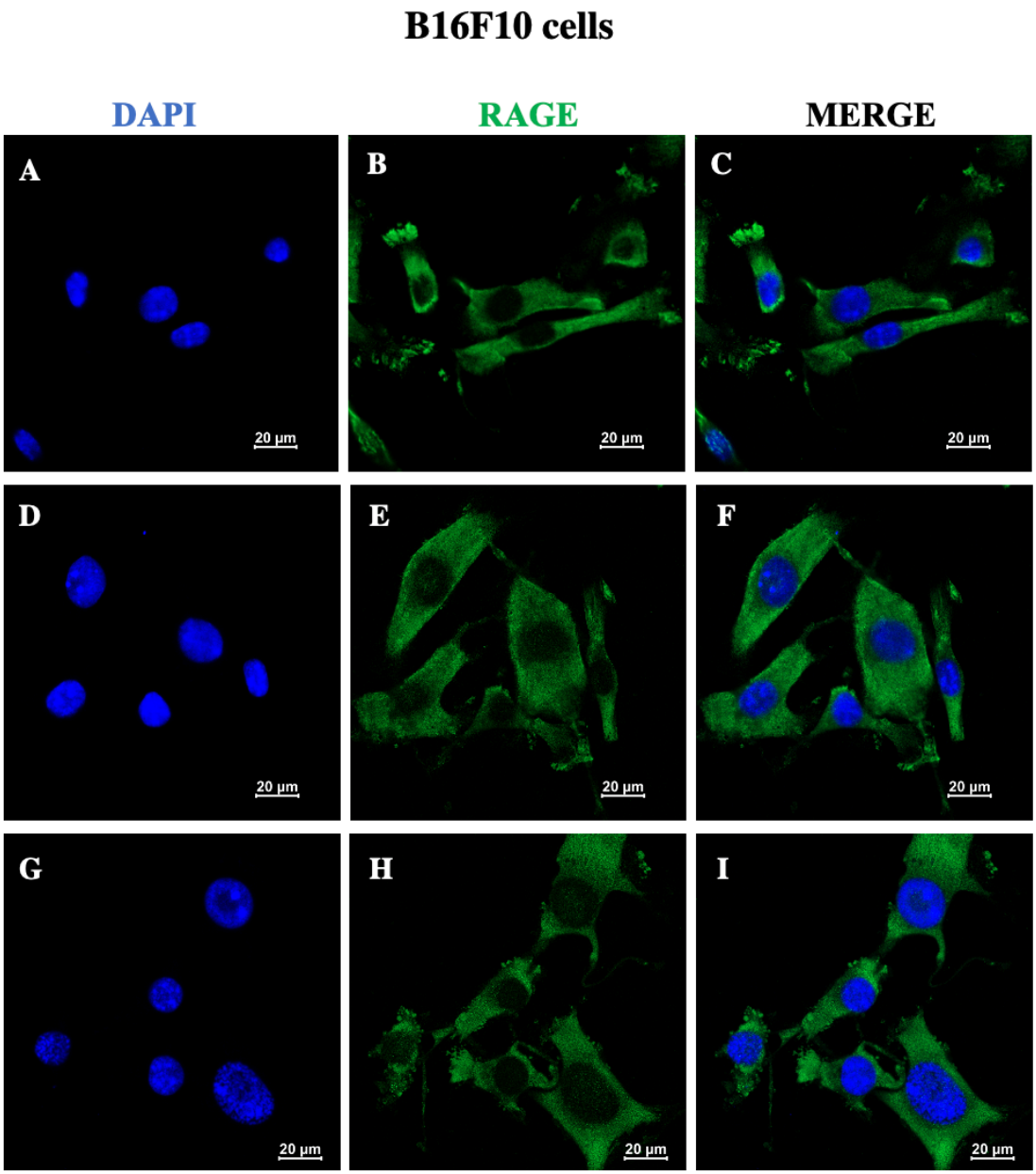

Figure 2.5. Localization of RAGE in 2D monoculture of B16F10 (n=3), WM115 (n=2), WM266 (n=3) cell lines – The green fluorescence of RAGE protein indicating that RAGE is localized intracellularly in B16F10, WM115, and WM266 cells. HEK RAGE cells (positive control) also showed green fluorescence of RAGE while HEK 293 (negative control) did not show any green fluorescence confirming specificity of the RAGE antibody used in the study. Green staining represents RAGE and blue staining represents cell nucleus (continued).

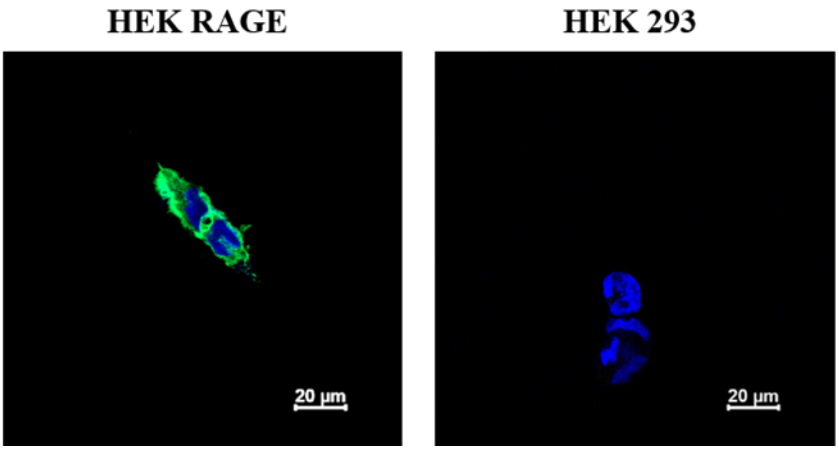

Figure 2.5. Localization of RAGE in 2D monoculture of B16F10 (n=3), WM115 (n=2), WM266 (n=3) cell lines – The green fluorescence of RAGE protein indicating that RAGE is localized intracellularly in B16F10, WM115, and WM266 cells. HEK RAGE cells (positive control) also showed green fluorescence of RAGE while HEK 293 (negative control) did not show any green fluorescence confirming specificity of the RAGE antibody used in the study. Green staining represents RAGE and blue staining represents cell nucleus (continued).

2.5.3. RAGE localization varied between spheroids of different melanoma cell lines

In spheroids generated from WM115 cells, we observed that there was a clear demarcation of green fluorescence, on the periphery of the spheroid and high fluorescence intensity on the surface of the cells (shown in figure 2.6. E). This suggests that RAGE is present on cell surface when present in the 3D microenvironment.

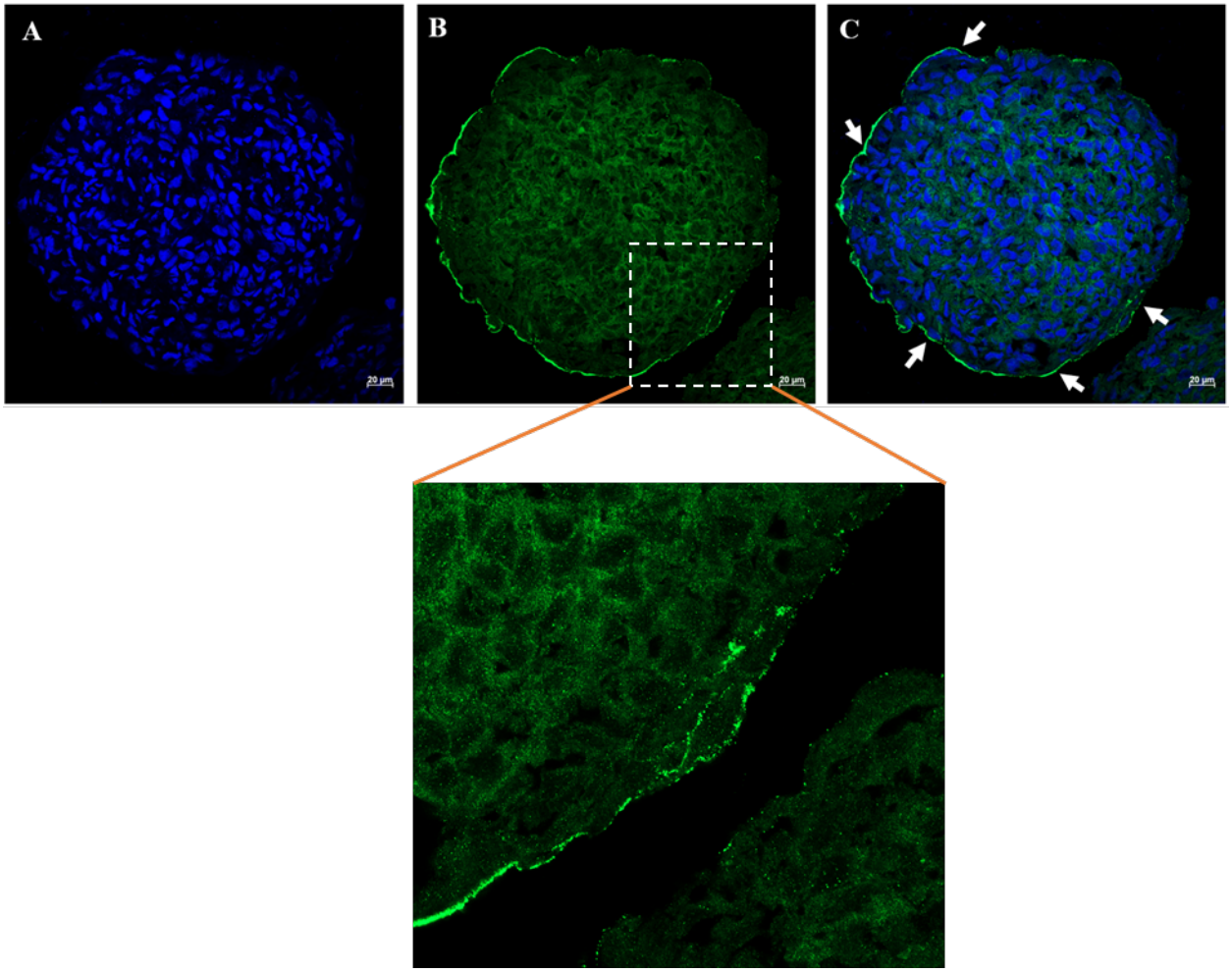

Figure 2.6. RAGE localization at peripheral edges in three batches (n=3) of WM115 spheroids. (A, D, G) represent blue nuclear stain DAPI. (B, E, H) represent green fluorescence RAGE. (C, F, I) represent merged image. (C, F, I – 3D view) represent 3D view of the merged images. Scale bar 20µm, magnification 40X.

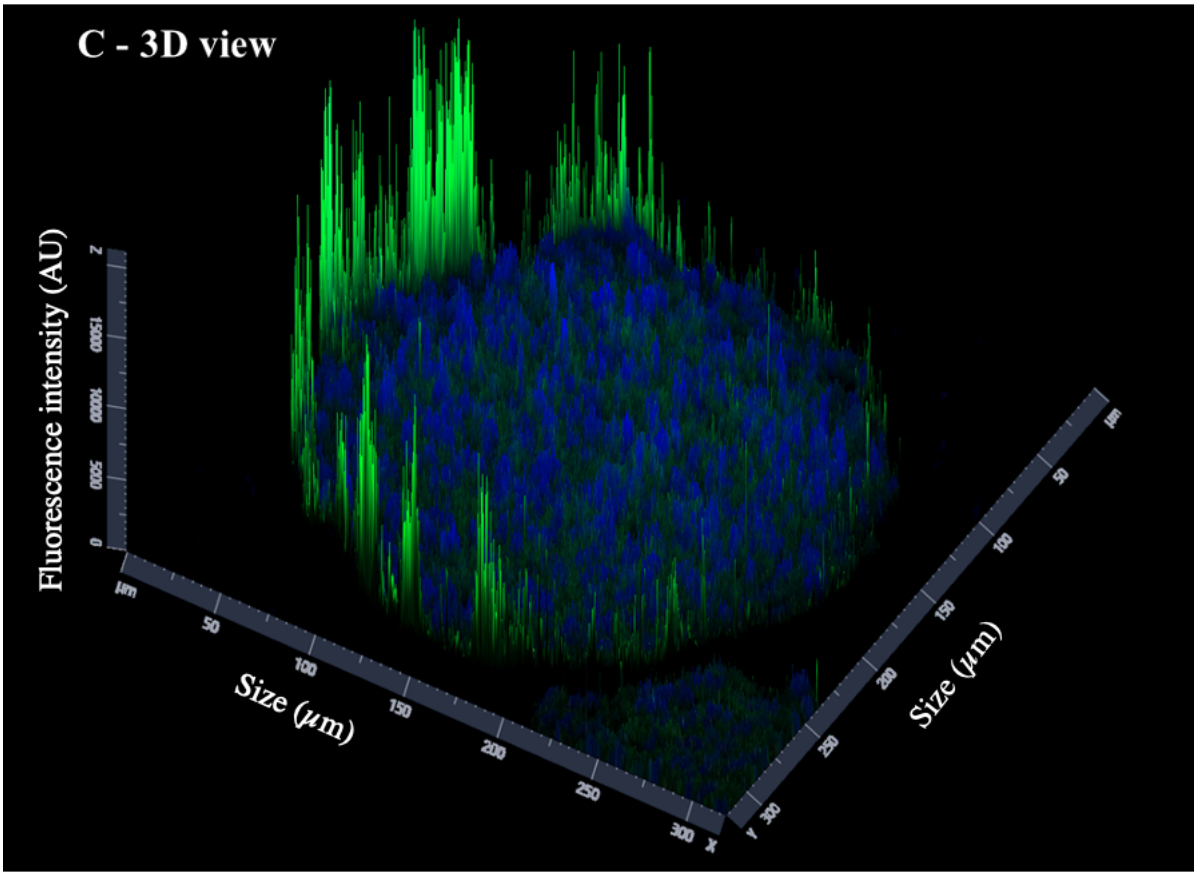

Figure 2.6. RAGE localization at peripheral edges in three batches (n=3) of WM115 spheroids. (A, D, G) represent blue nuclear stain DAPI. (B, E, H) represent green fluorescence RAGE. (C, F, I) represent merged image. (C, F, I – 3D view) represent 3D view of the merged images. Scale bar 20µm, magnification 40X (continued).

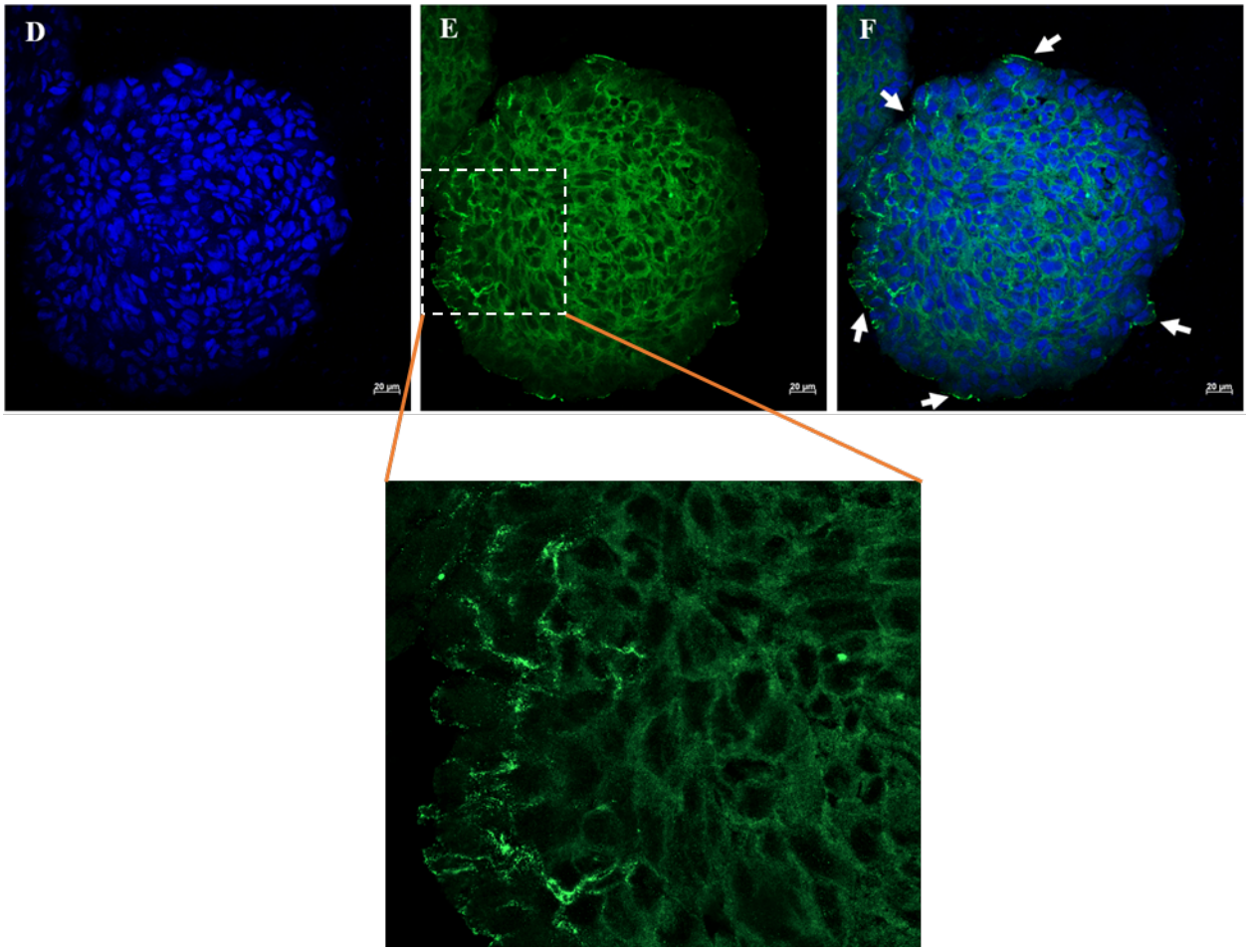

Figure 2.6. RAGE localization at peripheral edges in three batches (n=3) of WM115 spheroids. (A, D, G) represent blue nuclear stain DAPI. (B, E, H) represent green fluorescence RAGE. (C, F, I) represent merged image. (C, F, I – 3D view) represent 3D view of the merged images. Scale bar 20µm, magnification 40X (continued).

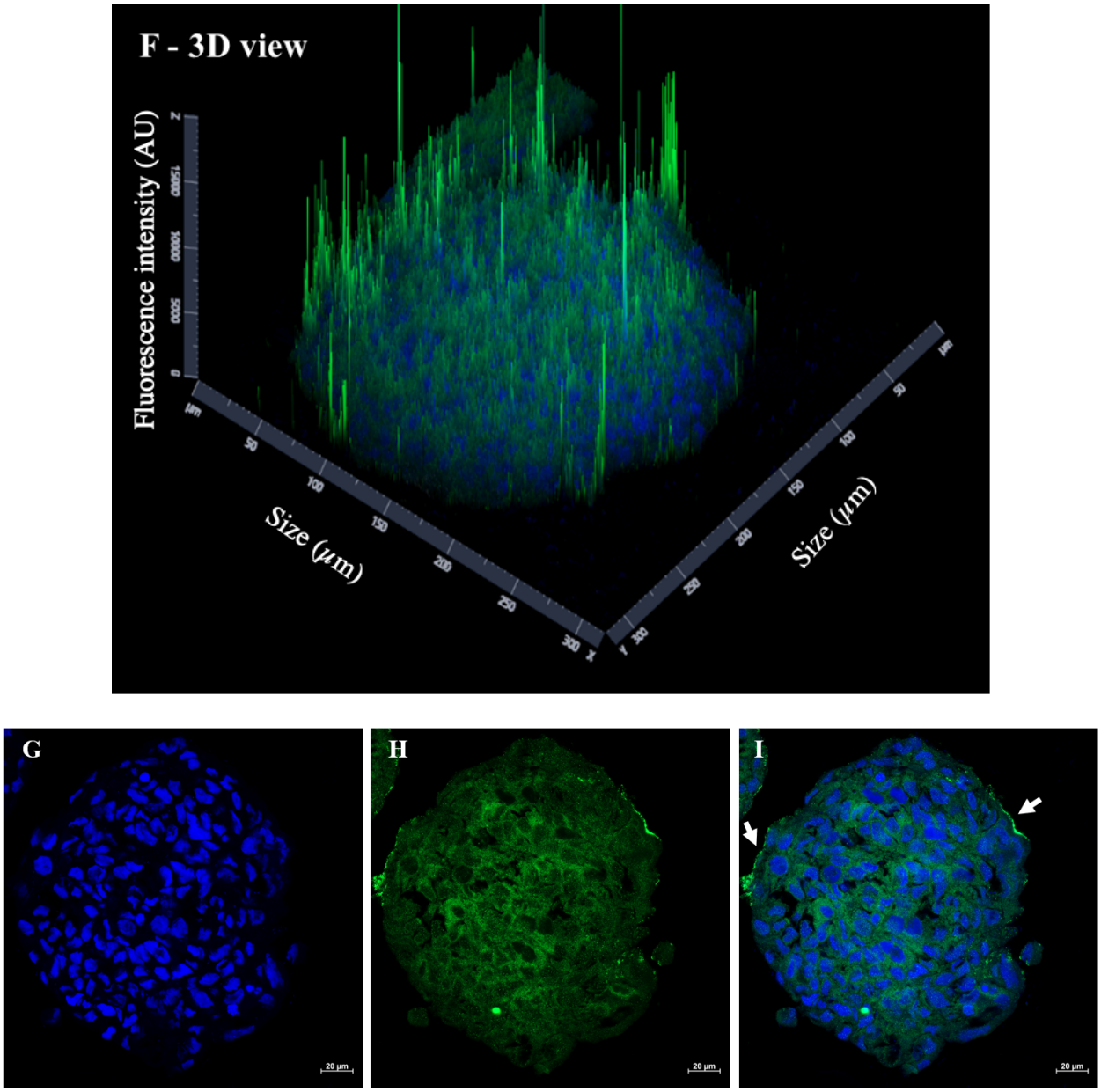

Figure 2.6. RAGE localization at peripheral edges in three batches (n=3) of WM115 spheroids. (A, D, G) represent blue nuclear stain DAPI. (B, E, H) represent green fluorescence RAGE. (C, F, I) represent merged image. (C, F, I – 3D view) represent 3D view of the merged images. Scale bar 20µm, magnification 40X (continued).

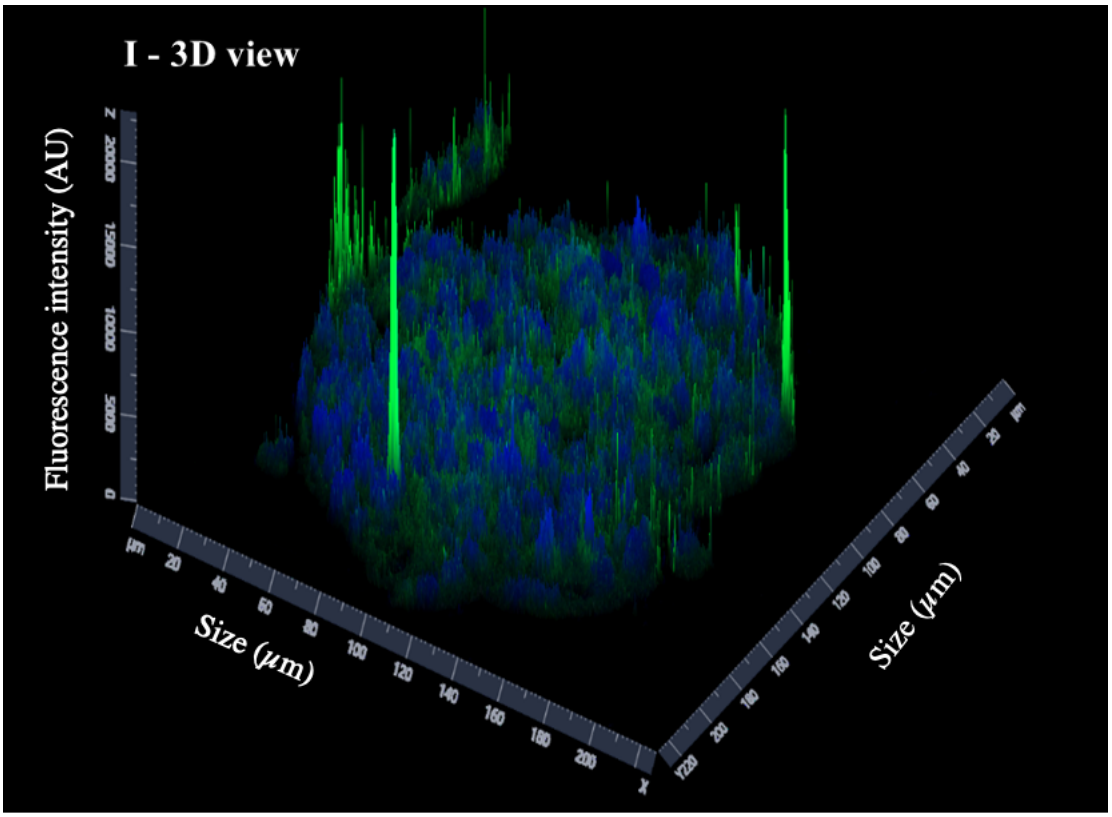

Figure 2.6. RAGE localization at peripheral edges in three batches (n=3) of WM115 spheroids. (A, D, G) represent blue nuclear stain DAPI. (B, E, H) represent green fluorescence RAGE. (C, F, I) represent merged image. (C, F, I – 3D view) represent 3D view of the merged images. Scale bar 20µm, magnification 40X (continued).

Next, we imaged WM266 spheroids to analyze RAGE localization. We observed that in WM266 spheroids, green fluorescence indicating RAGE was present intracellularly (major) and at the periphery of spheroids (at few sites) (shown with arrows in figure 2.7)

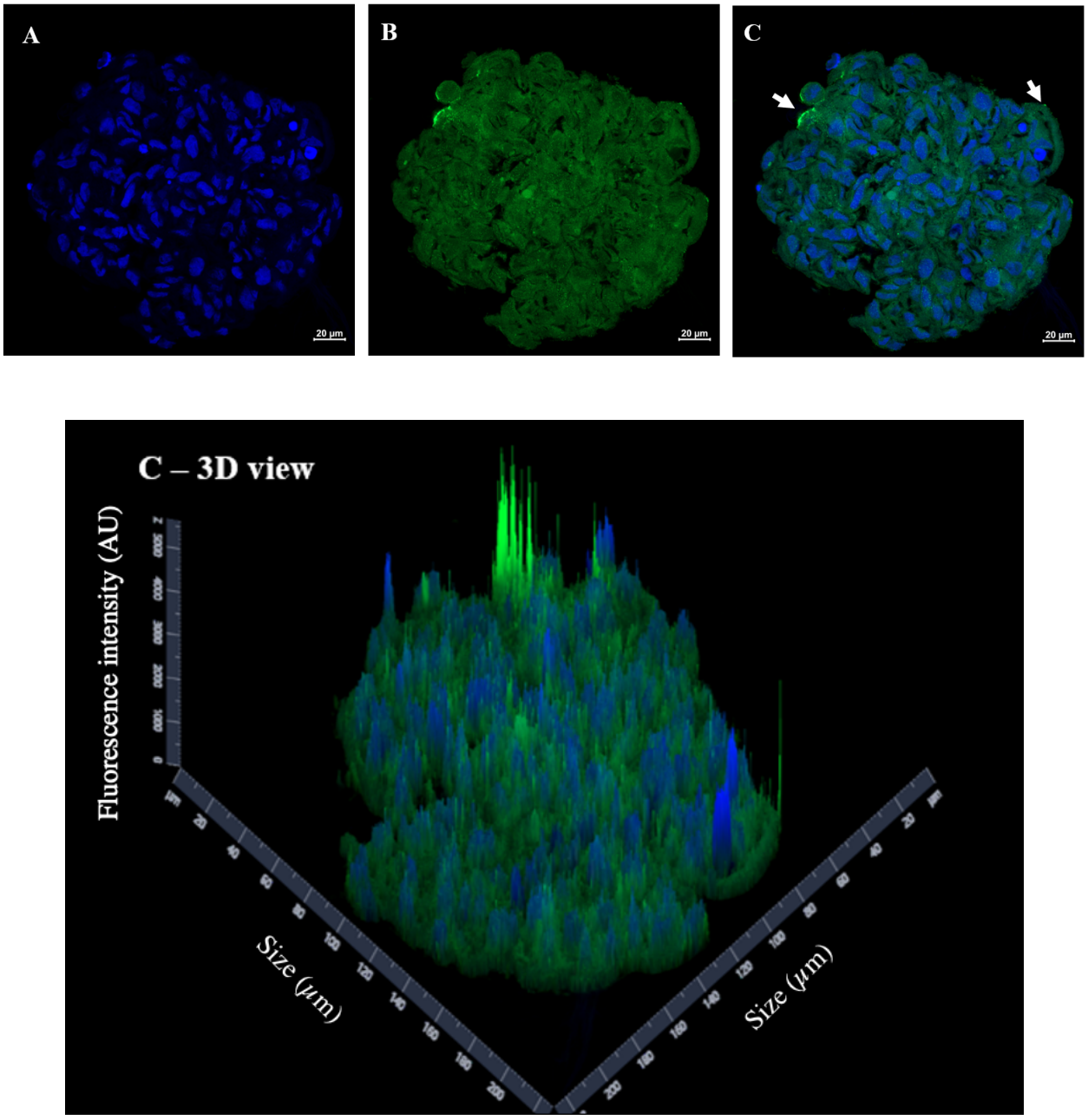

Figure 2.7. Localization of RAGE in the spheroid section of WM266 (n=2) is intracellular as well as peripheral at few sites (shown with arrows). (A and D) represent blue nuclear stain DAPI. (B and E) represent green fluorescence RAGE. (C and F) represent merged image. (C and F – 3D view) represent 3D view of the merged images. Scale bar is 20µm in A, B and C. Scale bar 10µm in D, E and F, magnification 40X.

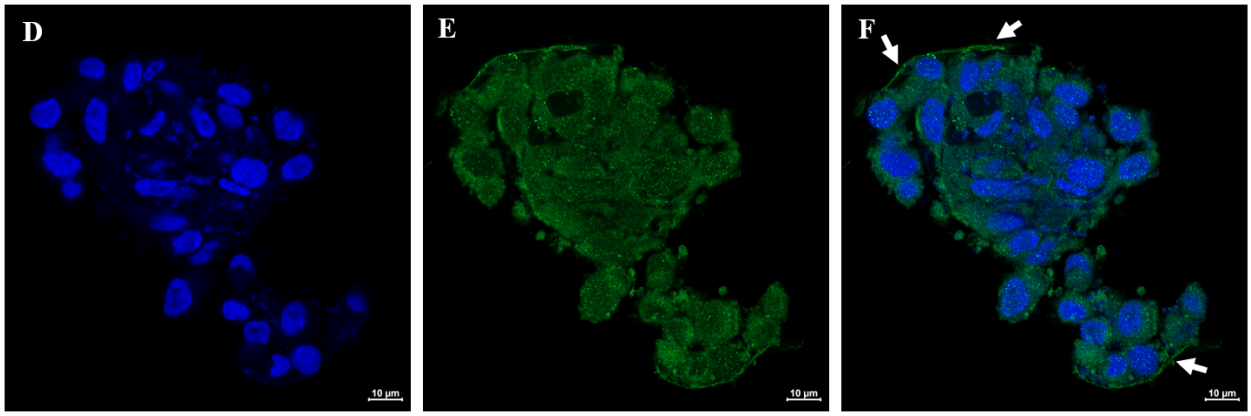

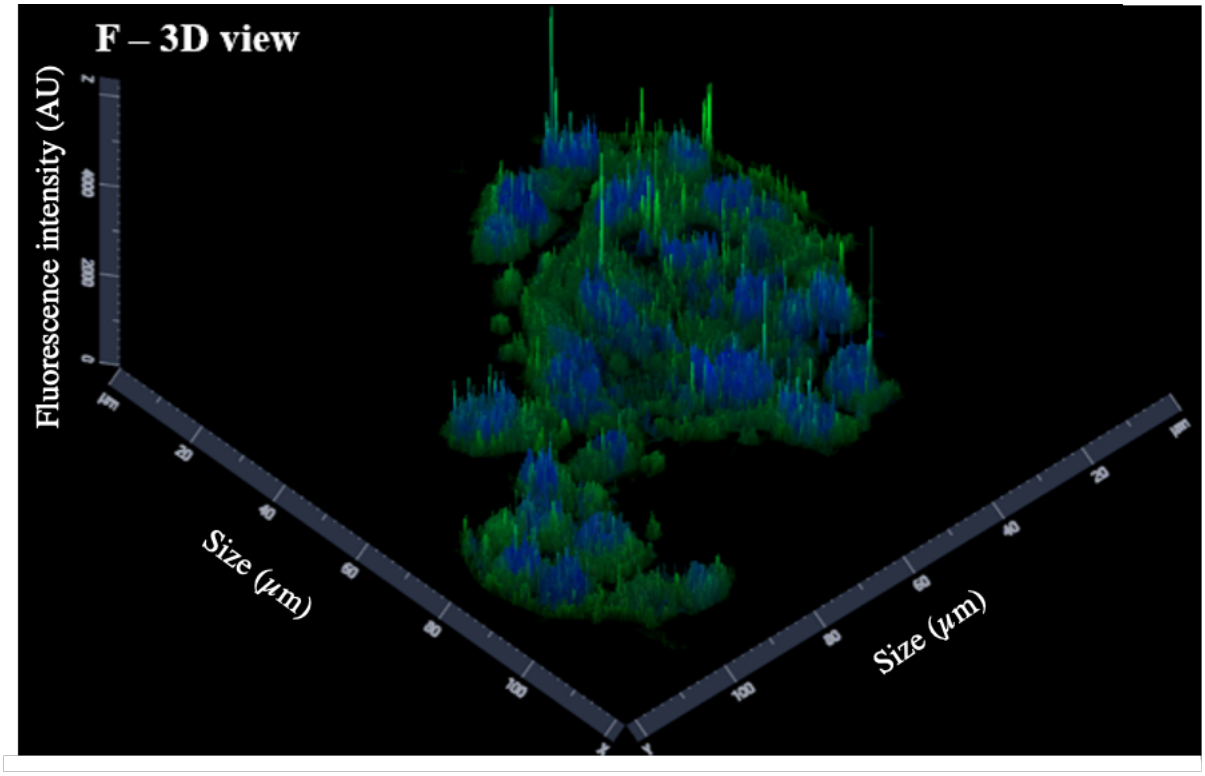

Figure 2.7. Localization of RAGE in the spheroid section of WM266 (n=2) is intracellular as well as peripheral at few sites (shown with arrows). (A and D) represent blue nuclear stain DAPI. (B and E) represent green fluorescence RAGE. (C and F) represent merged image. (C and F – 3D view) represent 3D view of the merged images. Scale bar is 20µm in A, B and C. Scale bar 10µm in D, E and F, magnification 40X (continued).

In B16F10 spheroids, we observed that green fluorescence was intensely present on cell surface. Interestingly, we also observed bright spots of green florescence inside the nucleus of B16F10 cells indicating the presence of RAGE inside the nucleus (figure 2.8).

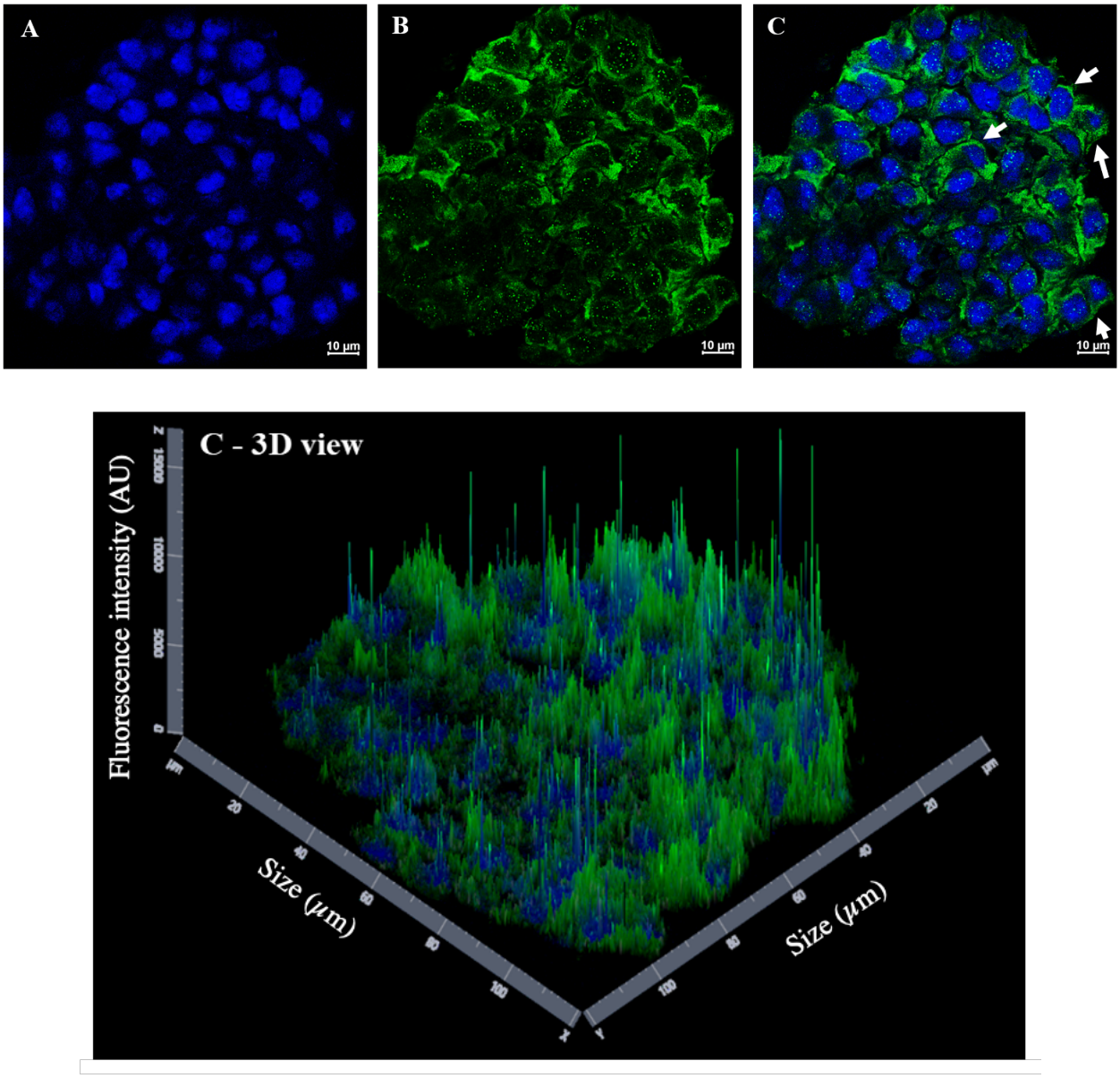

Figure 2.8. RAGE was observed to be present on cell surface (shown with arrows) and intracellularly in the spheroid section of B16F10 (n=3). (A, D, G) represent blue nuclear stain DAPI. (B, E, H) represent green fluorescence RAGE. (C, F, I) represent merged image. (C, F, I – 3D view) represent 3D view of the merged images. Scale bar 20µm, magnification 40X.

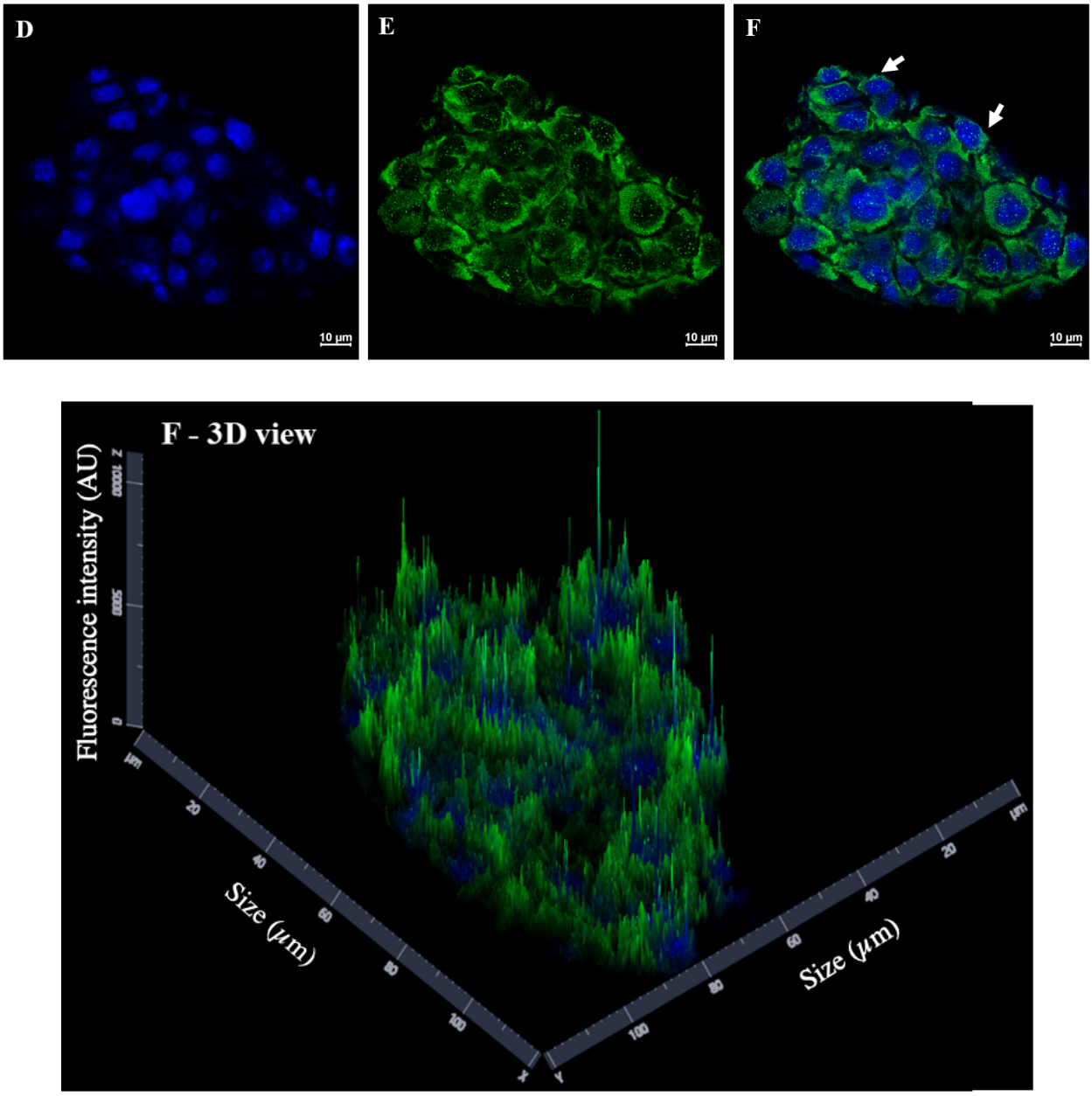

Figure 2.8. RAGE was observed to be present on cell surface (shown with arrows) and intracellularly in the spheroid section of B16F10 (n=3). (A, D, G) represent blue nuclear stain DAPI. (B, E, H) represent green fluorescence RAGE. (C, F, I) represent merged image. (C, F, I – 3D view) represent 3D view of the merged images. Scale bar 20µm, magnification 40X (continued).

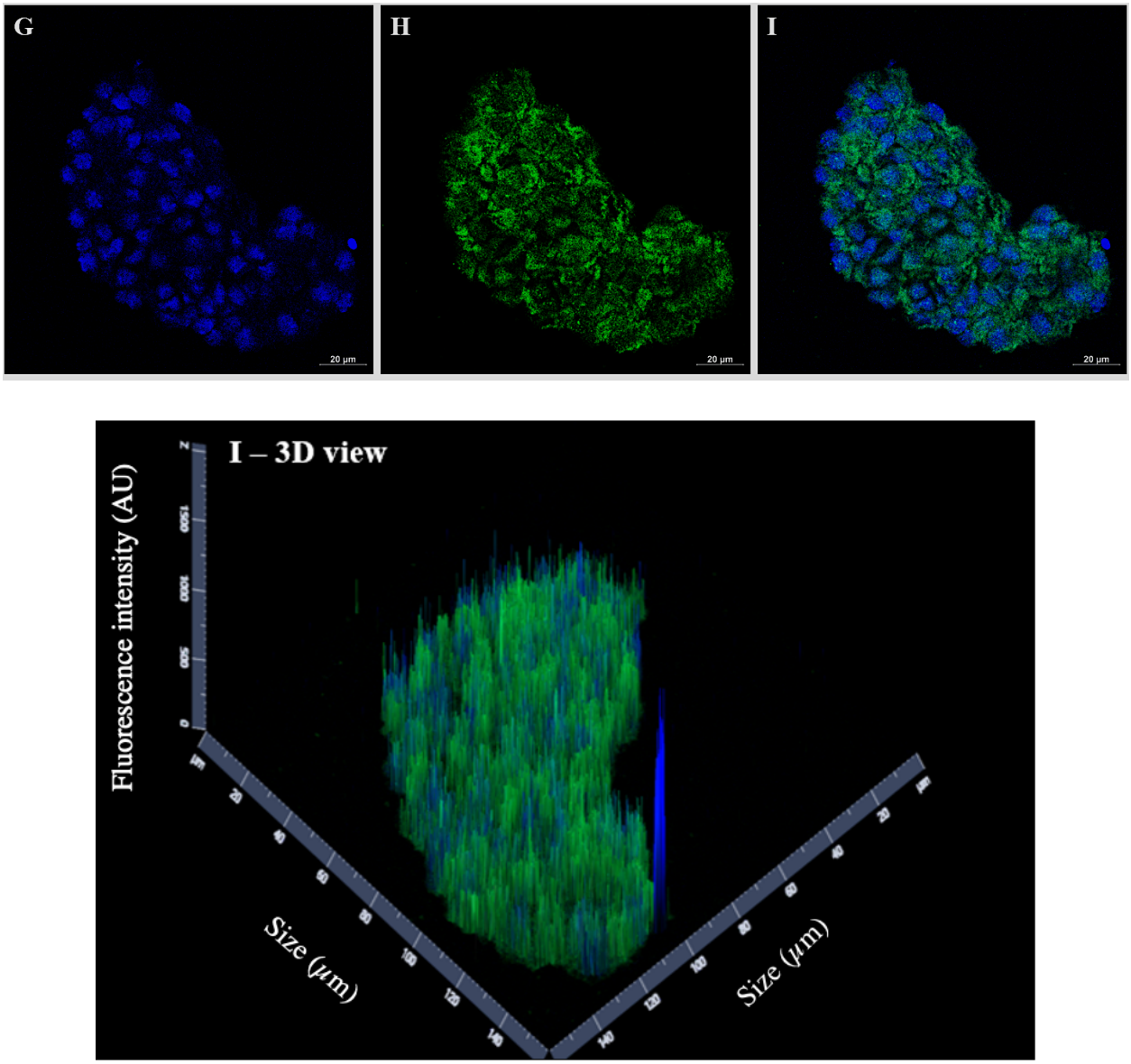

Figure 2.8. RAGE was observed to be present on cell surface (shown with arrows) and intracellularly in the spheroid section of B16F10 (n=3). (A, D, G) represent blue nuclear stain DAPI. (B, E, H) represent green fluorescence RAGE. (C, F, I) represent merged image. (C, F, I – 3D view) represent 3D view of the merged images. Scale bar 20µm, magnification 40X (continued).

2.5.4. Melanoma tumor nodules formation in lung colonization mice model

After injecting B16F10 melanoma cells via the tail vein in mice, tumor cells colonized to the lungs. After 21 days, we sacrificed the mice and harvested their lungs. Next, we examined the lung sections of tumor colonized mice and healthy mice using H&E staining (figure 2.9). We

observed brownish black pigment in the tumor nodules shown in H&E stained sections (figure 2.9), indicating the presence of melanin in the lung sections of the mice, confirming the colonization of melanoma cells in the lungs. It is reported that normal melanocytes are typically 7 µm in diameter [263]. However, we found that the average diameter of the invaded B16F10 tumor cells to be 20 µm (measured using image J software). This is inline with a published report where the average size of B16F10 melanoma cells was reported to be 15.4 ± 1.6 µm [264]. It also suggests that melanoma cells are larger in size than normal melonocytes.

Chakraborty et al. also showed that melanoma cells metastasized to lung contained large and atypical nucleus [266]. The average size of the nuclei of cancer cells in tumor nodules was found to be 10 µm. In comparison, the literature reports that the nuclei size of normal melanocytes measured around 5µm in diameter [265].

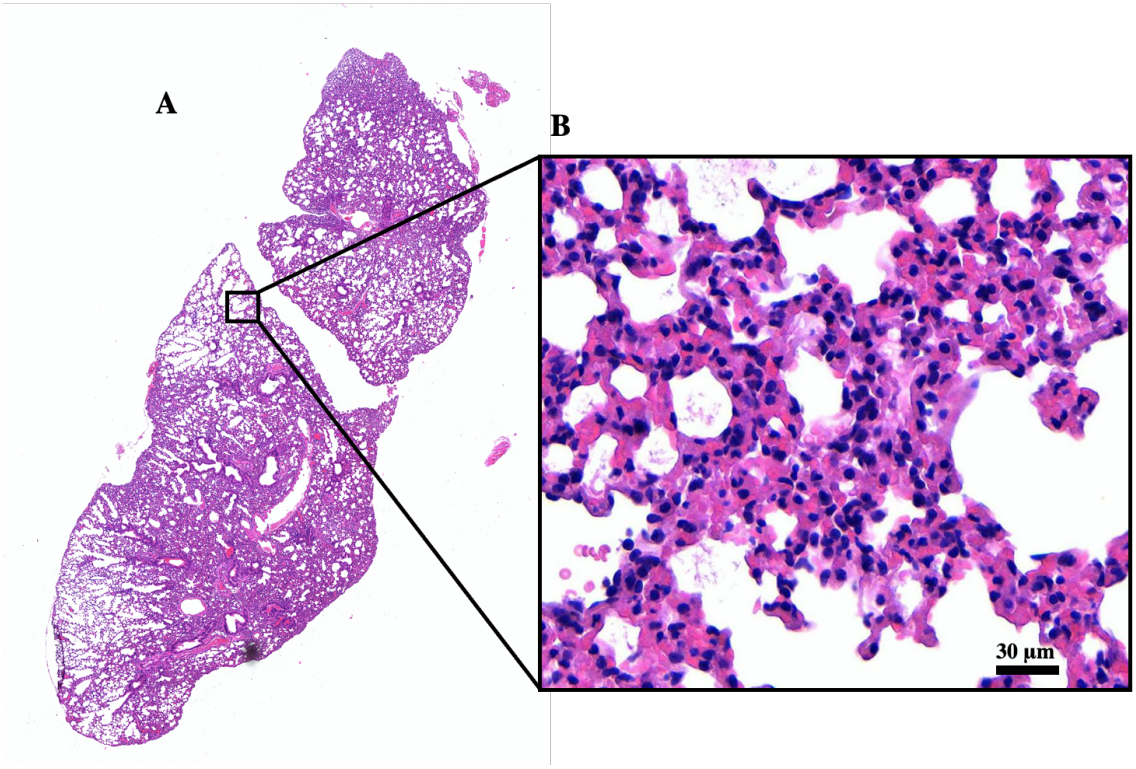

Figure 2.9. The representative images of H&E stain of full lung (A) and its corresponding magnified section (B) of healthy mice, full lung sections (C, E, and G) and its corresponding magnified section (D, E, and H) of tumor colonized lungs.

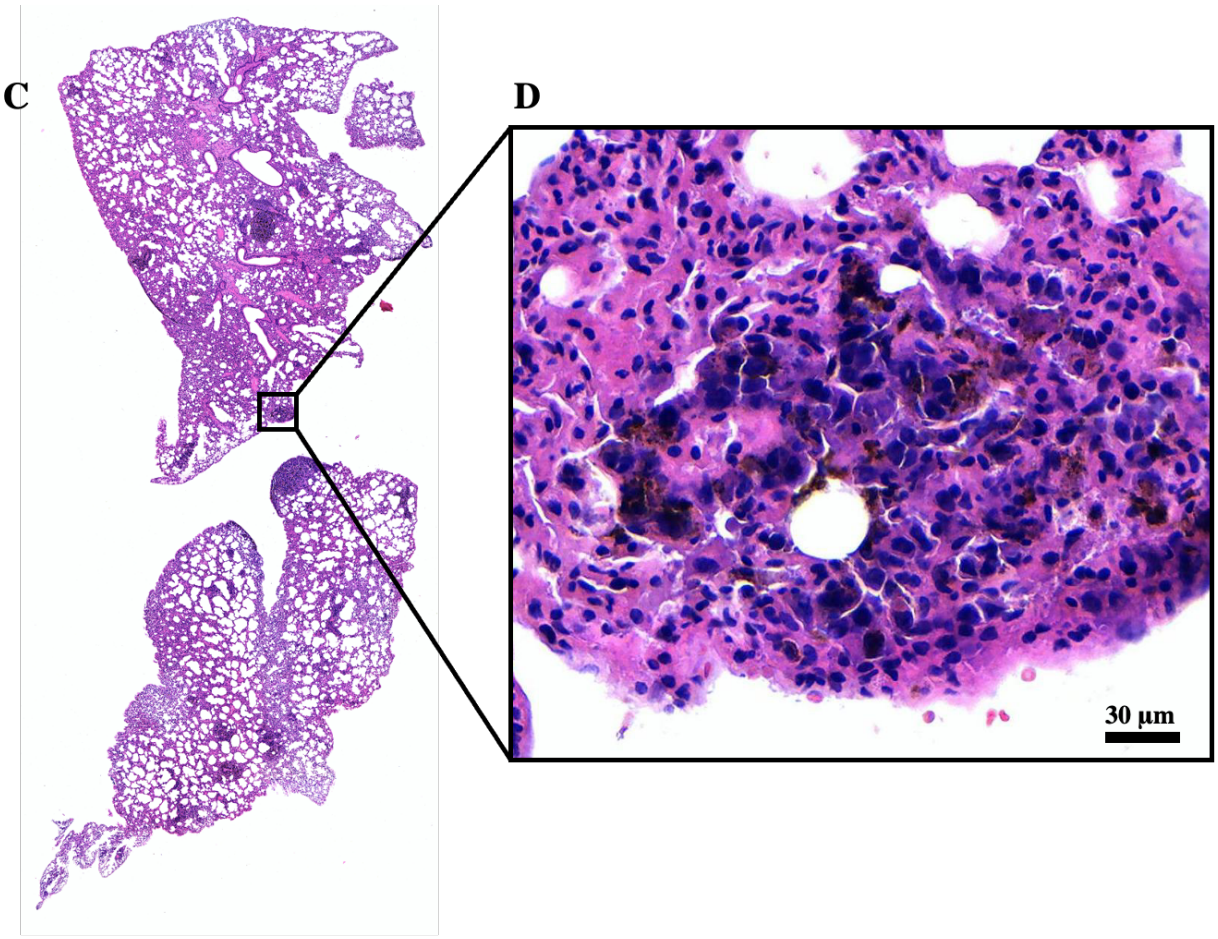

Figure 2.9. The representative images of H&E stain of full lung (A) and its corresponding magnified section (B) of healthy mice, full lung sections (C, E, and G) and its corresponding magnified section (D, E, and H) of tumor colonized lungs (continued).

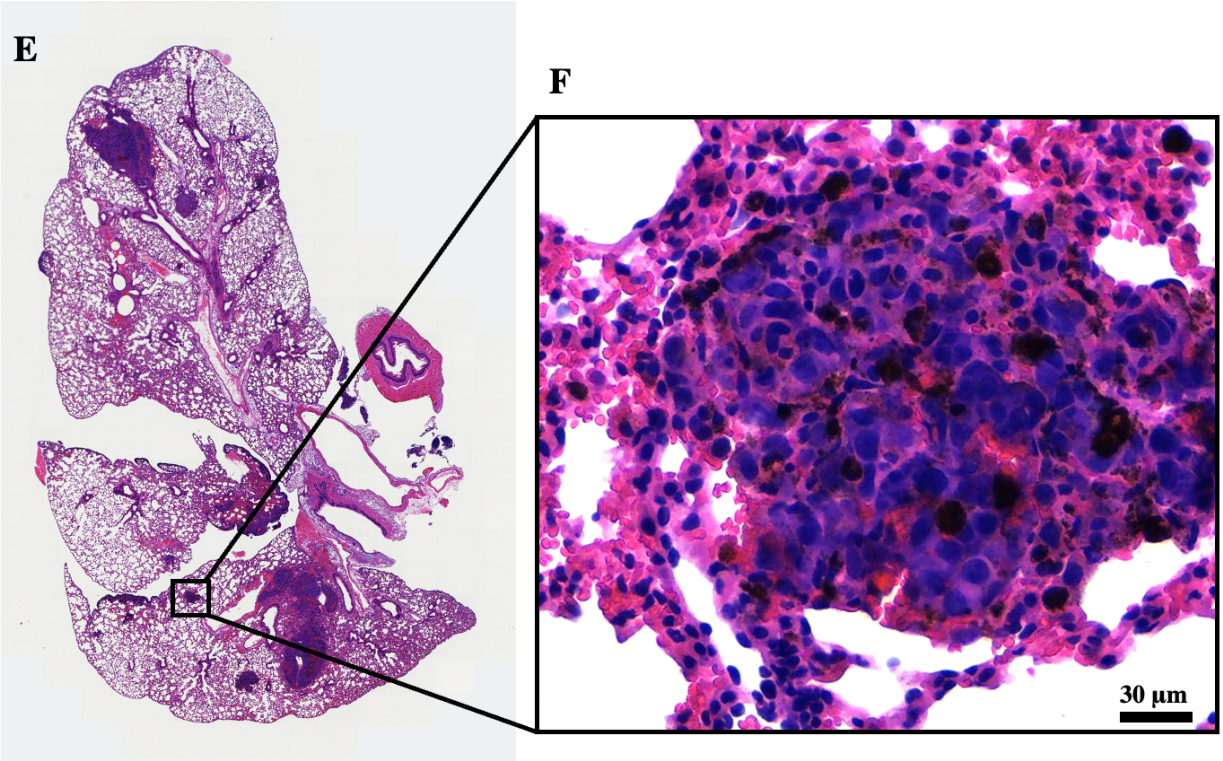

Figure 2.9. The representative images of H&E stain of full lung (A) and its corresponding magnified section (B) of healthy mice, full lung sections (C, E, and G) and its corresponding magnified section (D, E, and H) of tumor colonized lungs (continued).

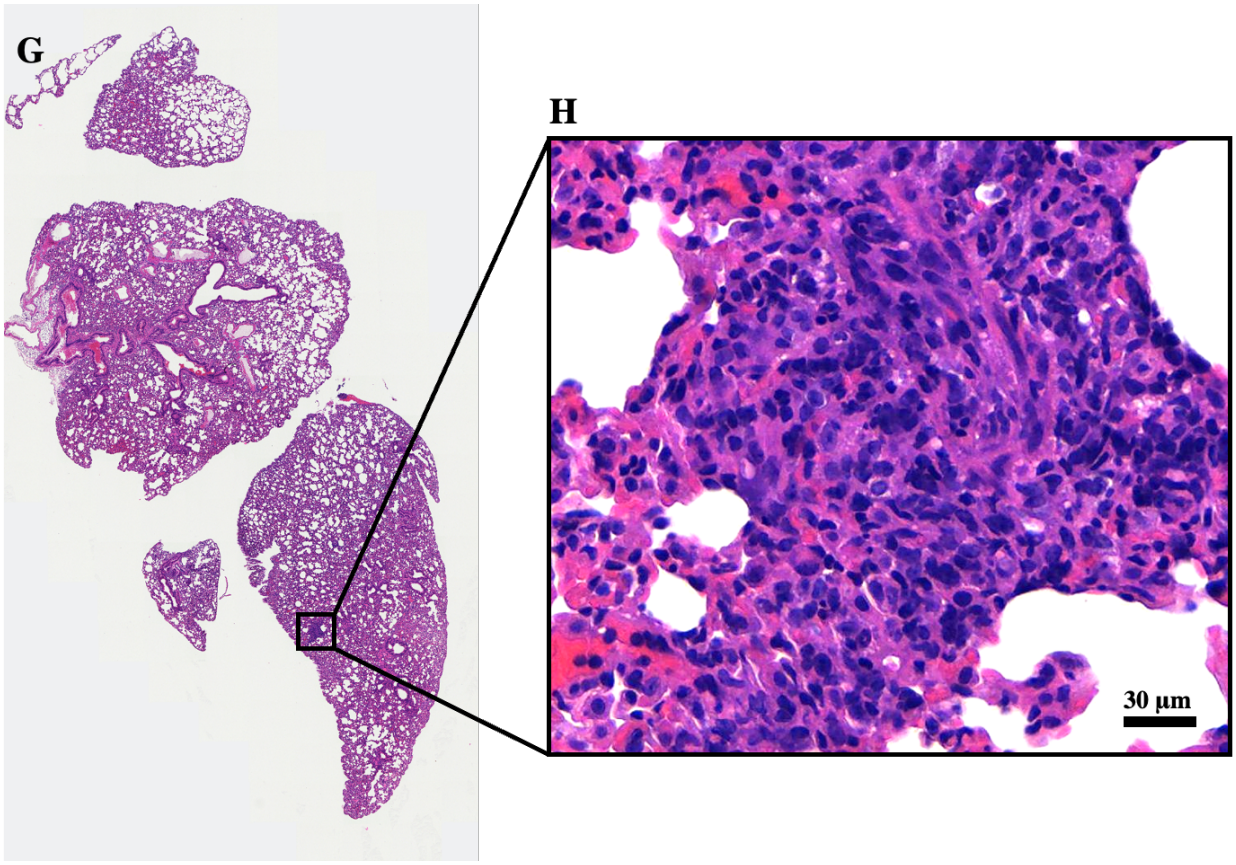

Figure 2.9. The representative images of H&E stain of full lung (A) and its corresponding magnified section (B) of healthy mice, full lung sections (C, E, and G) and its corresponding magnified section (D, E, and H) of tumor colonized lungs (continued).

2.5.5. Localization of RAGE in mice lungs

To investigate whether RAGE protein is expressed on the cell surface or intracellularly in the mice lung melanoma tumors, we examined RAGE expressions using immunohistochemistry (figure 2.10 – A and B). As we observed that tumor nodule is clearly demarcated from other tissue in the lung section, we indicated that with white dotted line (figure 2.10 – C and D). The immunofluorescent image of lung section showing green fluorescence in the area enclosed within white dotted line indicates high RAGE expression in the melanoma cells present in tumor nodule while blue staining indicates the cell nucleus. We observed that there was an intense staining of green fluorescence on cell surface than intracellularly indicating RAGE is highly expressed on cell

surface than inside the cell (figure 2.10 D). Moreover, we found that higher fluorescence intensity in tumor cells than healthy part of the lung section which indicates tumor cells express more RAGE than healthy cells.

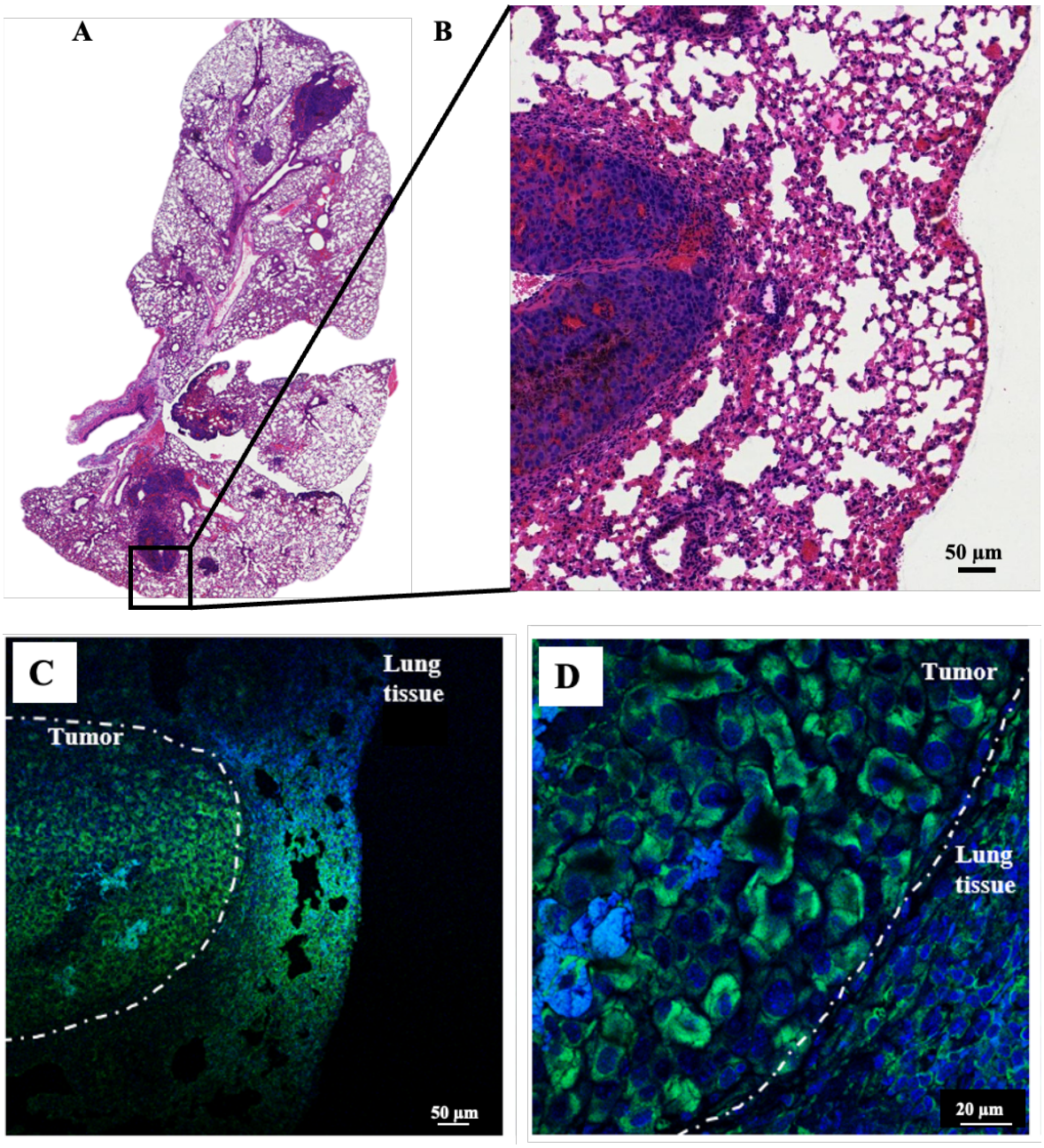

Figure 2.10. Lung section of the B16F10 tumor colonized lung. (A) represents H&E staining of the entire lung section while (B) is the magnified region of H&E-stained tumor nodule. Image (C) represents the immunofluorescence staining of lung section at 10X magnification, with tumor nodule enclosed inside the white dotted area while images (D) show the part of tumor section at 40X magnification. The green stain shows RAGE and blue stain shows the nucleus.

2.6. Discussion

In the present study, we investigated the localization of RAGE in the 3D architecture of melanoma cells compared to RAGE distribution in 2D monolayer. Previously, our group observed that in 2D monolayer RAGE was located intracellularly in melanoma cells (WM115). Moreover, Abe et al., have shown the presence of RAGE in the cytoplasm as well as on the membrane of melanoma cells (G361 and A375) in 2D cell culture [58]. Our group showed significant reduction in tumor growth of RAGE overexpressed melanoma cells (WM115-RAGE) implanted subcutaneously in mice compared to control WM115-MOCK melanoma cells upon targeting V-domain of RAGE with IgG 2A11 anti-RAGE antibody, indicating the presence of RAGE protein on cell surface [112]. Based on these reports, we hypothesized that RAGE is expressed on cell surface in 3D conditions and intracellularly in 2D monolayer cultures. To test our hypothesis, we generated 3D *in vitro* spheroids using three melanoma cell lines - B16F10, WM115 and WM266. We investigated the localization of RAGE in all three melanoma spheroids and compared our results with 2D monolayer culture. We observed a difference in RAGE localization among 3D spheroids of B16F10, WM266 and WM115. The immunofluorescence staining of WM115 spheroids showed high RAGE intensity over the periphery of spheroids compared to WM266 and B16F10. We also observed that RAGE is expressed more frequently on the cell surface in WM115 and B16F10 spheroid cells, whereas RAGE is mostly distributed intracellularly in WM266 spheroid. The difference in RAGE localization between WM266 and WM115 spheroids may be attributed to their phenotypic differences. As previously described, WM266 cells have mesenchymal-like morphology and are metastatic in origin while WM115 and B16F10 cells have epithelial-like morphology and were derived from a primary tumor and lung colonized tumor nodules respectively. Popa et al. has previously reported that the RAGE localization may vary

among different stages of melanoma progression. They observed that RAGE is clustered at the membrane ruffles and leading edges of primary melanoma cells (MelJuSo) while an intracellular localization was found in metastatic cells (SK-Mel28) [267]. However, these studies were carried out in 2D conditions, thus it is difficult to corelate the data from these studies with our results. So, future studies may be required to uncover the reason for the difference in RAGE localization in melanoma cells from different metastatic abilities.

Next, our immunofluorescence results of 2D monolayer cell culture showed that RAGE is mainly localized intracellularly in all three cell lines with some cells that have RAGE polarized at the edges. Our results are in-line with the past results of RAGE expression in WM115 and WM266 from our group. Moreover, a study showed the presence of RAGE in both cytoplasm and on the cell membrane of melanoma cells (G361 and A375) in 2D conditions [58]

To gain better understanding of RAGE localization in melanoma tumors in 3D microenvironment we further performed *in vivo* studies using B16F10 cells in a lung colonization mice model. We are also investigating RAGE localization in tumors generated with WM266 and WM115 cells, but this study is on-going. We chose the B16F10 cell line for the lung colonization model because B16F10 melanoma cells are of murine origin, are highly metastatic and colonize the lungs upon injection through the mice tail vein [262]. A study showed that overexpressed S100A8/A9 proteins in the lungs of mice served as a chemoattractant for RAGE that guides B16F10 melanoma cells to migrate and colonize in the lungs of mice [268]. Another study reported that S100A8/A9 interacts with RAGE on the surface of breast cancer cells [97]. Based on these two different studies it can be suggested that possibly B16F10 melanoma cells express RAGE on cell surface due to which they migrated to the lungs and interacted with S100A8/A9 ligands. However, a study by Abe et. al., indicated that RAGE is localized in the cytoplasm of G361

melanoma xenografts *in vivo* [58]. In the present study, we observed high intensity of green fluorescence on the cell surface of B16F10 melanoma cells present in tumor nodules of B16F10 tumor colonized lungs, indicating surface localization of RAGE in B16F10 cells within tumor.

2.7. Conclusion

In the present study, we investigated and compared RAGE localization in melanoma cells in their 3D architecture vs 2D conditions. WM115 and B16F10 spheroids showed intense green fluorescence of RAGE on cell surface indicating RAGE localization on cell surface while WM266 spheroids showed high green fluorescence intracellularly with few cell surface expressions. However, similar cells when cultured in 2D conditions showed intracellular expression of RAGE. Future studies are required to understand the difference in RAGE localization in WM266 cell spheroids. In our on-going studies we are generating tumors of WM155 and WM266 cells in a subcutaneous mice model to better understand the localization of RAGE in tumors. After analyzing lung tissue section of B16F10 tumors colonized lung we observed that RAGE is expressed intensely on cell surface of melanoma cells. Overall, we conclude that RAGE is expressed on the cell surface intensely in 3D microenvironment. Previously, Popa et al. studied RAGE localization in two genetically different cell lines (MelJuSo and SK-Mel28), by immunofluorescence, using cells grown in 2D conditions. They have demonstrated that RAGE clustered at membrane ruffles and leading edges, and at sites of cell-to-cell contact in primary melanoma cells (MelJuSo), in contrast to a more dispersed localization of RAGE in metastatic cells (SK-Mel28) [267].

However, in our study we used a different and novel approach by comparing the localization of RAGE in the same cell-lines, (we used three cell lines WM115, WM266, and B16F10) grown in different conditions: 2D cells, 3D spheroids and within tumors. Using B16F10 murine melanoma cells, we found that RAGE was more localized at the surface of cells within 3D

spheroids and tumors than within cells grown in 2D conditions. In-addition, we have also compared the localization of RAGE in two cell-lines that are genetically very similar (WM115 and WM266) under 2D and 3D conditions. We observed that WM115, which was established from a primary tumor, shows RAGE localization at the cell surface in 3D spheroids whereas RAGE was mostly found intracellularly in cells grown in 2D conditions. By comparison, WM266, which was established from a metastatic tumor from the same patient WM115 was established from, showed more intracellular expression both in 3D spheroids and 2D conditions. Overall, we concluded that RAGE localization differs based on the metastatic properties of the cells and the growth conditions.

The knowledge of RAGE localization would help future researchers to formulate and test RAGE specific antibodies and inhibitors that would target RAGE more effectively. Given that RAGE is present on the cell surface in primary tumors, antibody-like inhibitors that target the extracellular part of RAGE would provide an effective treatment. However, to target intracellular RAGE in metastatic tumors, small molecules RAGE inhibitors that can penetrate inside the cells would be more effective.

3. ROLE OF RAGE IN PANCREATIC CANCER UNDER HYPOXIA

3.1. Hypothesis

Our group has previously demonstrated that under normoxic conditions, RAGE promotes pancreatic tumor cell survival by enhancing autophagy following administration of gemcitabine, a chemotherapeutic agent [269]. Other studies also showed the crucial role of RAGE in mediating autophagy of pancreatic cancer cells under normoxic conditions, thus facilitating cancer cell survival [18, 19].

Under hypoxic conditions, it is reported that RAGE upregulation promotes autophagy in pancreatic cancer cell lines [2]. Moreover, it has been demonstrated that RAGE upregulation under hypoxic conditions enhanced migration and invasion of breast cancer and cervical cancer cells, and that migration and invasion were attenuated after gene silencing of RAGE using a specific siRNA [171]. Aforementioned studies revealed that RAGE has a crucial role in mediating autophagy and migration in different cancers under hypoxia. Thus, we hypothesized that in pancreatic cancer cells, RAGE upregulation under hypoxic conditions contributes to autophagy and migration and that the pharmacological inhibition of RAGE by FPS-ZM1 reduces autophagy and migration.

3.2. Abstract

In the present study we investigated the role of RAGE in autophagy and migration in the pancreatic cancer cell lines-PANC-1, CFPAC and MIA Paca-2 under hypoxia. Our results showed that the hypoxia marker, HIF-1α was stabilized in hypoxic conditions compared to normoxic conditions. Moreover, we observed an increase in RAGE levels in pancreatic cancer cell lines under hypoxic conditions. Next, we observed increased ratio of LC3-II/I in PANC-1 and MIA

Paca-2 in 1% oxygen levels. Furthermore, we observed increased migration of three pancreatic cancer cells under hypoxia.

We next investigated RAGE-dependent effect on autophagy and migration under hypoxia by using a RAGE antagonist, FPS-ZM1. We found that in the presence of FPS-ZM1, the ratio of LC3-II/I is decreased in PANC-1 and MIA PaCa-2, suggesting reduction in autophagy. Furthermore, we assessed migration by Boyden Chamber assay that showed a lower percentage of migration of FPS-ZM1 treated PANC-1, MIA PaCa-2 and CFPAC cells through the membrane of the insert as compared to untreated cells under hypoxia.

3.3. Introduction

Autophagy is a survival mechanism that fulfils the high metabolic and energetic demands of proliferating tumors by recycling intracellular components to supply metabolic substrates [270-273]. Hypoxia contributes to cell survival through the induction of autophagy [274]. In response to hypoxia, HIF-1α is stabilized and is translocated to the nucleus to initiate the transcription of genes such as Beclin 1, ATG5, BNIP3, ATG7, and ATG9A involved in autophagy [275]. A study demonstrated a strong link between autophagy and hypoxia in head and neck tumors [276]. The authors observed that LC3B, an autophagic marker was strongly expressed (identified by quantification of LC3B staining) in hypoxic tumor areas of head and neck tumor xenografts. During autophagy, the cytoplasmic proteins and organelles (cargo) are sequestered by phagophores and the cytosolic form of microtubule associated light chain protein 3 (LC3-I), a specific marker for autophagy, conjugates to phosphatidylethanolamine (PE) to form LC3-PE conjugate (LC3-II) [277] [278]. Expansion takes place when the two opposing ends of the elongating phagophore membrane fuse to form an autophagosome. The autophagosome then fuses with the lysosomes that allows the lysosomal hydrolases to degrade the autophagic cargo into basic

metabolic building blocks such as nucleotides, amino acids, sugars, fatty acids, which are exported to the cytosol for reuse by the cell. Thus, release of recycled molecules allows the maintenance of cellular metabolism and promotes the cell survival [279]. The schematic for autophagy is shown in figure 3.1.

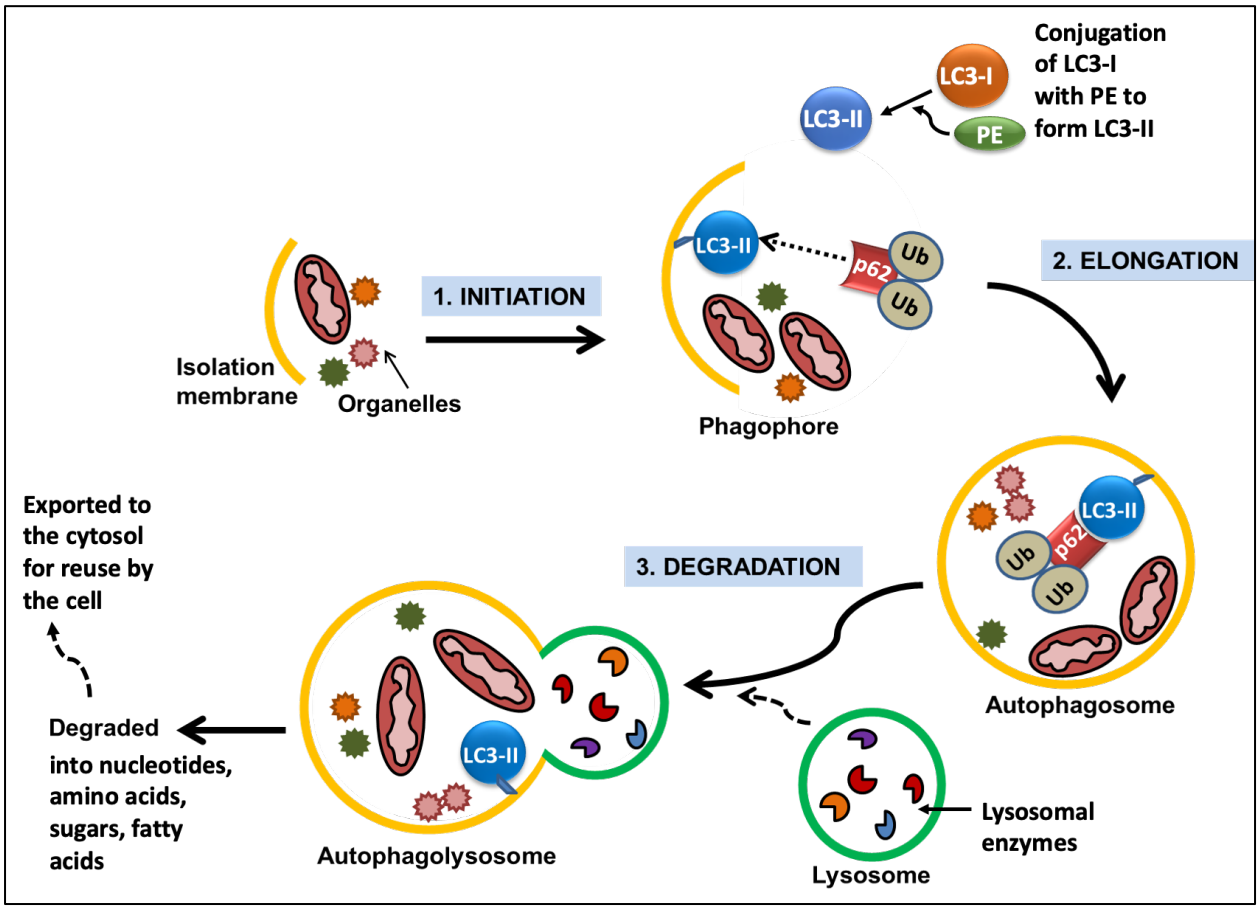

Figure 3.1. The specific stages of autophagy - (1) Initiation - includes formation of the isolation membrane (phagophore), the engulfment of cytoplasmic material and/or organelles (autophagic cargo) by the phagophore and the recruitment of LC3-II and p62-Ubiquitin complex, (2) Elongation – includes the elongation of the phagophore membrane, and fusion of its edges to form the autophagosome (3) Degradation - includes fusion of autophagosome with a lysosome and degradation of the autophagic cargo by lysosomal enzymes. The cargo is degraded to the metabolic building blocks (e.g., nucleotides, amino acids, sugars, fatty acids), which are exported to the cytosol for reuse by the cell. Adapted from [278].

It has been previously demonstrated that hypoxia promotes RAGE expression in different cancer types. Kang et. al., have shown increased in RAGE expression in pancreatic cancer cell

lines (Panc02 and Panc2.03) under hypoxia [2] while Tafani et al., have observed RAGE upregulation in breast cancer cells (MDA-MB-231 and MCF-7) and cervical cancer HeLa cells under hypoxic conditions [171].

Various studies in pancreatic cancer also illustrated a positive correlation between RAGE and autophagy under normoxic conditions. Kang et al., demonstrated that the overexpression of RAGE in pancreatic cancer resulted in increased autophagy that was reduced by RAGE knockdown [19].

The pivotal role of RAGE in migration has also been studied in different cancer types under normoxic conditions. Fuentes et al., observed increased migration of colon cancer cell lines (HT-29, LoVo, DLD-1, SW837, and WiDr) upon RAGE activation by S100P [280]. Similarly, a study showed RAGE activation by HMGB1 promotes the invasion and migration of hepatocellular carcinoma cells [281]. AGE-RAGE interaction was also shown to increase migration of breast cancer cells- MDA-MB-231 [114] and MCF-7 [282]. Moreover, in pancreatic cancer, Logsdon's group reported increased migration and invasiveness of human pancreatic cancer cell lines upon RAGE activation by S100P [283]. In-addition decreased cell migration and invasion in MDA-MB-231 and MCF 7 breast cancer cells and HeLa cervical cancer cells under hypoxic conditions via RAGE knockdown has also been observed [171].

However, the underlying mechanism of RAGE-mediated autophagy and migration under hypoxic conditions in human pancreatic cancer cells remains elusive. Therefore, in the current study, we intend to investigate if RAGE mediates the autophagy and migration in pancreatic cancer cells under hypoxic conditions. We investigated the effect of hypoxia on RAGE levels, autophagy and migration of PANC-1, CFPAC and MIA PaCa-2 pancreatic cell lines. Next, we blocked RAGE activation with a small molecule RAGE antagonist, FPS-ZM1 and compared autophagy and

migration results of treated and untreated cells to determine if autophagy and migration of pancreatic cancer under hypoxia are RAGE-mediated.

3.4. Materials and methods

3.4.1. Cell culture

PANC-1, CFPAC and MIA PaCa-2 pancreatic cancer cell lines were purchased from American Type Culture Collection (ATCC, Manassas, VA). Both PANC-1 and MIA PaCa-2 cells have been established from primary tumors, while the CFPAC cell line was isolated from liver metastasis. All these three cell lines express KRAS (v-Ki-ras2 Kirsten rat sarcoma viral oncogene homolog) and TP53 (encoding the p53 protein) mutations. KRAS mutations are very common in pancreatic cancer and account for 90% of pancreatic cancer cases while TP53 mutations are known to be reported in 50% of pancreatic adenocarcinomas [284]. In this study we chose these three cell lines because of their mutations in both KRAS and TP53. PANC-1 cells exhibit G12D KRAS mutation which is the most frequent mutation in pancreatic cancer. MIA PaCa-2 cells exhibit G12C mutation while CFPAC exhibit G12V mutations. These mutations are correlated with poor overall survivals in patients. Moreover, these three KRAS mutations have been identified in promoting autophagy via KRAS-mediated signaling pathways such as MEK-ERK and PI3K-AKT [285].

Cells were cultured and maintained in Dulbecco's Modified Eagle's Medium (DMEM, ATCC) containing 10% FBS (ATCC), penicillin (100 U/ml) and streptomycin (100 µg/ml) (ATCC) under standard culture conditions (5% CO_2 and at 37ºC). To achieve hypoxia-mimetic conditions, cells were treated with 300µM and 500µM cobalt chloride and placed in standard incubator. For hypoxia, flasks containing cells were incubated in hypoxic chamber with 94:5:1 mixture of $N_2/CO_2/O_2$ for 24 hours. In this study, we chose a hypoxic-mimetic agent, cobalt chloride for our preliminary studies. However, we performed similar experiments in the hypoxic

chamber to confirm our test results. Cobalt chloride is a synthetic agent that inactivates proline hydroxylases enzyme (PHD) by occupying its iron binding site [286]. The inactive PHD fails to carryout hydroxylation of HIF-1α, resulting in stabilization and accumulation of HIF-1α, thus producing hypoxia-mimetic conditions. However, creating hypoxia-mimetic conditions using cobalt chloride has the limitation that it does not produce realistic hypoxic conditions that require low oxygen levels. Therefore, for our further studies we exposed the cells with 1% oxygen in a hypoxic chamber to generate conditions that more resemble pathophysiological hypoxic conditions. We also investigated the role of RAGE under hypoxia using RAGE inhibitor in the hypoxic chamber.

3.4.2. Immunofluorescence

To analyze HIF-1α expression, 2.5 x 10^3 cells were seeded onto the 8 well chambered glass slide (Ibidi) and incubated with hypoxia mimetic agent (300µM and 500µM cobalt chloride) for 24 hours. Following this, the cells were fixed with 100 µl of 4 % PFA for 15 mins and permeabilized with 0.1 % triton X solution for 10 mins. Next the cells were blocked with 5% BSA for an hour at room temperature and incubated with HIF-1α primary antibody (Cell Signaling Technologies, Danvers, MA) overnight at 4ºC. Next day, the wells were washed thrice with PBS and incubated with Alexa Fluor conjugated anti-rabbit antibody 555 (Abcam, Cambridge, MA) for 1 hour. Finally, the cells were stained with DAPI and imaged under confocal microscope (Zeiss LSM 900, Carl Zeiss Microscopy LLC, White Plains, NY).

3.4.3. Western blotting

The cells grown under normoxic, hypoxia-mimetic and hypoxic conditions were detached using a cell scraper and centrifuged at 1100 rpm for 2 minutes to obtain a cell pellet (figure 3.2). Next, the cells were lysed with a RIPA buffer (PBS, Nonidet P-40 (NP-40)-1%, Na Deoxycholate

solid (0.5% w/v), SDS (0.1%)) and kept on ice for 45 minutes. The protein concentrations were determined using the BCA Protein Assay Kit (Pierce, Rockford, IL). For the detection of HIF-1α and LC3, 40 µg of protein were loaded and resolved using 10% and 15% SDS PAGE, respectively and transferred onto a nitro-cellulose membrane. The blots were then blocked with 5% milk in TBST for 1 hour at room temperature and incubated with a primary antibody (Table 1) overnight at 4ºC. Next day, the blots were washed with TBST three times and incubated with horseradish peroxidase (HRP) conjugated secondary antibody at room temperature for 1 hour. The blots were incubated with ECL substrate (Thermo Scientific, Waltham, MA). Chemiluminescence was detected using x-ray films and the films were developed on a developer. Finally, the band intensities of different proteins were measured by Image J software (National Institutes of Health, Bethesda, MD) [287] and normalized to the loading control protein, β-actin.

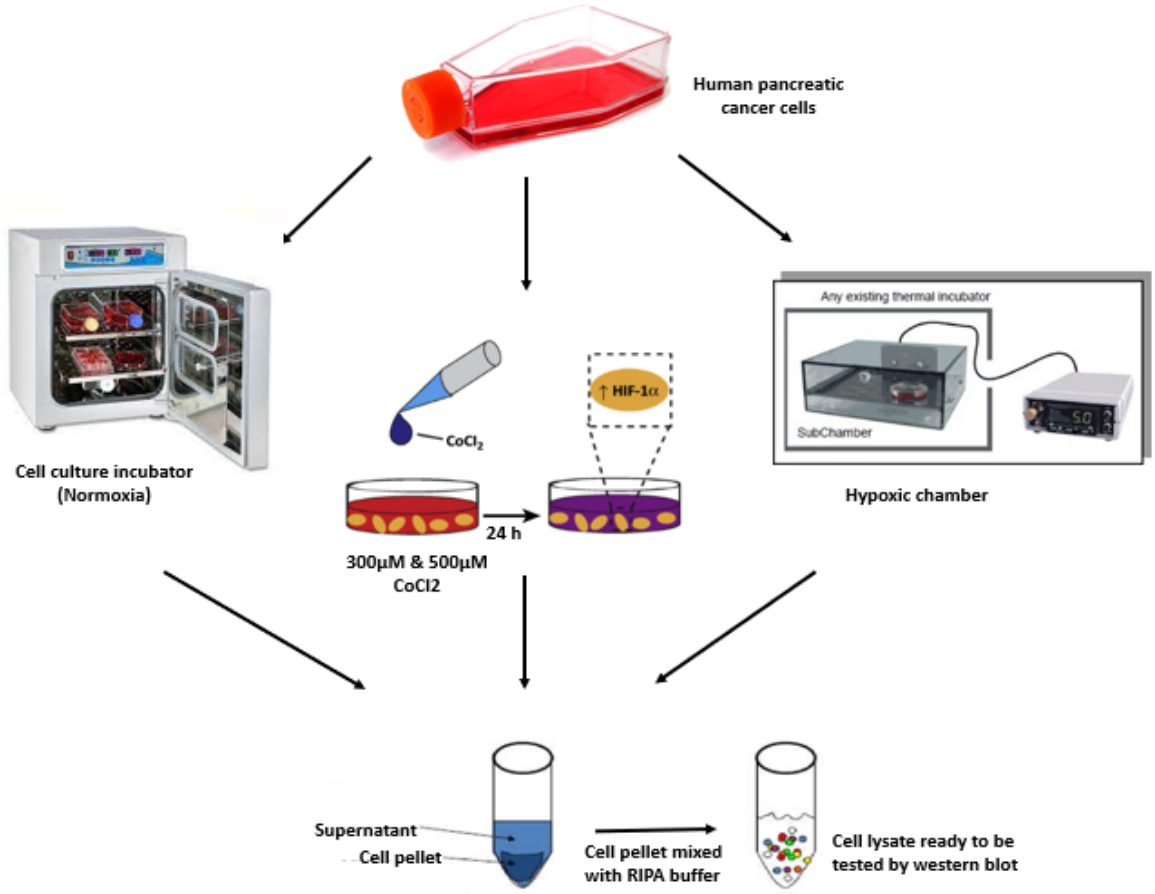

Figure 3.2. Schematic of the sample preparation under normoxia, hypoxia mimetic and hypoxic conditions.

3.4.4. Immunoprecipitation

For the detection of RAGE, 100 µl cell lysates were immunoprecipitated overnight with 30 µl of G-Sepharose beads pre-incubated with RAGE antibody (Santa Cruz Biotechnology Inc, Dallas, TX). Beads were washed three times with PBS. 15 µl of the lysate beads mixture was boiled with 5X SDS loading buffer and loaded on a 12% SDS-PAGE gel and transferred onto a PVDF membrane and blocked with Odyssey blocking buffer (LI-COR, Lincoln, NE) for 1h at room temperature. The primary and secondary antibody were diluted in Odyssey blocking buffer with 0.2% Tween 20. The membrane was incubated with the antibody for RAGE that corresponds to residues near the carboxy terminus of human RAGE 1 protein (Cell Signaling Technologies,

Dallas, TX, USA) overnight at 4ºC. After washing the membrane thrice with TBS-T, the membrane was incubated with IRDye 800CW secondary antibody (LI-COR, Lincoln, NE) for 1h at room temperature. The membrane was washed thrice with TBST and scanned using Odyssey CLx imaging system and densitometric analysis was performed using the LI-COR Image Studio Software.

Table 3.1. Details of antibodies.

Antibody	Company	Catalog no.	Species	Dilution
RAGE	R&D Systems	AF1145	Rabbit	1:1000 – WB 1:50 – IF
RAGE	Santa Cruz Biotechnology	sc-80653	Mouse	1:500 – IP pulldown
RAGE	Cell Signaling Technologies	D1A12 6996	Rabbit	1:1000 – IP blotting
HIF-1α	Cell Signaling Technologies	D1S7W XP	Rabbit	1:1000 – WB 1:200 – IF
LC3A/B	Cell Signaling Technologies	D3U4C	Rabbit	1:1000 – WB
Actin	Cell Signaling Technologies	13E5 4970	Rabbit	1:1000 – WB
Actin	Santa Cruz Biotechnology	sc-69879	Mouse	1:1000 – WB
HRP conjugated	Jackson Immuno Research	705-035-147	Anti-Mouse	1:10000 – WB
HRP conjugated	Jackson Immuno Research	711-035-152	Anti-Rabbit	1:10000 – WB
IR Dye 800CW	LI-COR	P/N 926-32214	Anti-Rabbit	1:10000 – IP
Alexa Fluor 555	Abcam	ab150074	Anti-Rabbit	1:200 – IF

3.4.5. FPS-ZM1 preparation

FPS-ZM1 is a high affinity antagonist of RAGE (Ki = 25 nM). It is a nontoxic tertiary amide compound that acts as an inhibitor specific to RAGE [288]. A study has confirmed the specificity of FPS-ZM1 for RAGE using ELISA by comparing the binding of Amyloid β (Aβ) ligands to RAGE and LDL receptor related protein-1 (LRP) in the presence of FPS-ZM1. LRP is a major clearance receptor for Aβ at BBB. The study showed that FPS-ZM1 blocks Aβ binding to the V domain of RAGE, however, does not inhibit Aβ40 and Aβ42 ligands binding to LRP. In-

contrast, Aβ binding to LRP was completely inhibited by a receptor-associated protein (RAP), which is a LRP specific inhibitor [288]. Moreover, authors have reported that FPS-ZM1 can penetrate blood brain barrier and showed no adverse effects on vital signs such as heart rate, blood pressure, respiration and liver functions in mice [289].

In this study, all three pancreatic cancer cell lines were treated with 50 nM of FPS-ZM1. 1mg/ml corresponding to 3.05 mM stock solution was prepared by dissolving 1 mg of FPS-ZM1 in 1 ml of DMSO. From 3.05 mM we prepared 500 nM solution in deionized water and used it at final concentration of 50 nM. The cells without any treatment (vehicle – DMSO at 0.001%) served as a control for the experiment.

3.4.6. Transwell migration assay

To evaluate the migration of pancreatic cancer cells, we performed transwell migration assays. We seeded all three pancreatic cancer cell lines - PANC-1, CFPAC and MIA PaCa-2 separately in the transwell inserts with 8µm pore diameter (Greener Bio, Monroe, NC). The cells were pretreated with media containing 1% FBS for 24 h. Next, 5×10^4 cells were added in the upper chamber of insert using 200 µl serum free media, and complete medium (DMEM media containing 10% FBS) was added to the bottom chambers. Next, the cells were cultured for 8h with hypoxia mimetic agents (300µM and 500µM of cobalt chloride) and their normoxic controls, and for 24 h under 1% oxygen levels (hypoxia chamber), normoxic control, FPS-ZM1 (50 nM) and DMSO (vehicle) treated cells. Finally, we used a cotton-tipped applicator to remove the media and non-migrated cells inside the inserts. Migrated cells were assessed quantitatively by analyzing fluorescence using alamar blue assay. The inserts were dipped in 300 µl of 0.1% alamar blue solution and incubated at 37 ºC for three hours. Finally, the fluorescence was measured at 545 (excitation) and 590 nm (emission) using spectrophotometer - Spectra Max M5 (Molecular

Devices, San Jose, CA). For crystal violet assay, the cells that migrated through the insert were fixed in 10% neutral buffered formalin solution for 30 min and stained with 0.05% crystal violet solution for 30 min. The cells that migrated through the pores to the lower surface of the inserts were imaged under a brightfield microscope (Olympus FV300, Tokyo, Japan) (figure 3.3).

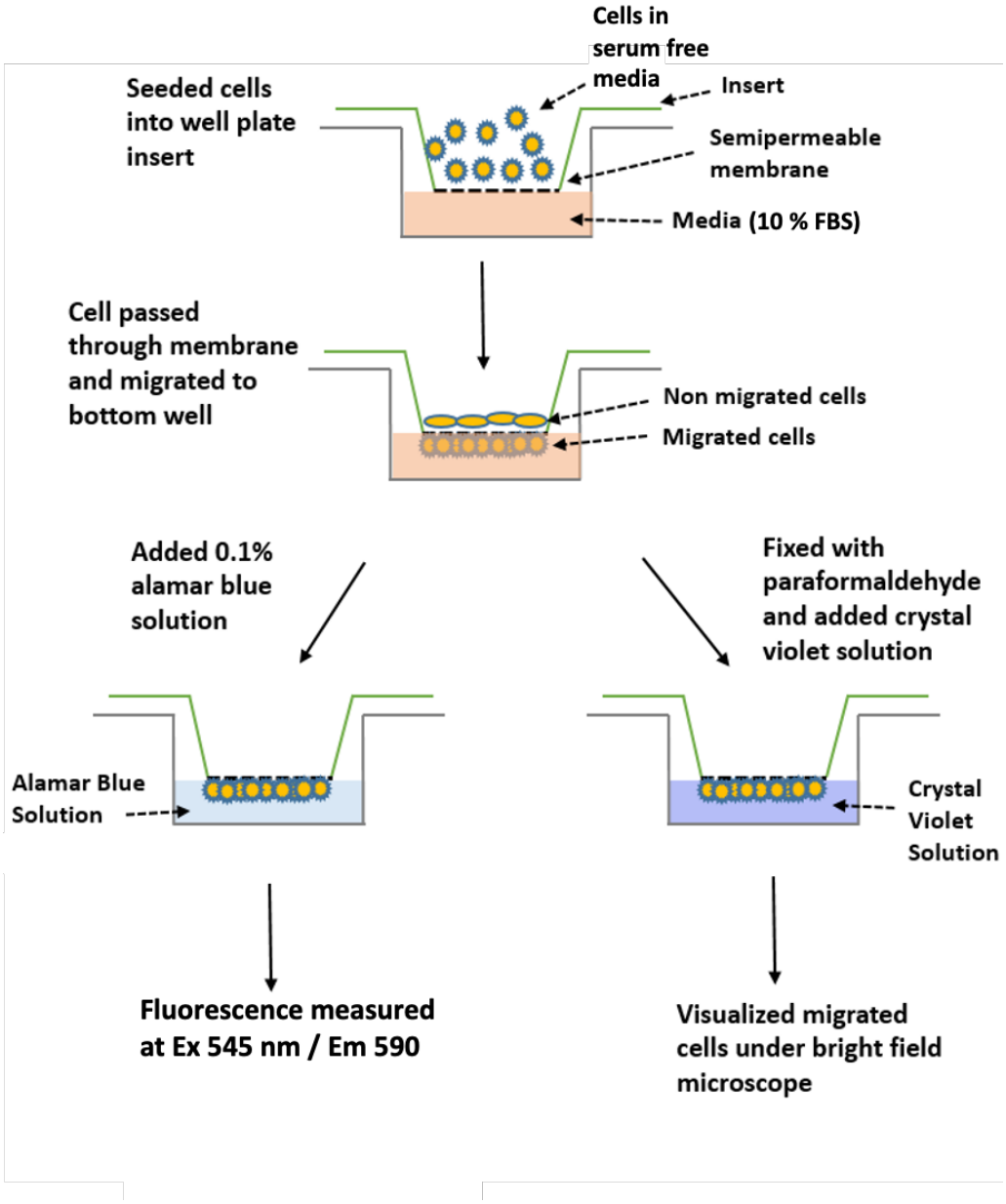

Figure 3.3. Schematic of Boyden Chamber migration assays. Migrated cells were quantified by measuring alamar blue fluorescence and stained with crystal violet for imaging.

3.4.7. Enzyme Linked Immunosorbent Assay (ELISA)

The amount of RAGE was determined using Quantikine RAGE ELISA kit following the manufacturer's instructions (DRG00, R&D Systems, Minneapolis, MN). Briefly, the cells under normoxic and hypoxic conditions (60 % confluent) were scraped and centrifuged at 1100 rpm for 2 minutes to obtain a cell pellet. Next, the cells were lysed with RIPA buffer to generate cell lysates of all cell lines. The protein concentrations of all cells were determined using the BCA Protein Assay Kit (Pierce, Rockford, IL, USA). Then 50 µl of standards and samples were incubated in ELISA plate overnight at 4ºC. Next the plate was incubated with anti-RAGE conjugate for 2 hours. Finally, the substrate solution was added and after adding the stop solution the absorbance was measured at 545 and 590 nm. The obtained values were normalized with their total protein and the RAGE levels were expressed as pg/mg protein.

3.4.8. Statistical analysis

HIF-1α and LC3 were analyzed by western blot from three different batches of cell lysate from PANC-1, CFPAC and MIA PaCa-2. RAGE was analyzed by immunoprecipitation from three different batches of cell lysate from PANC-1, CFPAC and MIA PaCa-2. Band intensities were calculated using Image J software. The band intensities of HIF-1α and RAGE were normalized with respect to Actin. Ratio of HIF-1α/Actin and RAGE/Actin were plotted as bar graphs. For LC3, first the band intensities for LC3-II and LC3-I were calculated and the ratios of band intensities of LC3-II/I were plotted as bar graphs. Immunofluorescence imaging for HIF-1α was performed once. Quantification of RAGE levels was performed by ELISA of three different batches (with two technical replicates) of each cell line. Transwell migration assay in hypoxia-mimetic conditions was done with one batch of cells with three technical replicates. Transwell migration assay in hypoxic chamber was done with three independent batches of cells with three

technical replicates for all conditions except for DMSO control for which two batch of cells with two technical replicates were used per cell line. Data are presented as mean ± SD and a p-value <0.05 was considered statistically significant. * $p<0.05$; ** $p<0.01$; *** $p<0.001$.

3.5. Results

3.5.1. HIF-1α is stabilized in hypoxic conditions

As a part of our preliminary studies, we analyzed the expression of HIF-1α by confocal microscopy in normoxic and cobalt chloride treated (hypoxic) samples (figure 3.4). We observed more staining for HIF-1α indicating higher levels of HIF-1α in cells treated with 300μM and 500μM cobalt chloride compared to untreated samples.

Cobalt chloride is a widely used chemical inducer of hypoxia that prevents HIF1α degradation and hence, stabilizes HIF1α expression. However, cobalt chloride also causes toxicity to cells and the toxicity is mainly caused by ionized cobalt. The mechanism of cobalt toxicity is not clear, but some of the toxic effects of cobalt relate to 1) its high affinity for sulfhydryl groups, which may cause inhibition of crucial enzymes in mitochondrial respiration [290], 2) the displacement of divalent cations by cobalt in the ion centers of metal-activated enzymes [291], 3) the inhibition of Ca^{2+} entry and Ca^{2+} signaling and competition with Ca^{2+} for intracellular Ca^{2+} binding proteins [292] and 4) the generation of reactive oxygen species in cells, resulting in oxidative damage to DNA, proteins and lipids [291, 293].

A study has shown decreased cell viability of mouse embryonic fibroblasts with increasing cobalt chloride concentration (0-200μM), indicating that cobalt chloride has toxic effect on cells [294]. Another study reported upregulation in HIF-1α m-RNA levels in C2C12 mouse myoblasts and 3T3L1 preadipocytes at 150μM concentration of cobalt chloride, however, cell viability was also reduced in these cells at the same concentration of cobalt chloride [295]. Because of these

limitations, we chose another approach to generate hypoxic conditions. It was reported that solid tumors have oxygen concentration of 1% or lower. Therefore, to create hypoxic conditions, we exposed the cells with 1% oxygen in a hypoxic chamber and performed our further experiments.

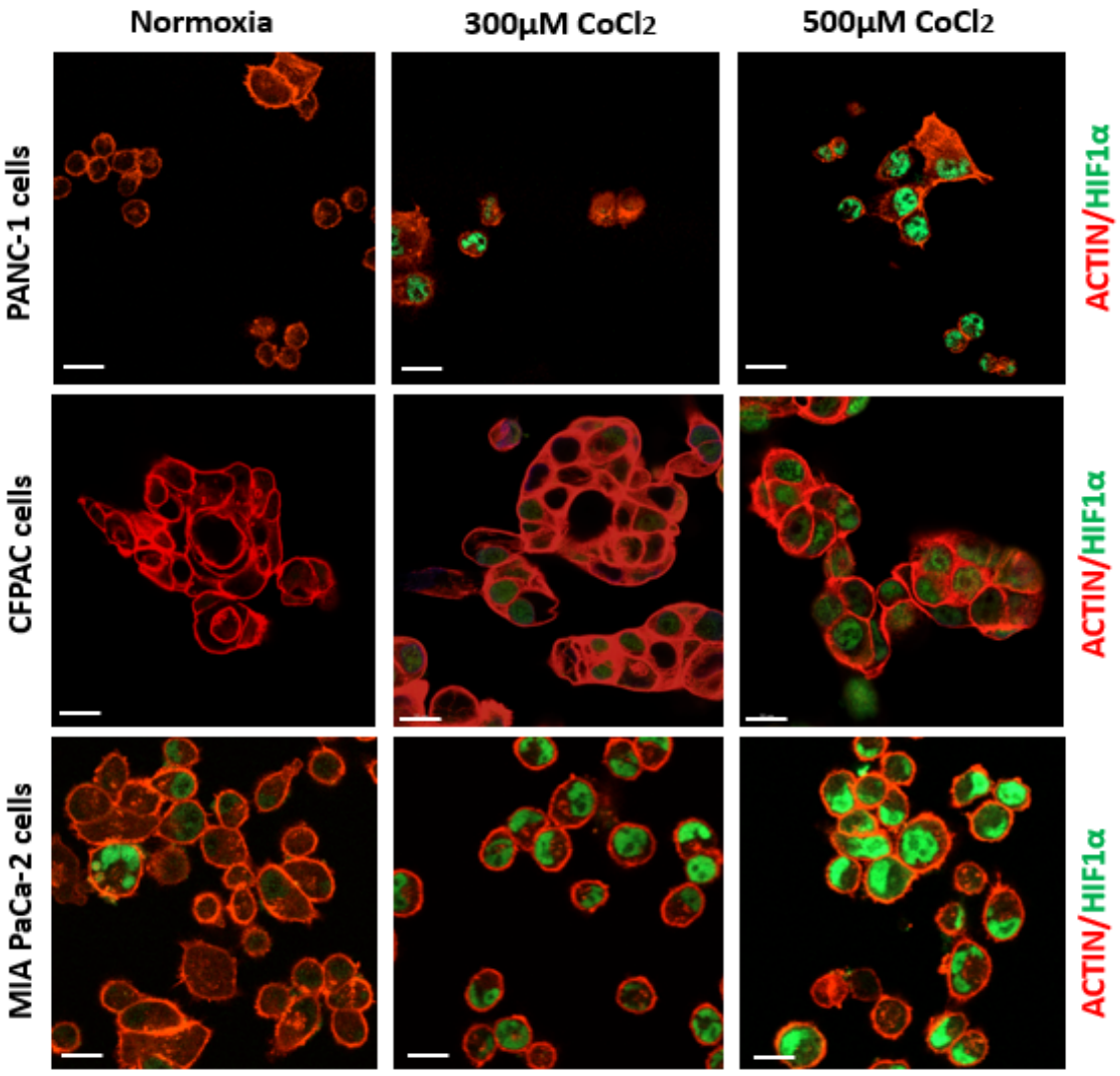

Figure 3.4. HIF-1α (green) and Actin (red) in PANC-1, CFPAC-1 and MIA PaCa-2 cells at normoxia, 300µM and 500µM cobalt chloride, (n=1). Scale bar 20µm.

Next, to investigate hypoxia generation in pancreatic cancer cell lines incubated in hypoxic chamber we determined HIF-1α expression in all three cell lines by Western blotting. We observed significantly higher levels ($p<0.05$) of HIF-1α in all three cell lines incubated in hypoxic chamber compared to their normoxic samples that confirms hypoxia generation in hypoxic chamber (figure

3.5, 3.6 and 3.7). As expected, the normoxic samples in all the cell lines showed very low HIF-1α expression levels compared to their hypoxic samples.

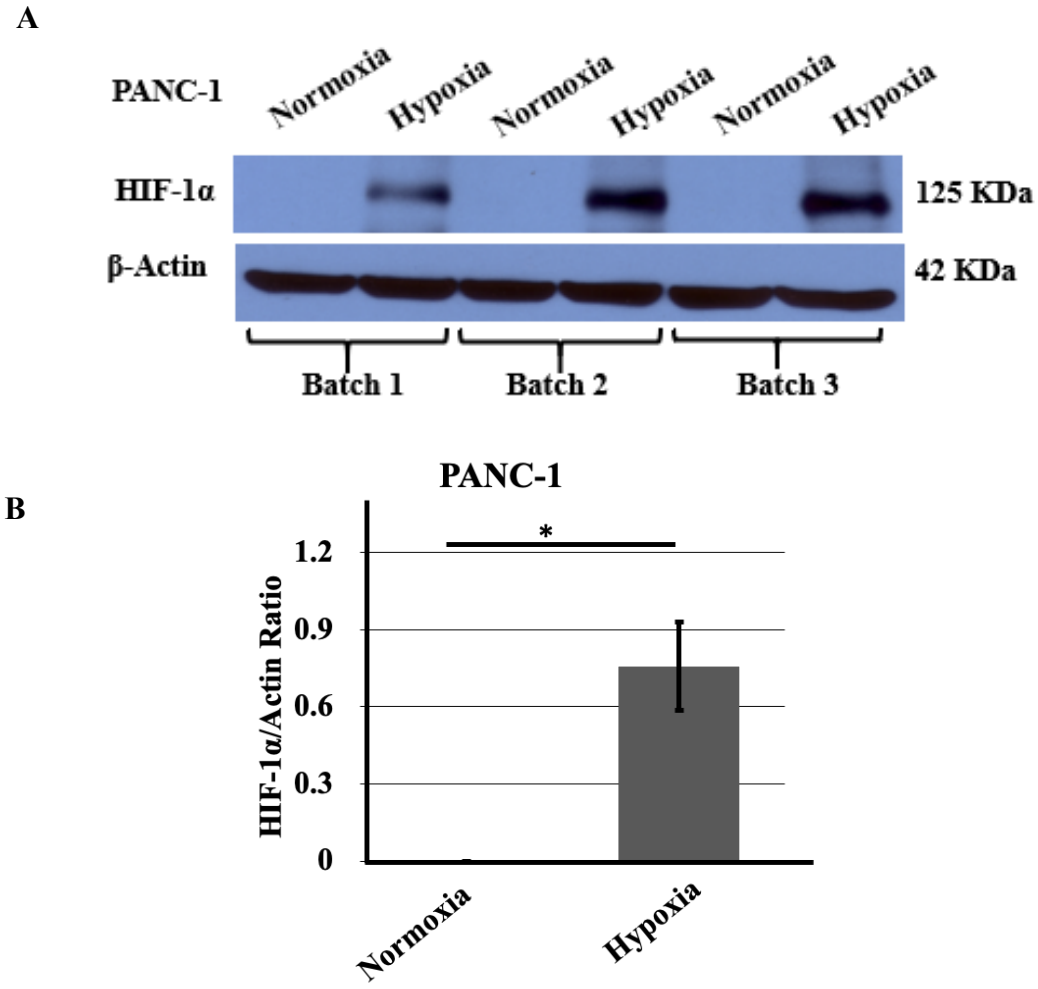

Figure 3.5. (A) Protein expression of HIF-1α and β-Actin (B) Increase in HIF-1α/Actin ratio in PANC-1 cells in hypoxic conditions versus normoxia, n=3, *p<0.05.

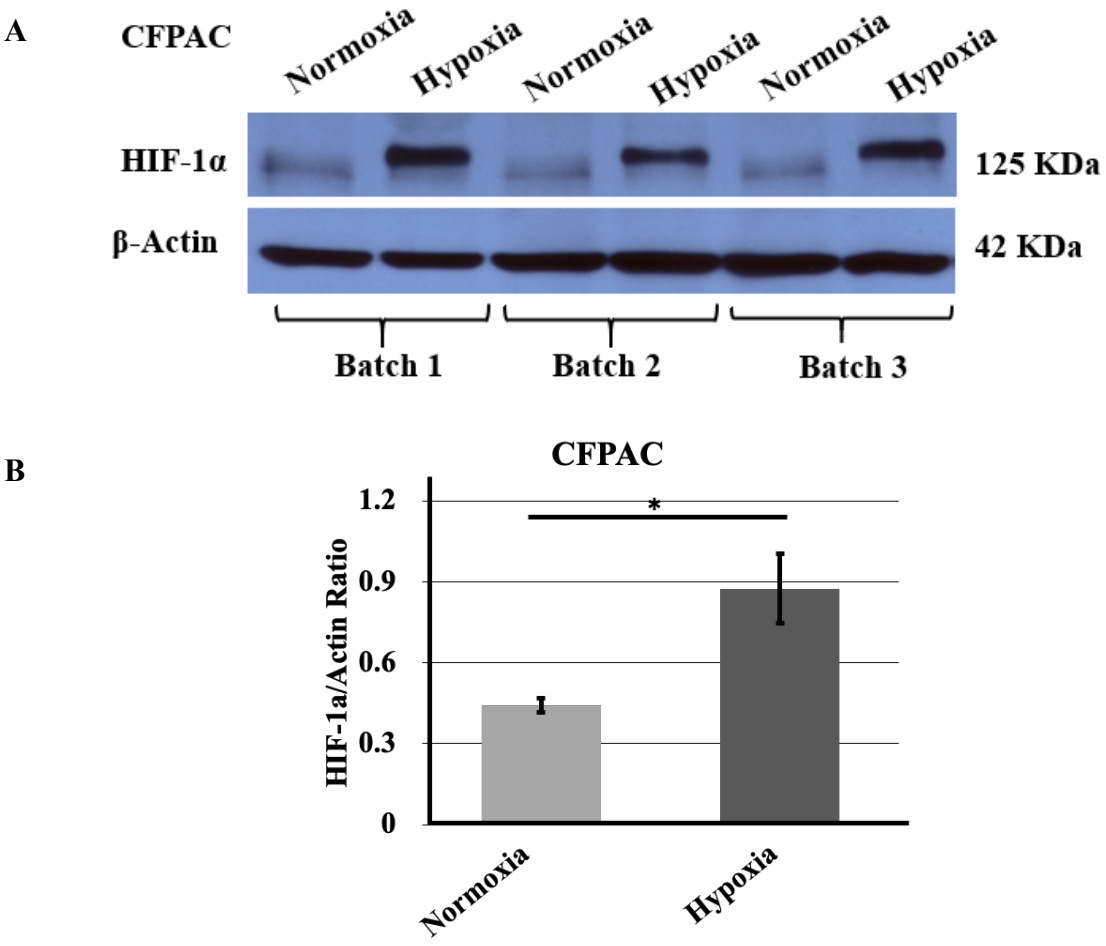

Figure 3.6. (A) Protein expression of HIF-1α and β-Actin (B) Increase in HIF-1α/Actin ratio in CFPAC cells in hypoxic conditions versus normoxia, n=3, *p<0.05.

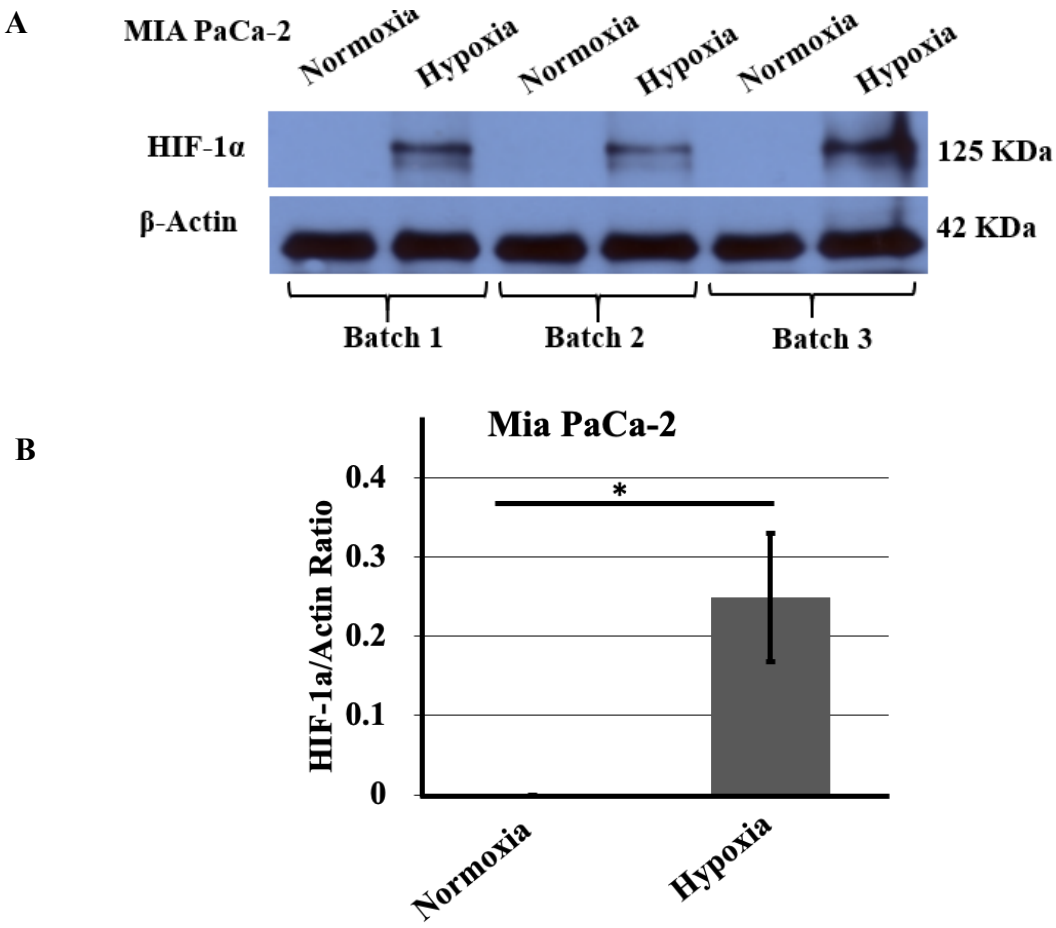

Figure 3.7. (A) Protein expression of HIF-1α and β-Actin (B) Increase in HIF-1α/Actin ratio in MIA PaCa-2 cells in hypoxic conditions versus normoxia, n=3, *p<0.05.

3.5.2. Hypoxic conditions upregulate RAGE levels

In our preliminary studies, we analyzed RAGE expression in hypoxia-mimetic conditions using 300µM and 500µM of cobalt chloride. Initially, we employed the Western blot technique to measure RAGE levels in the different lysates. However, we did not detect any RAGE band using this approach. This is probably due to very low levels of RAGE protein present in these samples. Indeed, we measured very low levels of RAGE by ELISA. Thus, we also utilized the immunoprecipitation technique to quantify RAGE levels because this technique can detect pg levels of proteins. One limitation of the immunoprecipitation method is that the sepharose beads used for immunoprecipitating the proteins might be saturated due to non-specific binding of lysate

components, resulting in an elevated background signal. Maybe due to that reason, we obtained RAGE bands with poor resolution and observed large variations among different sets of experiments.

As mentioned earlier, we used ELISA for the detection of RAGE levels in our samples. This technique is sensitive and detects RAGE even at low concentrations. The limit of detection of the ELISA kit we used was 4.12 pg/mL. However, the type of ELISA we employed during the study uses polyclonal antibodies that binds to the extracellular domain of RAGE. Thus, both the full-length form of RAGE and the soluble isoforms of RAGE can be detected by ELISA. This is one limitation of the ELISA approach.

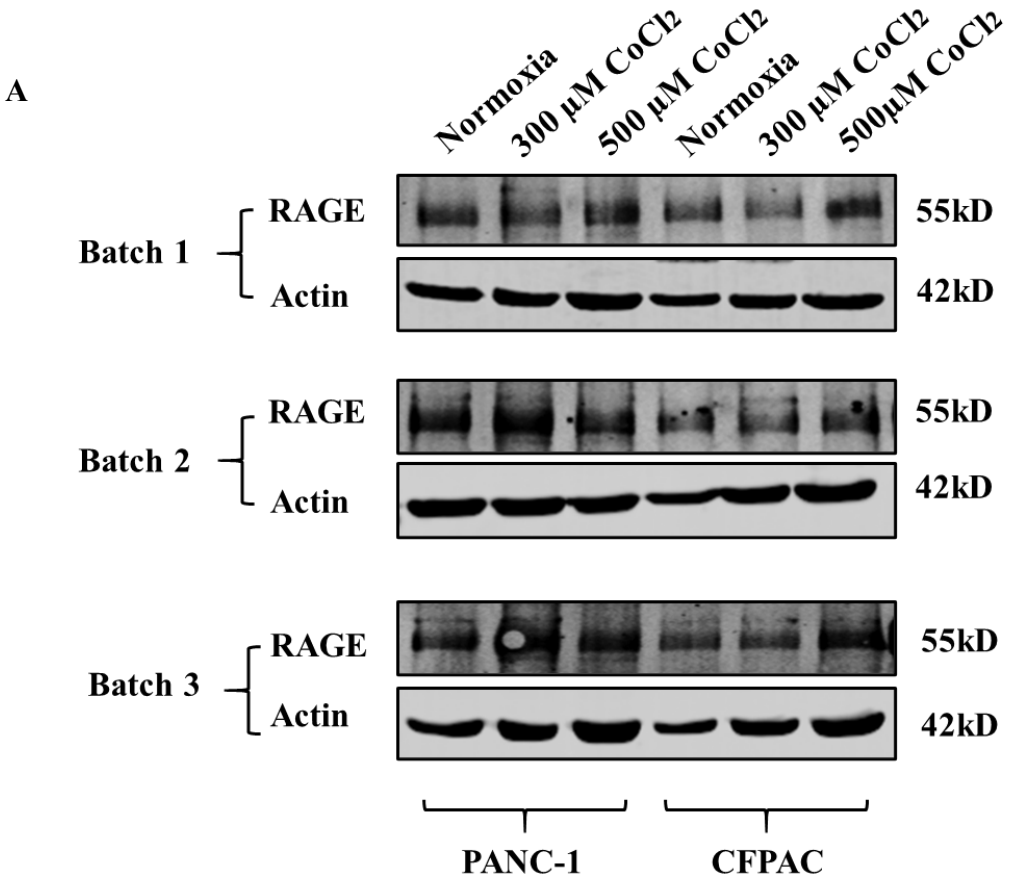

Figure 3.8. (A) Protein expression of RAGE and β-Actin (B) RAGE to actin ratio in PANC-1 and (C) RAGE to actin ratio in CFPAC cells at normoxia, 300µM and 500µM of cobalt chloride, n=3.

B

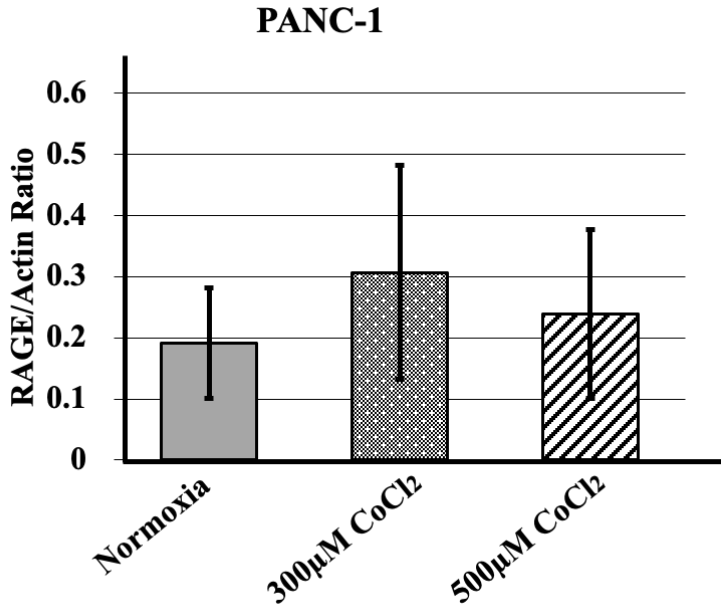

C

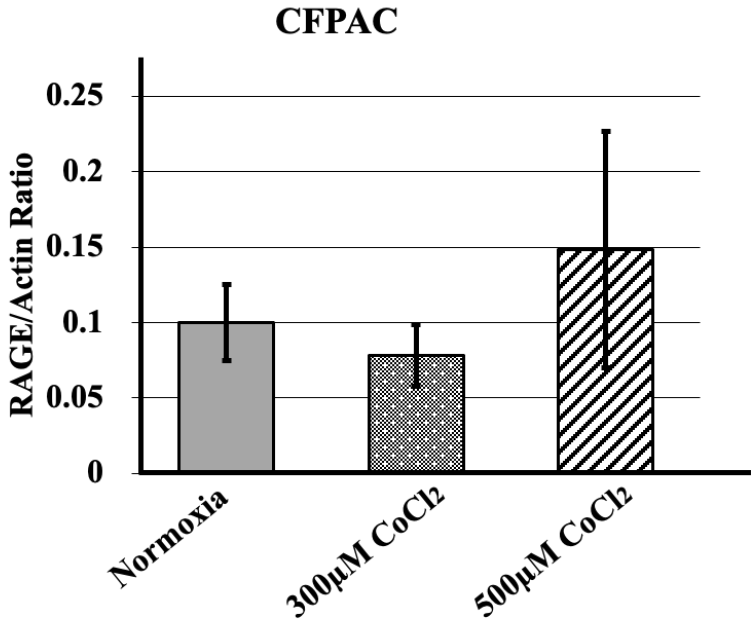

Figure 3.8. (A) Protein expression of RAGE and β-Actin (B) RAGE to actin ratio in PANC-1 and (C) RAGE to actin ratio in CFPAC cells at normoxia, 300µM and 500µM of cobalt chloride, n=3 (continued).

Next, to investigate the effect of hypoxia on RAGE level in hypoxic chamber, we performed ELISA for RAGE quantification under both normoxic and hypoxic conditions. We observed significant difference (***p<00.1) in RAGE levels between hypoxic and normoxic

conditions in all three cell lines (figure 3.9). CFPAC cell line showed ~1.6 fold increase in RAGE levels while PANC-1 and MIA PaCa-2 showed ~1.7 fold and ~2.3 fold increase in RAGE levels, respectively.

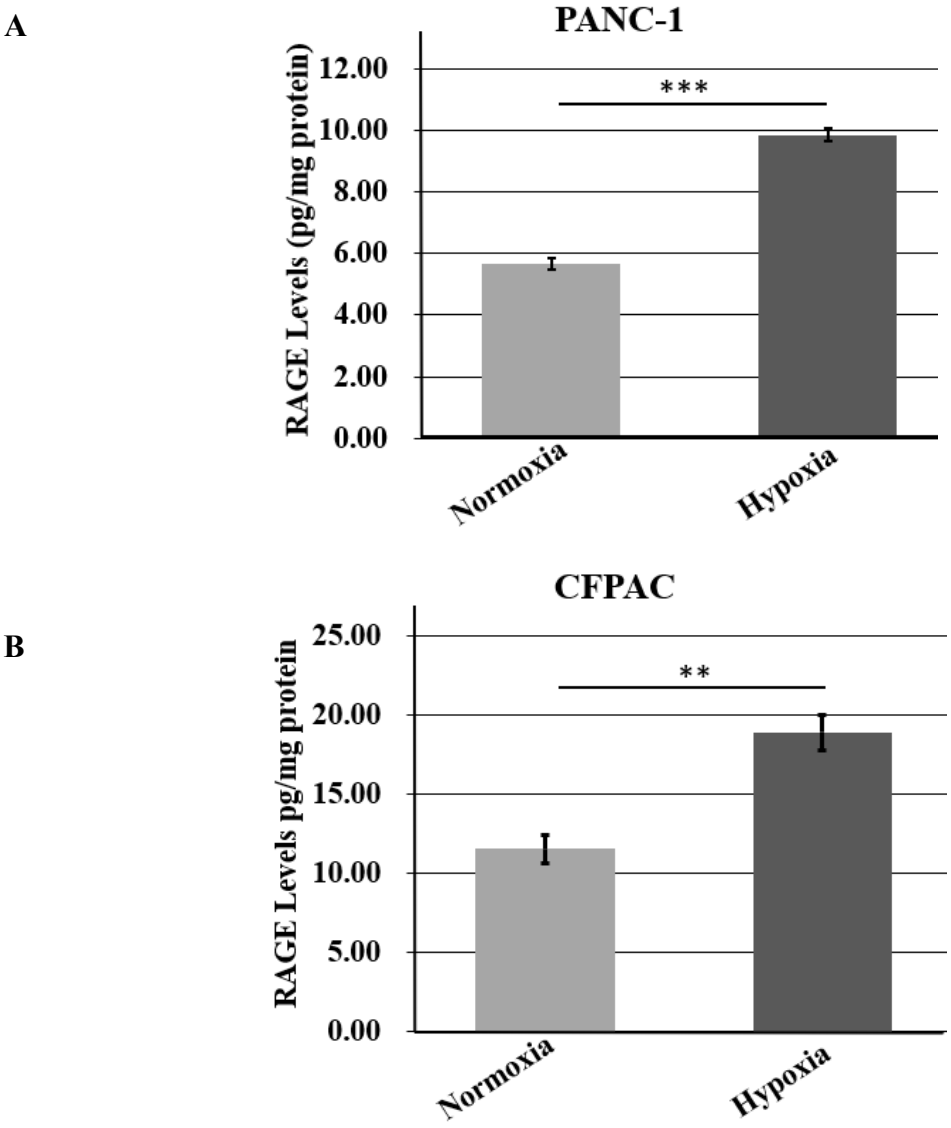

Figure 3.9. Increase in the RAGE levels in PANC-1, CFPAC and MIA PaCa-2 cells in hypoxia versus normoxia, n=3, **p<0.01, ***p<0.001. The limit of detection of ELISA kit is 4.12 pg/mL.

C

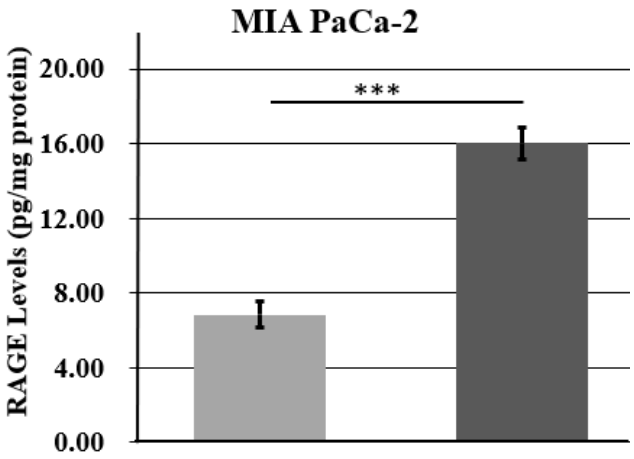

Figure 3.9. Increase in the RAGE levels in PANC-1, CFPAC and MIA PaCa-2 cells in hypoxia versus normoxia, n=3, **p<0.01, ***p<0.001. The limit of detection of ELISA kit is 4.12 pg/mL (continued).

3.5.3. Hypoxic conditions increase autophagy

We investigated the effect of hypoxia generated by hypoxia-mimetic agent on autophagy markers. We determined the expression levels of LC3-I and II in all three cell lines under hypoxia mimetic conditions using Western blot and compared our results with normoxic conditions. We observed increased ratios of LC3II/I in MIA PaCa-2 cells but not in CFPAC or PANC-1 after incubation with cobalt chloride. These differences may be attributed to differences in incubation time needed with the different cell lines. Indeed, a study reported that incubation of PANC-1 cells with cobalt chloride for 48h and 72h resulted in increased ratio of LC3II/I. We used instead incubation times of 0h, 12h and 24h in our present study [296]. Therefore, PANC-1 and CFPAC cells might need longer incubation time with cobalt chloride in order to observe increased ratios of LC3II/I. The data showed modest to no significant increase in the levels of LC3-II/I ratio in PANC-1 (1.23-fold at 300μM and 1.24- fold at 500μM) and CFPAC (300μM-1.09-fold and 500μM-1.18 fold) cells under hypoxia-mimetic conditions compared to their normoxic condition (bar graph not reported).

In MIA PaCa-2 cells, we did not observe any change in LC3-II/I ratio at 300μM cobalt chloride concentration compared to normoxic conditions. On contrary, we demonstrated a significant (*p<0.05) increase in the levels of LC3-II/I ratio (1.43-fold) in MIA PaCa-2 cells at 500μM cobalt chloride concentration compared to normoxia, suggesting increase autophagy level in hypoxia-mimetic conditions (figure 3.10).

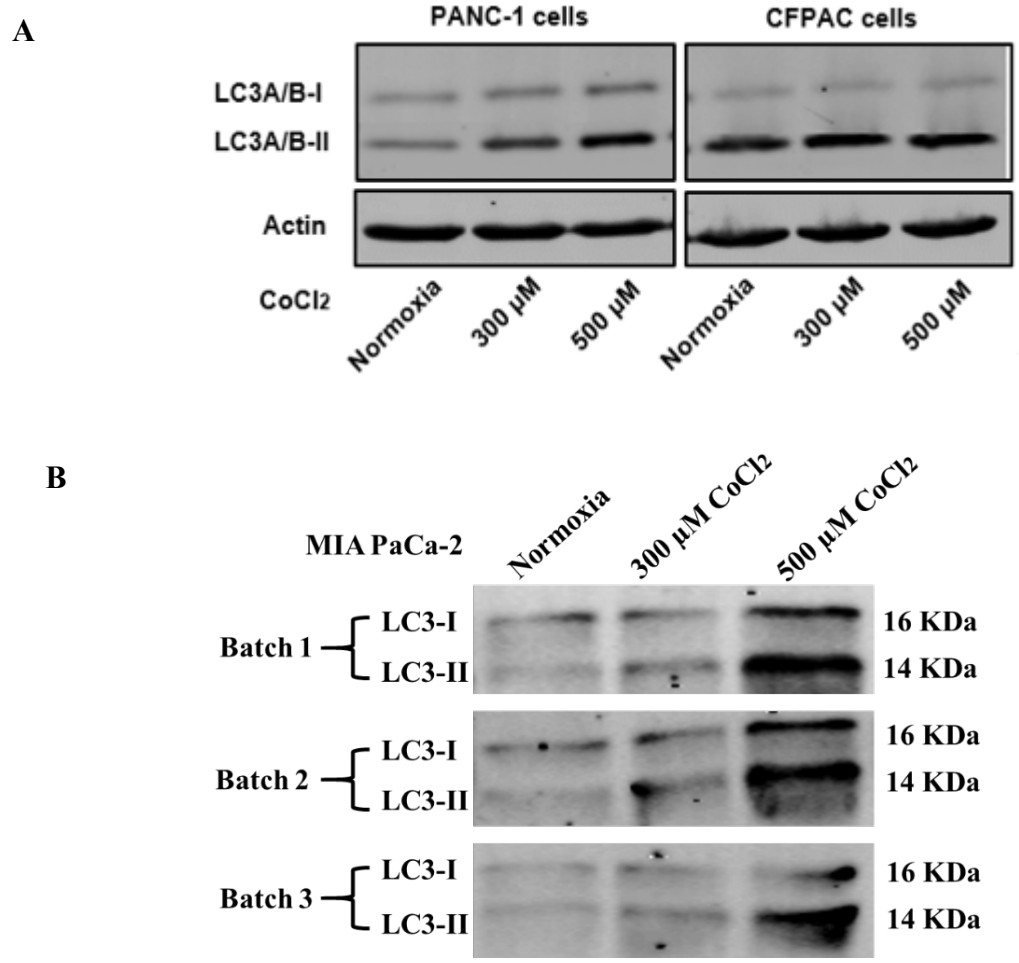

Figure 3.10. Expression of LC3-I and LC3-II in normoxia and cobalt chloride treated (A) PANC-1 (n=1) and CFPAC (n=1), (B) MIA PaCa-2 cells (n=3), (C) Quantification of LC3-II/I ratio in MIA PaCa-2 cells, n=3, *p<0.05.

C

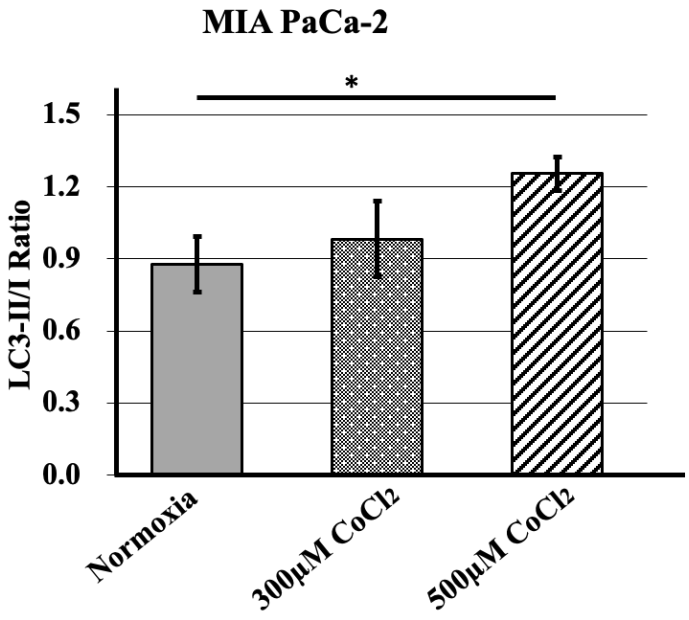

Figure 3.10. Expression of LC3-I and LC3-II in normoxia and cobalt chloride treated (A) PANC-1 (n=1) and CFPAC (n=1), (B) MIA PaCa-2 cells (n=3), (C) Quantification of LC3-II/I ratio in MIA PaCa-2 cells, n=3, *p<0.05 (continued).

Next, we investigated the expressions of LC3-I and II in PANC-1, CFPAC and MIA PaCa-2 cells in hypoxia chamber and compared our results with normoxic conditions. We observed significant increase in the level of LC3-II/I ratio in PANC-1 (***p<0.001) and MIA PaCa-2 (*p<0.05) cells under hypoxia compared to their normoxic samples. However, we did not observe significant change in the level of LC3-II/I ratio in CFPAC cells under hypoxia compared to CFPAC normoxia samples. Further, we observed significant reduction in the level of LC3-II/I ratio in PANC-1 (**p<0.001) and MIA PaCa-2 (*p<0.05) cells after FPS-ZM1 treatment compared to their untreated samples under hypoxic conditions, indicating the inhibitory effect of the RAGE inhibitor under hypoxic conditions. However, we did not find any change in FPS-ZM1 treated and untreated CFPAC samples under hypoxia. As a control, we observed no change in the levels of LCII/I ratio in all cell lines treated with the DMSO vehicle compared to untreated hypoxic samples (figure 3.11).

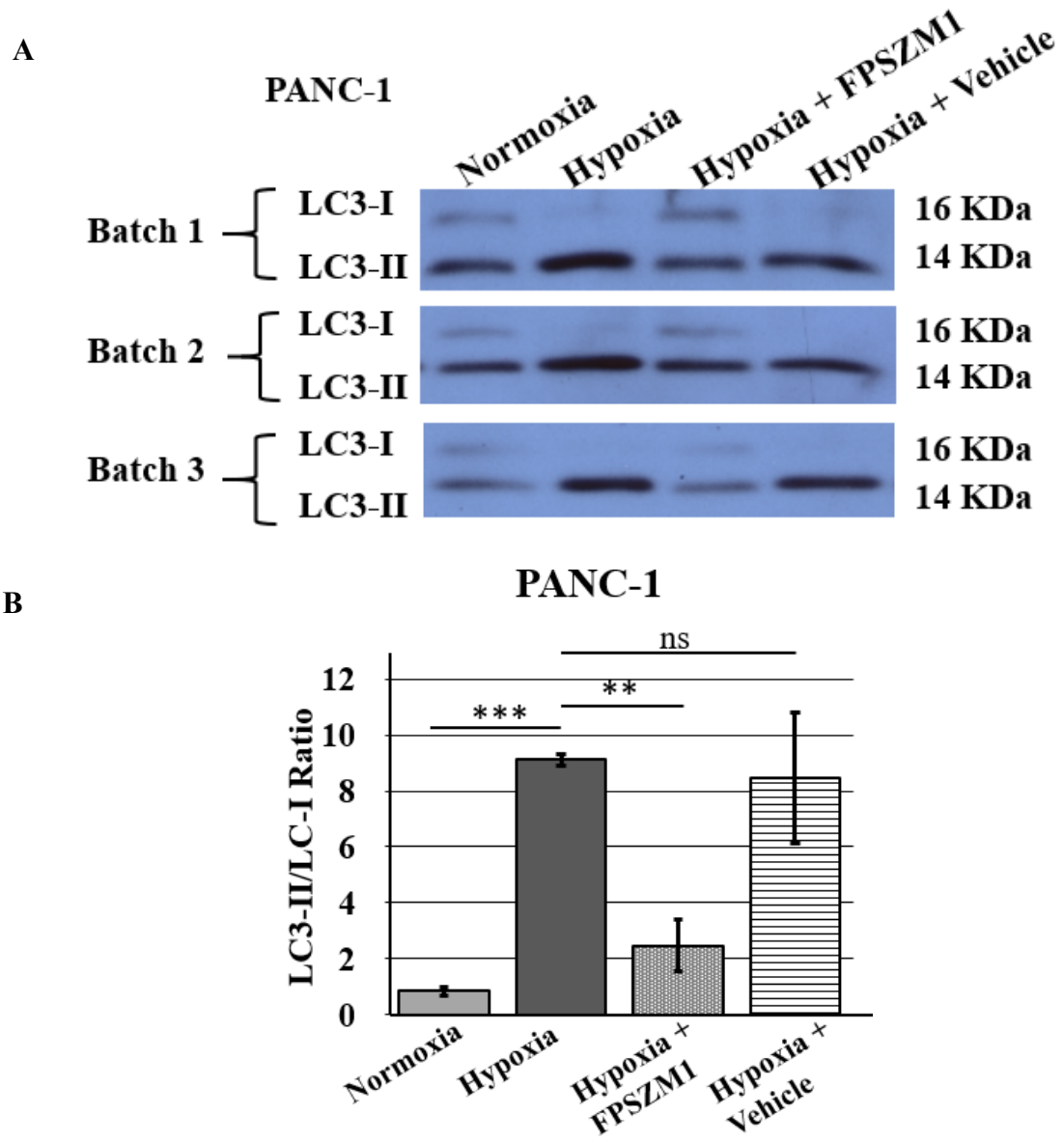

Figure 3.11. Expression of LC3-II and I in (A) PANC-1 (C) CFPAC and (E) MIA PaCa-2 cells. Ratio of LC3-II/I in (B) PANC-1, (D) CFPAC and, (F) MIA PaCa-2 cells in response to normoxia, hypoxia, FPSZM1 and vehicle (DMSO) treatment under hypoxia, n=3, *p<0.05, **p<0.01, ***p<0.001.

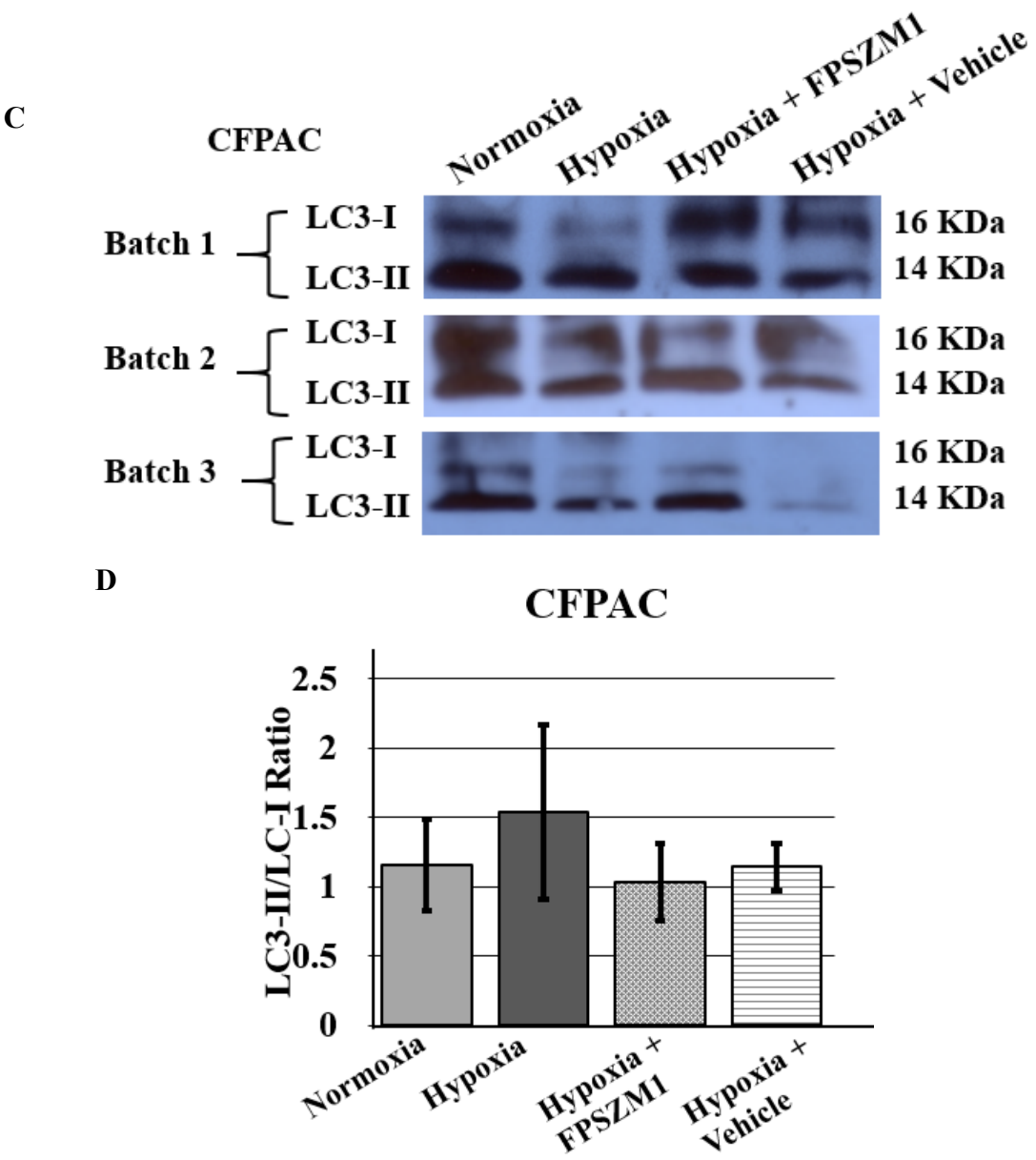

Figure 3.11. Expression of LC3-II and I in (A) PANC-1 (C) CFPAC and (E) MIA PaCa-2 cells. Ratio of LC3-II/I in (B) PANC-1, (D) CFPAC and, (F) MIA PaCa-2 cells in response to normoxia, hypoxia, FPSZM1 and vehicle (DMSO) treatment under hypoxia, n=3, *p<0.05, **p<0.01, ***p<0.001 (continued).

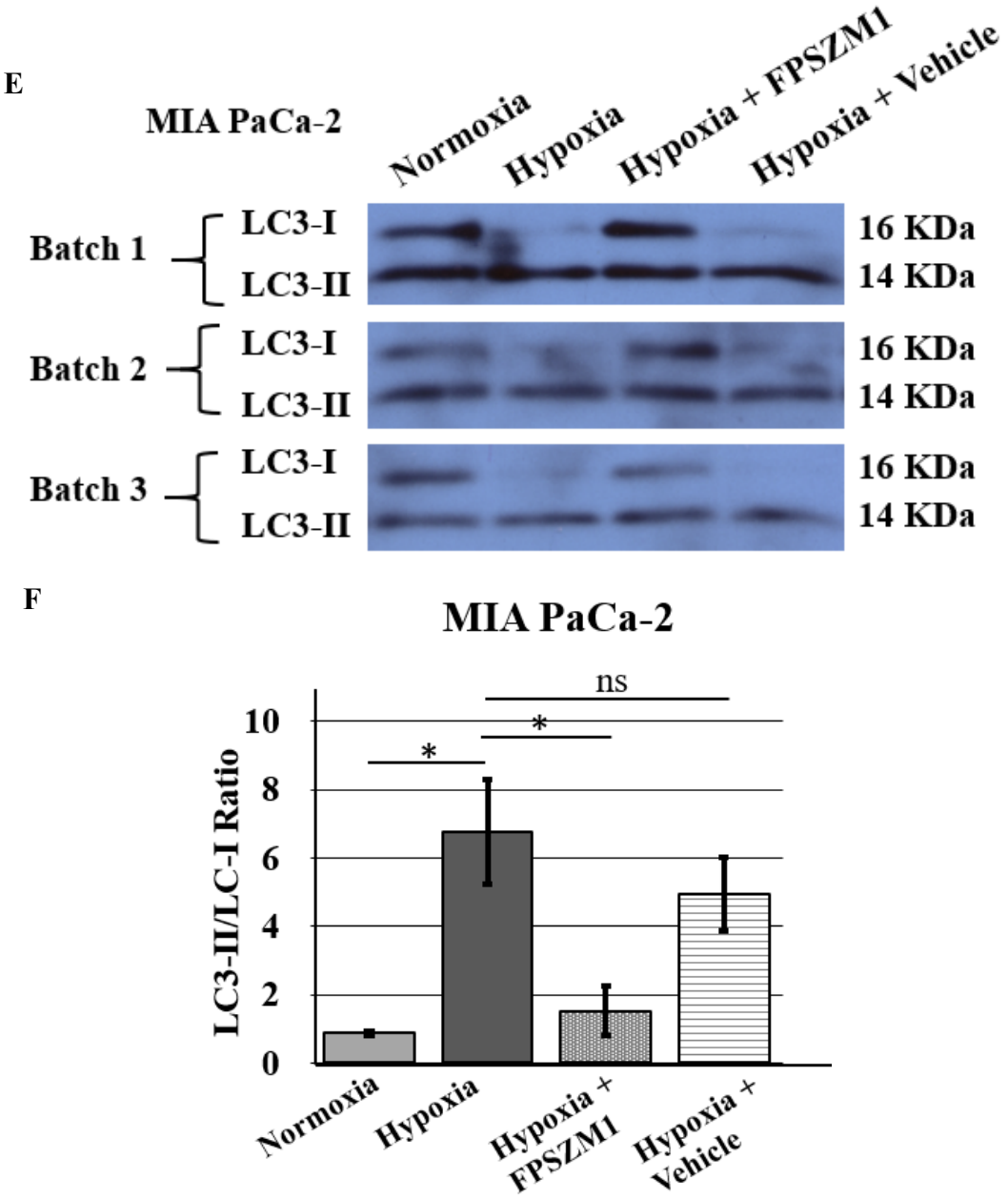

Figure 3.11. Expression of LC3-II and I in (A) PANC-1 (C) CFPAC and (E) MIA PaCa-2 cells. Ratio of LC3-II/I in (B) PANC-1, (D) CFPAC and, (F) MIA PaCa-2 cells in response to normoxia, hypoxia, FPSZM1 and vehicle (DMSO) treatment under hypoxia, n=3, *p<0.05, **p<0.01, ***p<0.001 (continued).

3.5.4. Increased cell migration under hypoxic conditions

To determine the effect of hypoxia-mimetic conditions on the migratory behavior of pancreatic cancer cells we employed the Boyden chamber transwell migration assay that measures

the migration of cells through transwell pores. The limitation of this technique is that there are many sources of assay-to-assay variation due to many washing steps that wash off loosely attached cells, resulting in underestimation of both migrated and non-migrated cells. Moreover, when wiping off the transwell membranes with cotton swabs, extra precautions are required in terms of force applied. Wiping off with too much force may break the membrane, while wiping off too gently does not adequately remove all cells that have not migrated, leading to overestimation of the number of migrated cells. Furthermore, cells near the edge of the membrane are always more difficult to wipe off due to limited accessibility. These limitations may generate variations in the results; however, taking precautions mentioned above can reduce the variations.

We observed significant increase (***$p<0.001$) in migration at both 300 μM and 500 μM cobalt chloride concentrations in PANC-1 and CFPAC cells compared to normoxic conditions determined by Alamar blue assay. While MIA PaCa-2 showed significant increase (***$p<0.001$) in migration only at 500 μM (figure 3.12). The crystal violet staining also showed increased cell migration in response to cobalt chloride treatment versus normoxia. We also observed that overall migration of CFPAC cells was higher than that of the other two cell lines. The representative images are shown in figure 3.13.

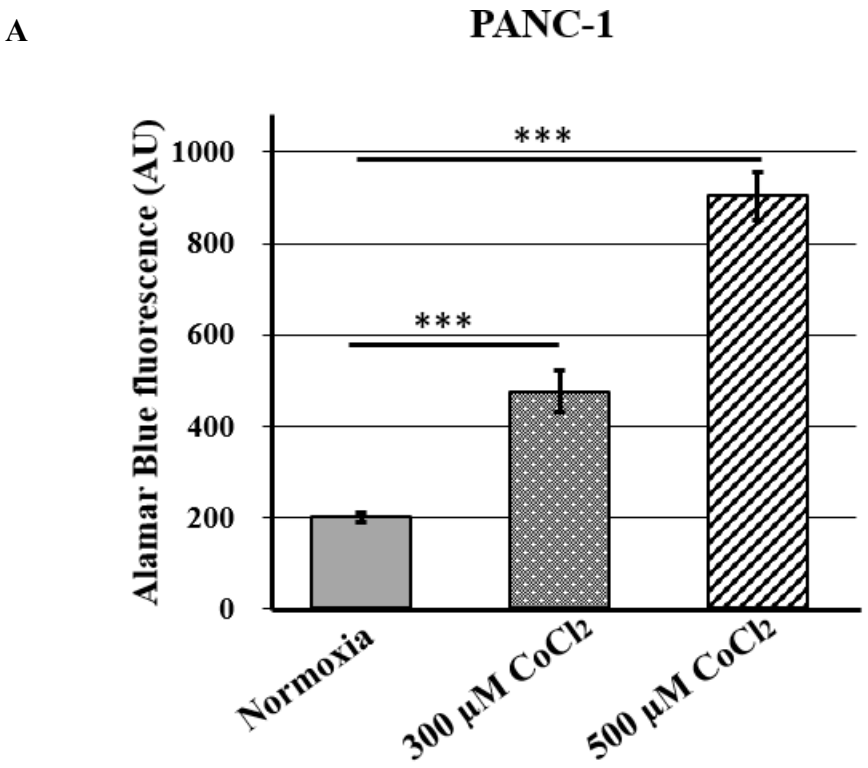

Figure 3.12. Alamar blue fluorescence of migrated PANC-1, CFPAC and MIA PaCa-2 cells through transwell inserts after normoxia, 300 µM and 500 µM of cobalt chloride, ***$p<0.001$, n=1; with 3 technical replicates.

B

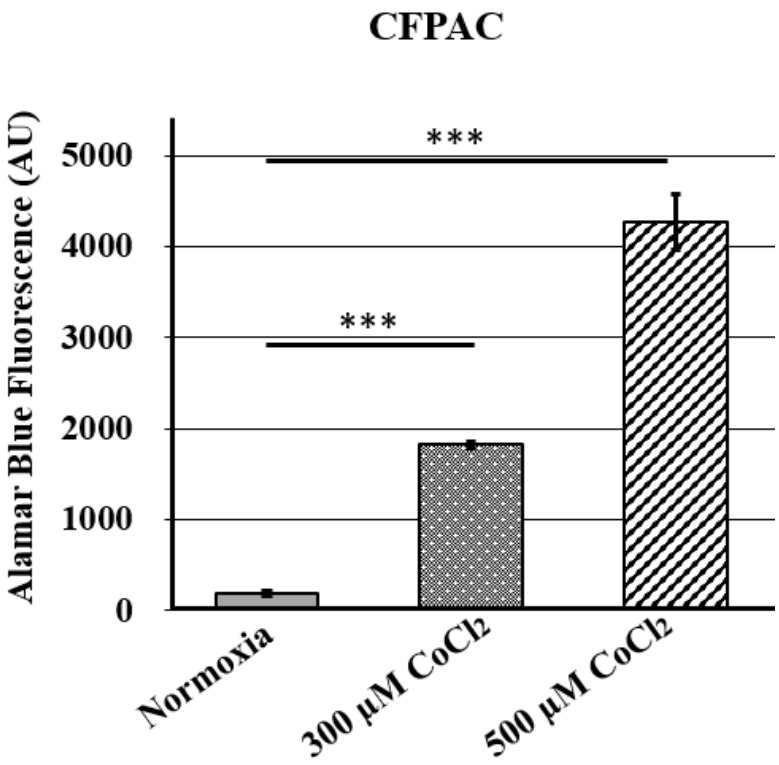

C

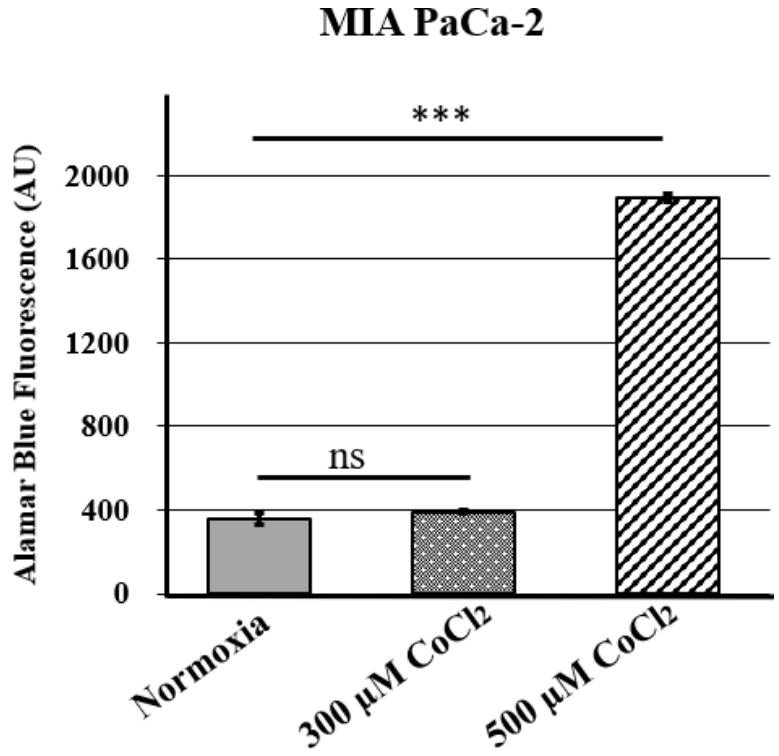

Figure 3.12. Alamar blue fluorescence of migrated PANC-1, CFPAC and MIA PaCa-2 cells through transwell inserts after normoxia, 300 µM and 500 µM of cobalt chloride, ***$p<0.001$, n=1; with 3 technical replicates (continued).

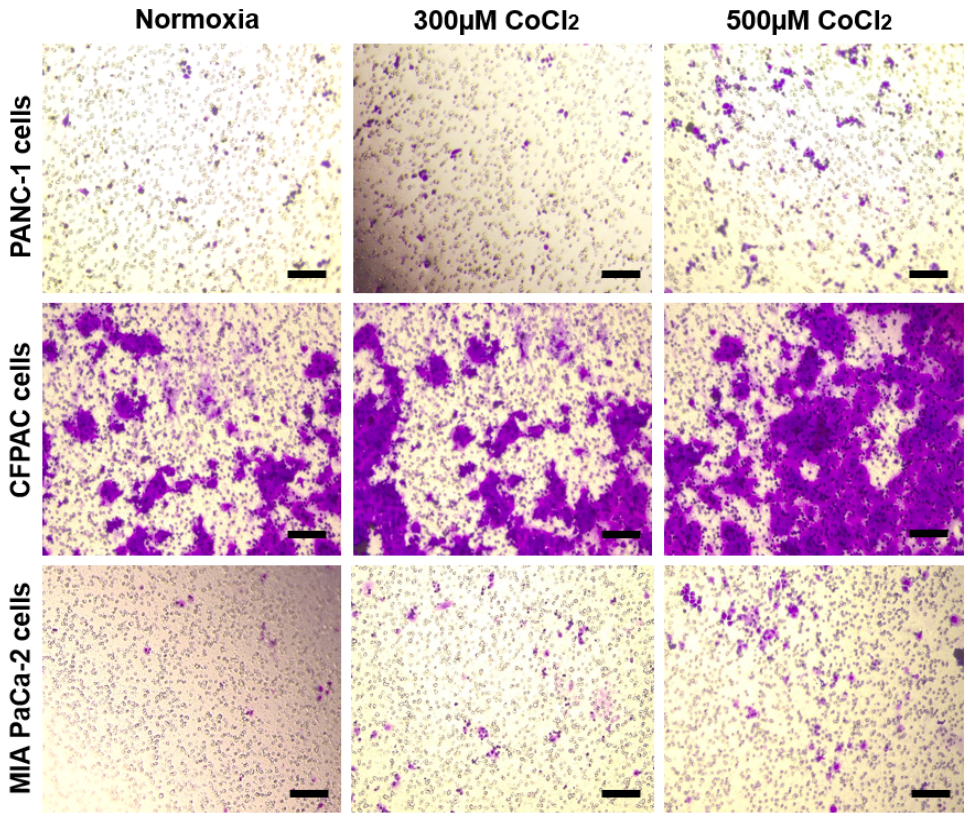

Figure 3.13. Crystal violet staining of migrated PANC-1, CFPAC and MIA PaCa-2 cells through transwell inserts after normoxia, 300 μM and 500 μM of cobalt chloride, n=1. Scale bar 150μm.

Next, to investigate the migration in hypoxic chamber and to evaluate the role of RAGE in changing migration behavior of pancreatic cancer cells we performed transwell assays and measured the difference in migration rate using alamar blue assay. We observed significant increase in migration rate in cell-lines under hypoxic conditions - MIA PaCa-2 (**$p<0.01$), CFPAC (*$p<0.05$) and PANC-1 (**$p<0.01$) compared to normoxic conditions. Next, we treated all cell lines with FPS-ZM1, a RAGE antagonist, and we observed significant decrease in migration rates in all cell lines under hypoxic conditions. However, we did not observe any change in migration in the presence of FPS-ZM1 under normoxic cells. We did not find any inhibitory effect from the vehicle of FPS-ZM1 that confirms that inhibitory response does not come from the vehicle (DMSO) (figure 3.14).

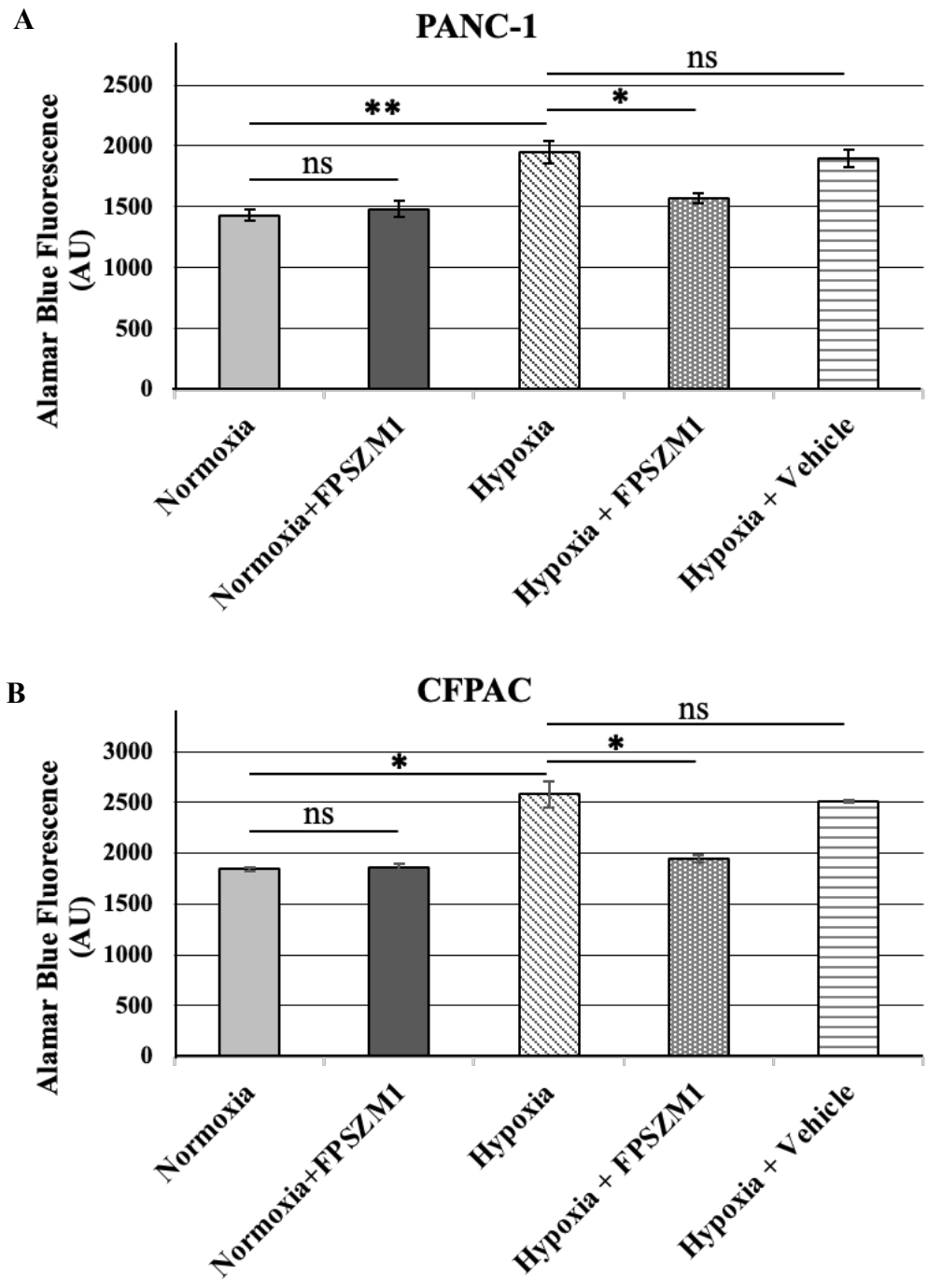

Figure 3.14. Migration of PANC-1, MIA PaCa-2 and CFPAC cells in response to normoxia, hypoxia, FPSZM1 and vehicle (DMSO) treatment under hypoxia, n=3, *p<0.05 **p<0.01.

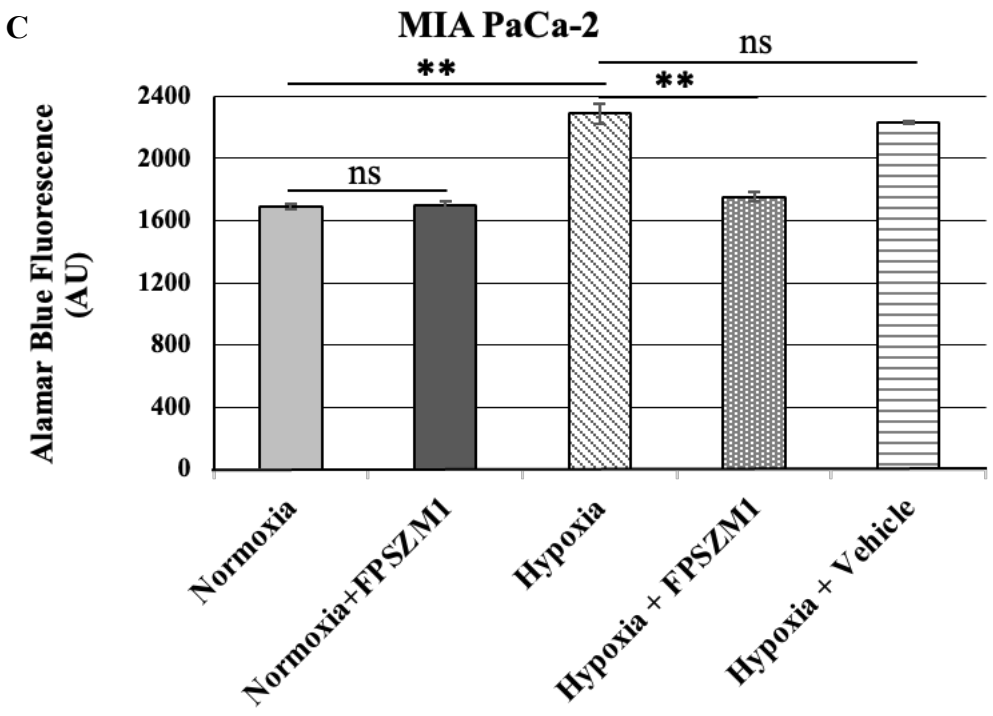

Figure 3.14. Migration of PANC-1, MIA PaCa-2 and CFPAC cells in response to normoxia, hypoxia, FPSZM1 and vehicle (DMSO) treatment under hypoxia, n=3, *p<0.05, **p<0.01 (continued).

3.6. Discussion

In the present study, we used three human pancreatic cancer cells lines - PANC-1, MIA PaCa-2 and CFPAC to demonstrate the role of RAGE in autophagy and migration of pancreatic cancer cells under hypoxia. Emerging evidence suggests that hypoxia governs cancer cell resistance to chemotherapy drugs and promoting tumor survival by inducing autophagy. Yang et al., showed enhanced autophagy under 1% oxygen levels in T24 human bladder cancer cells that further promoted the resistance to gemcitabine treatment. The authors demonstrated that the hypoxia stabilized HIF-1α upregulated BNIP3 and Beclin1 expression levels in human bladder cancer cells. In-addition, suppression of HIF-1α was observed to downregulate the expression levels of BNIP3 and Beclin1, indicating hypoxia-mediated autophagy in bladder cancer cells [297]. Beclin-1 is a central regulator of autophagy that participates in forming the isolation

membrane, a double-membrane structure that engulfs cytoplasmic material to form the autophagosome [278]. BNIP3 also assists in autophagy by forming a dimer with LC3 and facilitating the formation of an autophagosome [298].

Autophagy is also reported to be increased in pancreatic cancer cells in resected tumors that can be correlated with poor patient outcome [299]. The findings from previous studies of our group indicated that overexpressed RAGE in pancreatic cancer cells (PANC-1 FLR) under normoxic conditions participated in promoting autophagy [19]. However, in the present study we investigated the role of RAGE in promoting autophagy in pancreatic cancer under hypoxic conditions.

Kang et al., have also reported hypoxia mediated autophagy in pancreatic cancer cells (Panc02 and Panc2.03) via RAGE-RAF-MEK-ERK and RAGE-PI3K-AKT signaling pathways [2]. The authors demonstrated that upon RAGE knockdown with RAGE specific siRNA, there is a reduction in the level of LC-II/LC-I ratio. Moreover, authors have also showed about 1.5-fold increase in RAGE levels in PANC-1 and CFPAC pancreatic cancer cell lines incubated under 1% hypoxic conditions for 24 hours, however, they did not carry out further any studies related to autophagy studies with these cell lines. Interestingly, in-line to these results, we also observed approximately 1.5-fold increase in RAGE expression in all three cancer cell lines incubated in hypoxic chamber for 24 hours compared to normoxic conditions. We also investigated the expression of RAGE via immunoprecipitation method, however, did not get reproducible results in all three sets due to excessive background. In another study, Kang et al., have investigated the role of HMGB1 in promoting autophagy under normoxic conditions in pancreatic tumor cell lines. The authors demonstrated that tumor cell death release HMGB1 proteins that interact with RAGE present on neighboring cancer cells and enhance their cell survival by inducing autophagy.

Additionally, the knockdown of HMGB1 resulted in reduction of the intracellular pool of HMGB1 that further reduced the autophagy.

In the present study, we also revealed that the autophagy in PANC-1 and MIA PaCa-2 cells under hypoxia is RAGE mediated, that we determined after RAGE blockage with small molecule RAGE inhibitor, FPS-ZM1 resulting in decrease in the level of LC3-II/I ratio. However, we did not observe significant change in LC3-II/I ratio in CFPAC cells under hypoxia, which may be possible because of existing levels of HIF-1α in CFPAC cells even under normoxic conditions. Presence of HIF-1α in CFPAC cells under normoxic condition suggests that there is some degree of hypoxia under normal conditions (figure 3.6). Future studies may be required to elucidate the underlying mechanism of RAGE activation under hypoxia. It is reported that HIF-1α upregulates many RAGE ligands under hypoxic conditions including HMGB1 [175] [176] , S100A8/9 [186] and S100A4 [181] by interacting with their HRE promoter region. However, the clear evidence for RAGE activation in pancreatic cancer via these ligands under hypoxic conditions is not well established.

The role of hypoxia in regulating tumor cell migration and invasion through numerous molecular pathways have been discussed. Ming et. al, have reported increased migration of MCF7 breast cancer cells under hypoxic conditions. The authors demonstrated that hypoxia in breast cancer cells promotes miRNA levels of miR-302a gene responsible for increased migration [300]. Similarly, another study showed increased migration of breast cancer cells (MDA-MB-231 and MCF-7) in a hypoxic chamber and discussed the role of HIF-1α mediated CXCR6 overexpression (chemokine receptor) in increasing the migration [301]. Another study by Lin et al. demonstrated about 10% increase in migration of hepatocellular carcinoma (HCC) cells under hypoxic conditions. The study indicated that HIF-1α (stabilized under hypoxic conditions) plays a critical

role in promoting SNAI1 mediated EMT in HCC cells [302]. Furthermore, Tafani et. al. demonstrated increased migration and invasion of MDA-MB-231 and MCF-7 breast cancer cells and HeLa cervical cancer cells are mediated via RAGE upregulation under hypoxic conditions. The authors further explained that silencing of RAGE in these cells resulted in decrease migration rate [171].

In the present study, we observed increased cell migration of all three pancreatic cell lines under hypoxic conditions. We also observed that RAGE upregulation under hypoxia is the possible mechanism of increase in migration of pancreatic cancer cells that we investigated via RAGE blocking with FPS-ZM1, a RAGE inhibitor. We found that migration in all pancreatic cell lines decreased by approximately 20 % after RAGE inhibition, indicating the contributing role of RAGE in migration under hypoxia. Moreover, we have investigated the effect of RAGE inhibitor in migration of pancreatic cancer cells under normoxic conditions. However, we did not observe any significant change in the migration of cells after RAGE inhibition. The possible reason for insignificant change in migration might be attributed to the relatively low-level RAGE (close to the limit of detection) in pancreatic cancer cell lines under normoxic conditions that elicit minor response after using RAGE inhibitor.

3.7. Conclusion

In the present study we investigated the role of RAGE in migration and autophagy of pancreatic cancer cells - MIA PaCa-2, PANC-1 and CFPAC under hypoxic conditions. We observed about 1.5-fold increase in RAGE levels in all cell lines incubated in the hypoxic chamber for 24 hours. Upregulation of RAGE levels under hypoxic conditions in cancer cells is supported by many other studies however, how RAGE upregulation under hypoxia promotes pancreatic cancer progression is still poorly explored. In the present study, we focused majorly on RAGE

mediated autophagy and migration under hypoxic conditions, however, future studies are required to uncover the involvement of RAGE ligands that would participate in autophagy and migration via RAGE activation under hypoxic conditions. We observed that under 1% oxygen levels cell migration was increased in all selected pancreatic cancer cell lines compared to their normoxic conditions. We anticipated that hypoxia promotes migration of cancer cells however to evaluate the role of RAGE in the migration we blocked RAGE with RAGE antagonist, FPS-ZM1 and observed that the migration of pancreatic cancer cells reduced by approximately 20% in all cell lines. Interestingly, we did not observe significant change in percent migration in cells under normoxic conditions after RAGE blockage. We also observed increased autophagy in PANC-1 and MIA PaCa-2 cell lines under hypoxia determined by their LC3-II/I ratio indicating that hypoxia mediates autophagy. To investigate that autophagy in PANC-1 and MIA PaCa-2 cell lines under hypoxia is RAGE mediated we blocked RAGE with FPS-ZM1. We observed decrease in the level of LC3-II/I ratio after drug treatment.

Previously, Kang et al. have shown that hypoxia mediates autophagy via RAGE in two pancreatic cancer cell-lines (Panc02 and Panc2.03). These authors showed that silencing RAGE with specific siRNAs led to a reduction in autophagy. These authors also showed an increase in RAGE levels under 1% hypoxic conditions in the two human PANC-1 and CFPAC pancreatic cancer cell lines, however, they did not carry out further studies on the association between RAGE upregulation and autophagy in these cell lines [2]. In this work, we expanded on the study of Kang et al. and we showed for the first time, in the three human pancreatic cancer cell-lines PANC-1, CFPAC and MIA PaCa-2 cell lines, that pharmacological inhibition of RAGE by FPS-ZM1, a RAGE-specific small molecule inhibitor, resulted in decrease of autophagy under hypoxia. In addition, we also explored the role of RAGE on the migration of pancreatic cancer cells, under

hypoxic conditions. We observed that targeting RAGE with FPS-ZM1 led to decrease in cell migration under hypoxia. Overall, we concluded that targeting RAGE by FPS-ZM1 in pancreatic cancer is a promising targeting approach that has the potential to reduce both autophagy and migration in pancreatic cancer cells. Our findings on role of RAGE in pancreatic cancer progression under hypoxia may contribute to reduce the expansion of pancreatic cancer.

4. ADVANCED GLYCATION ENDPRODUCTS INCREASE MIGRATION AND NF-κB ACTIVITY OF KPC CELLS

4.1. Hypothesis

Advanced glycation end-products (AGEs) are well known ligands for RAGE that participates in the proliferation and migration of various cancers [57, 58]. Previously, our group has generated a series of biologically active AGE compounds. Among them ribose modified BSA proteins have shown strong binding affinity with RAGE (Dissociation constant $K_d = 2.0 \pm 0.8$ μM) [303]. Moreover, our group has demonstrated that KPC cell lines express high level of RAGE protein (data not shown).

Based on these studies, we hypothesize that ribose modified BSA induced RAGE activation could alter proliferation and migration of pancreatic cancer cells thus contributing to the growth of pancreatic cancer. To test our hypothesis, we chose KPC 5517 cells based on their high RAGE expression levels among a set of KPC cell lines, determined by the former student of our group, Priyanka Swami. Next, we performed the cellular assays related to cell proliferation and migration.

4.2. Abstract

The objective of this chapter was to investigate proliferation and migration of pancreatic cancer cells after treatment with AGEs. For this purpose, we performed alamar blue assay to determine cell proliferation of AGE treated and untreated samples. We observed that AGE treated samples showed reduction in the proliferation in one set of data and no change in another set. Next, we performed migration studies with Boyden chamber assay and observed that treated samples showed higher migration than untreated samples. We also employed NF-κB -luciferase reporter construct to monitor NF-κB activity after AGE treatment. We found that modest increase in NF-

κB activity of treated samples in comparison to untreated samples in one set of data. However, upon repetition for the second time the increase in the NF-κB activity upon AGE stimulation was not significant. Collectively, we observed that AGEs-RAGE interaction in KPC 5517 cells increases their migration with no change in their proliferation rate.

4.3. Introduction

Advanced Glycation Endproducts (AGEs) are formed during the non-enzymatic glycation reaction between a reducing sugar and a free amino group on a protein or nucleic acid. Glycation has been reported to be linked with altered structure and functionality of native proteins [304, 305]. Glycated bovine serum albumin is a type of AGEs that has been well studied in cancer [306-308]. In this study, we utilized ribose modified bovine serum albumin protein (Rib-vH BSA) as a ligand for RAGE. Previously, our group has synthesized various modified forms of BSA proteins and characterized them on the basis of their side chain modifications, thermal stability, secondary structure, aggregation and surface charge. Then the binding affinity of these modified BSA proteins for RAGE was determined based on their K_d values [303]. It was found that Rib-vH BSA express strong binding affinity to RAGE [303].

AGEs have been reported to promote proliferation, migration and invasion of cancer cells [58, 59, 309].It has been observed that AGE (glycated BSA) treatment increased the proliferation of pancreatic cancer cells by 25% compared to the untreated samples [310]. Abe et al. demonstrated that glyceraldehyde-derived AGE (AGE2) and glycolaldehyde-derived AGE (AGE3) enhances both proliferation and migration of melanoma cells (G361 cells) *in vitro*. [58]. Moreover, researchers have also reported the role of AGEs-RAGE interaction in increasing cell migration of human oral cancer cell [58, 311, 312] and colorectal cancer [313]. AGE-RAGE interaction was also shown to increase migration of breast cancer cells- MDA-MB-231 [114] and

MCF-7 [282]. In our study, to investigate the role of AGE-RAGE interaction in promoting proliferation and migration in pancreatic cancer cells we employed KPC mice derived cells that express a high level of RAGE.

In the present study, we investigated the effect of ribose modified AGEs on the proliferation of KPC 5517 cells using different AGEs concentration (2 μg/ml, 50 μg/ml and 1000 μg/ml). Next, we carried out migration studies with 1000 μg/ml of AGEs concentration. Finally, we evaluated NF-κB activity of cells to investigate the mechanism for increased migration.

4.4. Materials and methods

4.4.1. Cell culture

The murine KPC pancreatic cancer cell line 5517 was received as a gift from Dr. Hollingsworth, University of Nebraska, Omaha Medical Center (NE). The KPC mouse is a genetically engineered mouse which incorporates conditional activation of mutant endogenous alleles of the KRAS and Trp53 genes through Cre-Lox technology [299]. KPC cell line 5517 was cultured and maintained in DMEM (ATCC) containing 10% FBS (ATCC) and 1% mixture of penicillin (100 U/ml) and streptomycin (100 μg/ml) (ATCC) under standard culture conditions (5% CO_2 and at 37ºC).

4.4.2. Preparation of Advanced Glycation End-products (AGEs)

In this study, ribose modified bovine serum albumin (Rib-vH BSA) proteins were utilized as AGE ligands that were prepared and purified in-house by Dr. Stefan Vetter in the Department of Pharmaceutical Sciences, NDSU [314]. Briefly, the preparation steps include solubilization of 20 mg/ml BSA in sodium phosphate buffer containing 1 mM EDTA and 1mM sodium azide (pH 8) and subsequent incubating BSA solution with 500 mM ribose at 37 ºC for 21 days. The obtained

protein ligands were dialyzed two times with 200 volumes of PBS at 4 ºC and sterile filtered prior to use for cell culture experiments.

4.4.3. Cell proliferation

The cells (70 % confluent) were detached using 0.25% trypsin, centrifuged at 150 x g for 5 minutes to obtain the cell pellet. The cells were resuspended in the media and counted using a hematocytometer. Next, 5 x 10^3 cells were seeded in each well of a 96 well plate. The cells were kept under low serum (1% FBS in DMEM) conditions for 24 hours before treatment with AGEs at the concentrations of 2 µg/ml, 50 µg/ml and 1000 µg/ml. The wells without any AGE treatment served as a control. After 24 hours of drug treatment, 10% v/v of Alamar Blue solution (0.1 mg/ml stock) was added to each well. After 2 hours of incubation, the fluorescence intensity was measured using emission wavelength at 590 nm and excitation wavelength at 545 nm.

4.4.4. Cell migration

For the migration assay, we seeded KPC 5517 pancreatic cancer cells in the transwell inserts with 8µm pore diameter (Greener Bio, Monroe, NC). 5×10^4 cells were added in the upper chamber of insert using 200 µl serum free media and complete medium (DMEM media containing 10% FBS) was added to the bottom chambers. Next, the cells were incubated with 1000 µg/ml AGEs for 16 hours. Upon the completion of the incubation, we used a cotton- tipped applicator to remove the media and non-migrated cells inside the inserts. Migrated cells were assessed quantitatively by analyzing fluorescence using alamar blue assay. Briefly, the inserts were dipped in 300 µl of 0.1% alamar blue solution and incubated at 37 ºC for three hours. Finally, the fluorescence was measured using emission wavelength at 590 nm and excitation wavelength at 545 nm with a Spectra Max M5 spectrophotometer (Molecular Devices, San Jose, CA).

4.4.5. Immunofluorescence

2.5 x 10^3 cells were seeded in each well of 8-well chambered glass slides (Ibidi GmbH, Martinsried, Germany) and allowed to grow 70% confluency. The cells were fixed using 4% PFA in PBS for 15 minutes, permeabilized for 10 minutes with 0.1% triton X-100 solution and finally blocked with 5% bovine serum albumin (BSA) for 1 hour. Next, the cells were incubated with RAGE primary antibody (PA1-075, Invitrogen, dilution 1:100) at 4ºC overnight. The cells were washed three times with TBST for 5 minutes each and incubated with secondary antibody - FITC conjugated donkey anti-rabbit (#705095147, Jackson Immuno Research Labs, dilution 1:100). Finally, the cells were stained with DAPI and scanned under confocal microscope (Zeiss LSM 900, Carl Zeiss Microscopy LLC, White Plains, NY) and processed using Zeiss Zen software (blue edition, version 3.1).

4.4.6. NF-κB luciferase assay

KPC 5517 cells were seeded at a density of 2.5 x 10^4 cells per well in a 24 well plate for 24 hours. Next, the cells were transfected with 500 ng/well of NF-κB/luciferase reporter plasmid for another 24 hours. This reporter plasmid contained a firefly luciferase gene under the control of a NF-κB responsive element. Lipofectamine 3000 (L3000008, Invitrogen, Waltham, MA) was employed as a transfection reagent. The cells without any transfection served as a control. Next day, the cells were incubated with fresh media containing AGE 1000µg/ml for 16 hours. At the end of the incubation, cells were washed thrice with PBS and lysed using NanoLuc lysis buffer (Promega, Madison, WI). 10µl of the resultant cell lysate was mixed with 100µl of luciferase substrate to measure the luminescence using a Quick Pak luminometer.

4.4.7. Statistical analysis

Data are presented as mean ± standard deviations. Statistical analysis was performed by using the student's t-test. The p value of less than 0.05 was considered as statistically significant. *$p<0.05$; **$p<0.01$; ***$p<0.001$. A single representative image was taken for RAGE staining by immunofluorescence. For proliferation assay, the experiment was performed twice with four technical replicates for each dataset. Migration assay and NF-κB activity were also performed twice with three technical replicates in each dataset.

4.5. Results

4.5.1. KPC cell lines express different RAGE levels

A previous student in our group, Priyanka Swami, has determined RAGE levels in all seven KPC cell lines using quantitative ELISA and the results showed that KPC cell lines contained various levels of RAGE. Cell lines 5517 expressed relatively higher levels of RAGE among the seven cell-lines tested (657.2 ± 84.7 pg of RAGE). Hence, we chose high RAGE expressing KPC 5517 cell line for further experiments.

4.5.2. RAGE is expressed in KPC cells

The immunofluorescence staining of KPC 5517 cells performed by a former student of our group, Sultan Kadasah, confirmed expression of RAGE protein in KPC 5517 cells. We also observed that RAGE was not only expressed on the cell surface but was also distributed in the cytoplasm.

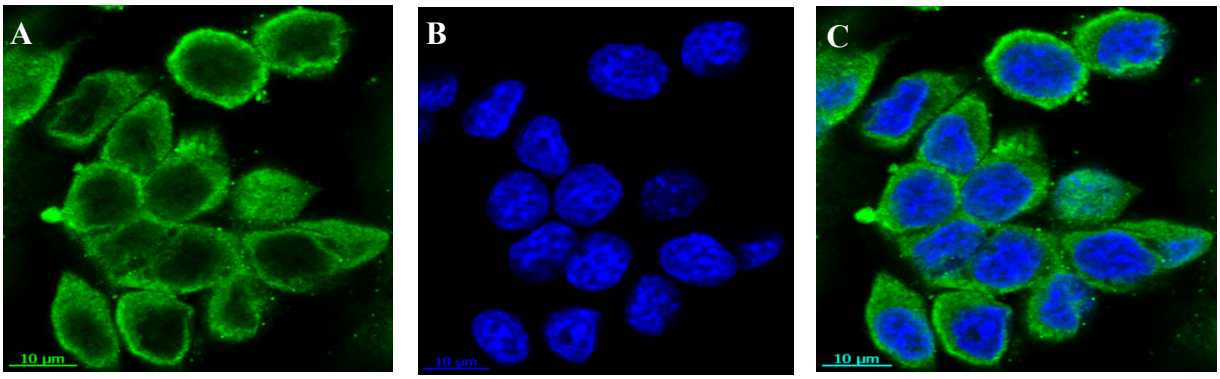

Figure 4.1. Expression of RAGE in KPC 5517 cell line as determined by immunofluorescence (Sultan Kadasah). A: RAGE staining. B: DAPI staining. C: Merged image, n=1, scale bar 10µm.

4.5.3. Cell proliferation decreases in the presence of AGEs

We determined the effect of various AGEs concentrations on the cell proliferation of KPC cell line 5517 over a period of 24 hours. The data showed that after AGE treatment of 2 µg/ml, 50 µg/ml and 1000 µg/ml there was a modest decrease in proliferation in one batch of cells (figure 4.2 A) and no change in second batch of cells (figure 4.2 B) relatively to control untreated samples. These variations in experimental outcomes might have occurred because we used an indirect method (Alamar Blue assay) to measure cell proliferation. Viable cells reduce alamar blue reagent's active compound resazurin into resorufin, through the activity of NADPH dehydrogenase in mitochondria. Resorufin can be measured by fluorescence spectrometry. Other direct methods could have been used: one method consists in counting directly viable cells in a sample, after staining with Trypan blue. Using this more direct method, only viable cells are counted. Dead cells are not counted because they are stained blue.

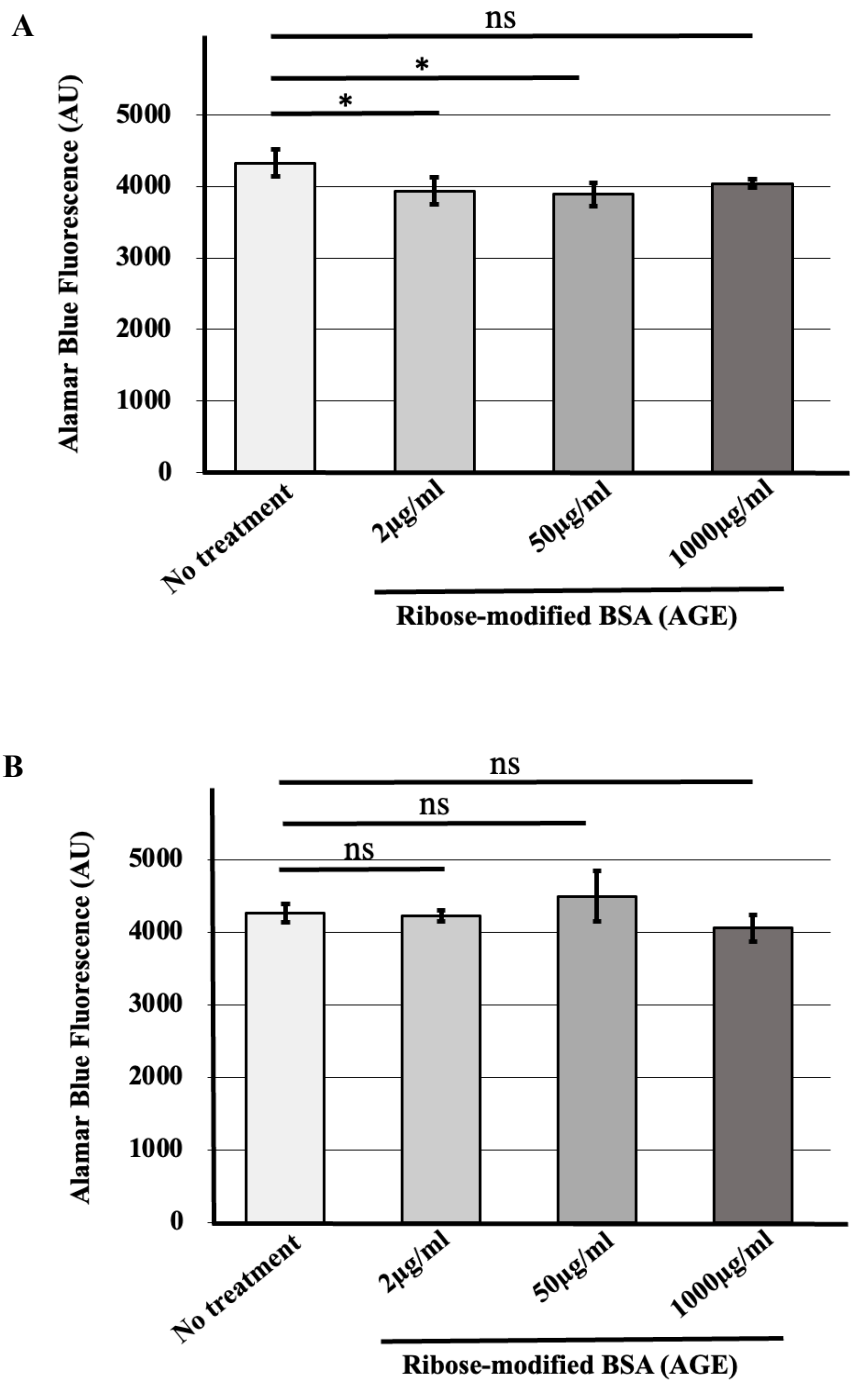

Figure 4.2. Proliferation of KPC 5517 (A) Batch 1 and (B) Batch 2 in the presence of 2 µg/ml, 50 µg/ml and 1000 µg/ml of AGE as determined by alamar blue fluorescence assay. * $p<0.05$, n=2; with 4 technical replicates each experiment.

4.5.4. Cell migration increases in the presence of AGEs

Next, we examined the migration potential of KPC 5517 cell line with the Boyden Chamber assay upon treatment with 1000 µg/ml of AGE. We observed significant increase in percent migration of KPC 5517 cells compared to untreated cells.

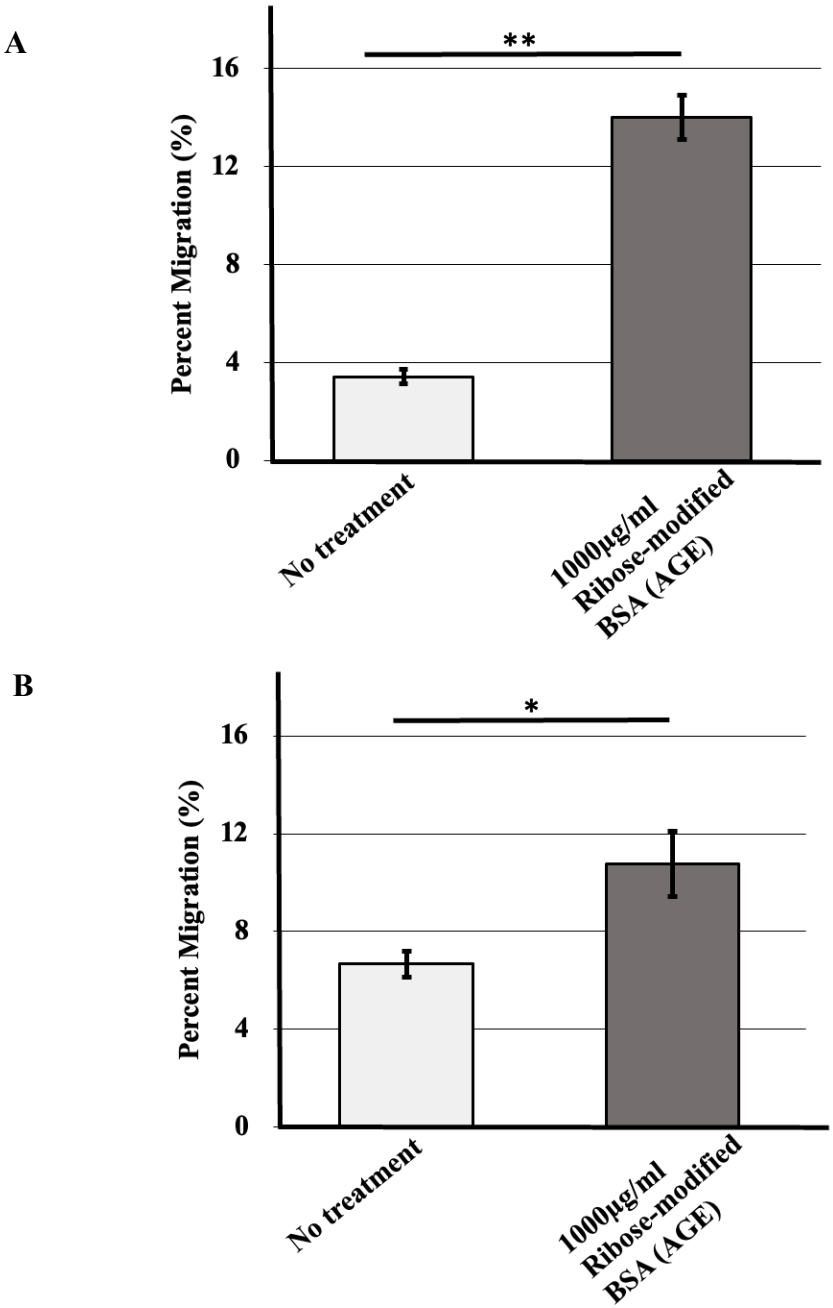

Figure 4.3. Migration assessed of KPC 5517 (A) Batch 1 and (B) Batch 2 cells upon treatment with AGEs at concentration of 1000 µg/ml using boyden chamber assay, ** $p<0.01$, * $p<0.05$, n=2; with three technical replicates each experiment.

4.5.5. AGEs stimulation leads to an increase in NF-κB activity

We measured the activity of NF-κB by transiently transfected KPC 5517 cells with a luciferase reporter plasmid containing NF-κB response elements. We observed a modest increase in NF-κB activity in one batch of cells (figure 4.4 A) and no significant increase in second batch of cells (figure 4.4 B) in AGE treated cells (1000 µg/ml) compared to untreated cells.

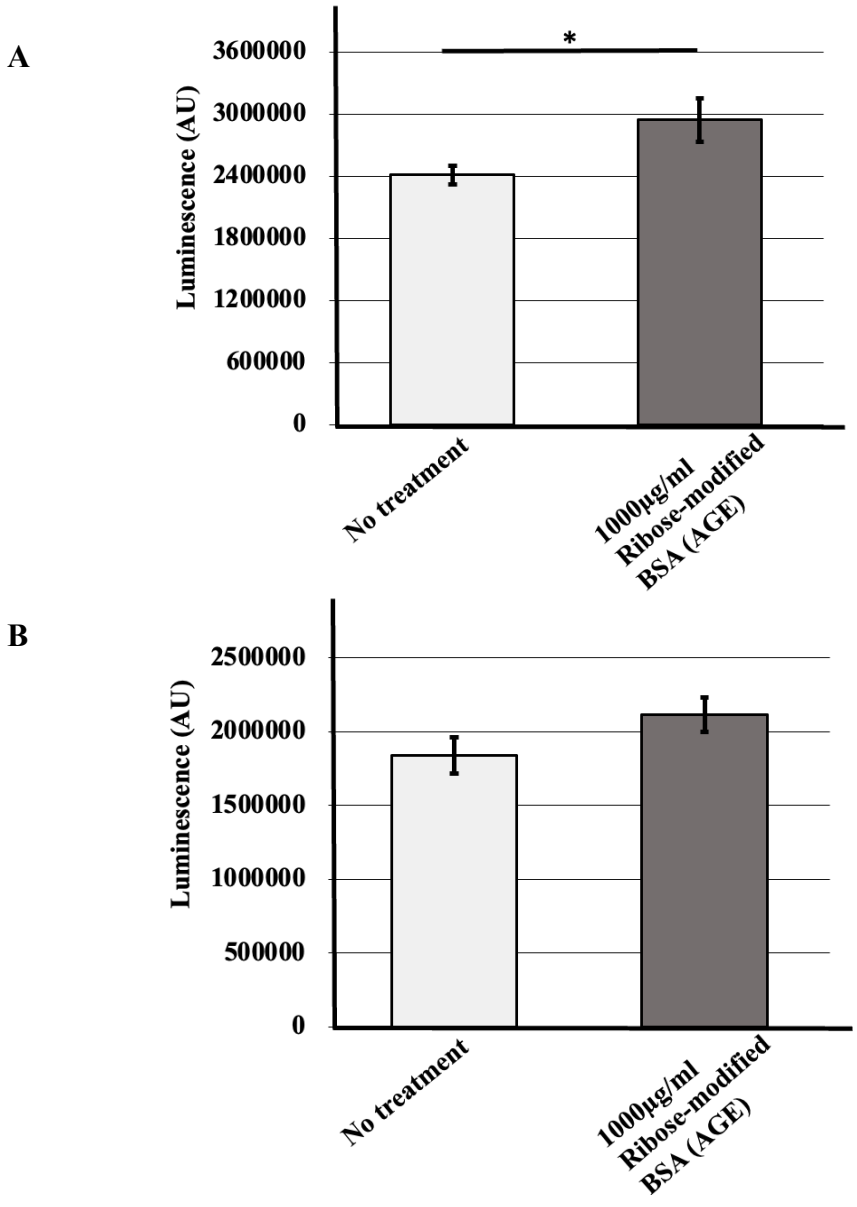

Figure 4.4. NF-κB activity was measured by transfecting the KPC 5517 (A) Batch 1 and (B) Batch 2 cells with luciferase reporter plasmid containing NF-κB response elements, * $p<0.05$, n=2; with three technical replicates each experiment.

4.6. Discussion

In this chapter we investigated the effects of AGE-RAGE interaction on the proliferation and migration of KPC 5517 pancreatic cancer cell line. It is reported that AGE-RAGE interaction can act differently in different cancers. Abe et al., demonstrated the interaction between different AGE types (AGE1, glucose-derived AGE; AGE2, glyceraldehyde-derived AGE; AGE3, glycolaldehyde-derived AGE; AGE4, methylglyoxal-derived AGE; AGE5, glyoxal-derived AGE) with RAGE and observed significant increase in proliferation of melanoma cells (G361 cells) with AGE2 and AGE3 stimulation whereas other AGEs (AGE1, AGE4 and AGE5) did not show any effect on proliferation [58]. On contrary, Kim et. al, observed increased proliferation of acute myeloid leukemia (HEL) cells after treatment of cells with 200 μg/ml of glucose-derived AGEs for 12 hours [57]. In another study, Ko et al., demonstrated that the treatment of SAS human oral cancer cells with glyceraldehyde-derived AGEs inhibited cell proliferation [315]. In Mia PaCa-2 pancreatic cancer cells, Yamamoto et. al, investigated the effect of glucose-derived AGE in a dose dependent manner and observed that treatment with 1 μg/ml AGE concentration increased the proliferation by 25% compared to the untreated control sample [310]. In the present study we also utilized glucose derived AGEs based on their strong affinity with RAGE, demonstrated by previous member of our group. In our findings, the effect of AGEs on KPC 5517 proliferation appeared to be different than the results seen by Yamamoto et al. and Kim et al, because we did not observe any significant change in proliferation with the treatment of different AGE concentrations. However, our results are consistent with the results observed by Abe et al., where they utilized various concentrations of glucose derived AGEs ranging from 0-1000 μg/ml and did not observe any change in proliferation.

Next, we examined the effect of AGE-RAGE interaction on migration of KPC 5517 pancreatic cancer cell line. Deng and colleagues have demonstrated that glucose-derived AGEs treatment (200 μg/ml) resulted in increase in the migration and invasion rates of LoVo and SW620 colorectal cancer cells [313]. Moreover, it has been reported that glyceraldehyde-based AGEs promoted migration of human oral cancer cells (SAS) [315] and lung cancer cells (A549) [312]. Moreover, Abe. et. al., have observed 138% and 108% increase in the migration by glyceraldehyde-derived and glycolaldehyde-derived AGEs, respectively after 16h of migration assay [58]. To the best of our knowledge, we did not see any AGE-RAGE interactions in pancreatic cancer migration. However, our former group member, Priyanka Swami observed decreased migration in RAGE overexpressed PANC-1 FLR2 pancreatic cancer cells that was reverted upon RAGE knockdown with siRNA specific for RAGE [316]. Our results are not in-line with these results, because we observed modest increase in migration in KPC 5517 pancreatic cancer cells. Moreover, we found that the NF-κB activity of KPC 5517 cells were modestly increased after 1000 μg/ml AGEs treatment. Several reports suggested that NF-κB is associated with cancer cell migration, invasion, metastasis [317, 318]. Menini S et al., showed increased proliferation of PANC-1 and MIA PaCa-2 pancreatic cancer cells via increased NF-κB activity upon RAGE activation by Nϵ-carboxymethyllysine (CML) AGEs [319]. Another study indicates ROS/ERK/NF-κB mediated migration in BxPC-3 and PANC-1 pancreatic cancer cells that were reduced by the treatment of curcumin, N-acetylcysteine (NAC) and PD 98059 (an ERK inhibitor) drugs [317]. Similarly, Yan et al., showed increased expression levels of NF-κB p65 in squamous carcinoma of the head and neck cancer (SCCHN) that was associated with increased cell invasion. Further, authors demonstrated that treatment of highly metastatic SCCHN cells with NF-κB inhibitors resulted in reduced cell invasion [318]. Our former group member, Sultan Kadasah has

also observed 1.5-fold increase in NF-κB activity upon 500 μg/ml of ribose modified BSA (AGE) treatment in PANC- 1 and MIA PaCa-2 pancreatic cancer cells compared to non-treated cells. It was also observed that pre-incubation with anti- RAGE antibody IgG 2A11 abolished AGE-induced NF-κB activation.

4.7. Conclusion

The accumulation of AGEs in human serum through exogeneous consumption or endogenous production has been associated with several chronic inflammatory diseases such as diabetes, nephropathy and as well as cancer. AGE-RAGE mediated interactions have been shown to regulate multiple signaling pathways in cancer such as the JAK/Stat or Ras-Raf-MAPK pathways, which are involved in cell proliferation. AGEs have been reported to promote pancreatic cancer cell proliferation of MIA PaCa-2 cells with increasing concentration from 0μg/ml-1μg/ml [310]. In the present study, we investigated the effect of AGEs on the migration of pancreatic cancer cells using the murine KPC 5517 pancreatic cancer cell line: this forms the novelty of our study. In a parallel study, we also investigated the effect of AGEs on the proliferation of KPC 5517 pancreatic cancer cells. KPC 5517 cells were derived from a genetically engineered PDAC orthotopic mouse model and express high RAGE levels. We found modest decrease in one batch of cells and no change in proliferation in another batch of cells after treatment with ribose-modified AGEs. We also observed increase in cell migration upon treatment with ribose-modified AGEs. Furthermore, we also investigated NF-κB activity in KPC 5517 cell lines. We observed significant increase in one set of experiment but not in another set. Since data from proliferation assay and NF-κB activity were not reproducible, we cannot establish the effect of ribose-modified AGEs on KPC 5517 cells. Therefore, further studies are required to demonstrate the effect of ribose-derived AGEs on proliferation and NF-κB activity. Effect of other AGEs can also be studied to investigate

AGE-RAGE mediated proliferation and migration. Overall, our findings on AGE-RAGE interactions in the proliferation and migration in pancreatic cancer cells may contribute to reduce the progression of pancreatic cancer.

5. SUMMARY AND CONCLUSION

Emerging evidence suggests that activation of RAGE occurs in pathological conditions such as cancer, thus we need to understand the biology of RAGE to design therapeutic agents that can inhibit the activation of this receptor. Various studies have demonstrated high expression of RAGE in melanoma that indicate the crucial role of RAGE in melanoma pathogenesis. However, it is equally important to understand the exact location of RAGE inside the cells to design specific inhibitors or blockers that could target RAGE effectively.

In chapter 2 of our study, we investigated RAGE localization in melanoma cells in their 3D architecture using WM115, WM266 and B16F10 cells. We performed immunofluorescence assay to determine the localization of RAGE. Our results showed RAGE is localized at the surface of cells present in WM115 and B16F10 spheroids. However, WM266 spheroids showed more intracellular expression. We also observed surface localization of RAGE in B16F10 tumors generated in lung colonization mice compared to intracellular localization of RAGE in 2D monolayer conditions. In our ongoing studies, we are also generating tumors of WM115 and WM266 cells in a subcutaneous mice model to better understand the localization of RAGE in these tumors.

In chapter 3 of our study, we investigated the role of RAGE in migration and autophagy of pancreatic cancer cells - MIA PaCa-2, PANC-1 and CFPAC under hypoxic conditions. Hypoxia is marked by increased expression of HIF-1α. We performed Western blotting for analyzing the expression of HIF-1α and found increase in its expression in hypoxic conditions versus normoxia. RAGE upregulation has also been reported in various cancers. We have found increases in RAGE levels in all three pancreatic cancer cell lines under hypoxia using ELISAs. Studies show that hypoxia promotes autophagy and migration of cancer cells. However, the importance of RAGE

mediated autophagy and migration of pancreatic cancer cells under hypoxia is not completely understood. We observed that the migration of pancreatic cancer cells reduced by approximately 20% in all cell lines under hypoxic conditions after RAGE blockage with a RAGE antagonist, FPS-ZM1. Moreover, we observed a decrease in the level of LC3-II/I ratio in PANC-1 and MIA PaCa-2 cell lines upon RAGE inhibition under hypoxia, indicating reduction in autophagy upon RAGE inhibition. However, we did not observe significant effect of RAGE inhibition on CFPAC cells under hypoxia.

RAGE also plays an important role in proliferation and migration of various cancer cells. Studies report increased level of RAGE ligands in many cancer types. In the third study, we investigated the effect of one of the RAGE ligands, ribose-modified AGEs, on the proliferation and migration of murine pancreatic cancer cell line KPC 5517. We did not observe significant change in proliferation of KPC 5517 cells after treatment with ribose-modified AGEs. However, we found increased migration of pancreatic cancer cells upon RAGE activation by AGEs. We also observed significant increase in NF-κB activity in KPC 5517 cells in one set of experiments but not in another set. Thus, we cannot conclude that AGEs treatment increase NF-κB activity in KPC 5517 cells.

6. FUTURE DIRECTION

We have studied RAGE localization in melanoma cells in chapter 2. Our immunofluorescence studies revealed that RAGE localization is influenced by 3D cellular architectures. However, to further compare RAGE levels between cell surface RAGE and intracellular RAGE, we could utilize the Western blot technique and quantify RAGE levels in the membrane cell lysate fraction and cytoplasmic fraction of the cells.

We observed that RAGE is expressed mainly at the surface of WM115 cell spheroids, however, its sister cell line WM266 (derived from the same patient) showed intracellular localization of RAGE, that may be attributed to their phenotypic differences. Thus, future studies are required to understand the difference in RAGE localization between WM115 and WM266 cell lines in their 3D spheroid models. To evaluate this difference in localization, RAGE internalization process can be studied in these cell lines by transfecting both cell lines with chromophores (Texas Red chromophores) containing RAGE protein and monitor their RAGE internalization. Furthermore, to rule out the possibility of the presence of RAGE isoforms intracellularly, we could measure the levels of RAGE isoforms using western blot technique.

In chapter 3, we have established hypoxic conditions using chemical inducer and hypoxic chamber to understand the effect of hypoxia on pancreatic cancer progression. To determine that hypoxic conditions were achieved, we analyzed HIF-1α expressions by Western blot. However, to measure the activity of HIF-1α that participates in the transcription of VEGF, LDHase and PGKinase genes under hypoxic conditions, we could measure the transcriptional levels of these HIF-1α targeted genes. Our results showed that RAGE promotes autophagy under hypoxia that we determined by evaluating LC3-II/I ratio, however, these results can be supported by analyzing other autophagy related proteins. p62 interacts with polyubiquitinated proteins and these

complexes are selectively sequestered in the autophagosomes through direct binding with LC3. p62 is efficiently degraded in autophagosomes, therefore, p62 degradation directly correlates with autophagic activity. Thus, in future, western blot analysis of p62 degradation would be beneficial to investigate increased autophagy in hypoxic conditions. It is also worthwhile to uncover what RAGE ligands would be upregulated under hypoxic conditions that participates in RAGE dependent autophagy and migration. To investigate RAGE ligands, a western blot of both cell lysate and the media concentrate can be carried out and a specific antibody against HMGB1, S100 proteins can be used to detect their levels both in cell lysate and in culture media (in case of extracellular release).

We assessed migration of pancreatic cells by transwell migration assay, and we found that migration increases under hypoxic conditions. To further investigate migration, it would be interesting to identify the expression of migratory proteins such as vinculin, talin and paxillin by western blot to better understand the influence of hypoxia on migration of pancreatic cancer cells. Migration involves cell motility and proteins involved in focal adhesion form crucial parts of this process. Focal adhesion involves a multi-protein complex made up of vinculin, talin and paxillin. Focal adhesion complexes provide a stable connection between the cytoskeleton of cells and the substratum. Vinculin is attached to talin at one end and paxillin at another end, forming a critical part of focal adhesions. Thus, western blot analysis of the levels of vinculin, talin and paxillin would support the changes in cell migration observed under hypoxic conditions upon RAGE inhibition. Accordingly, decreases in the expression levels of these proteins would corelate with increased cell migration.

In chapter 4, we have found that RAGE activation by glucose modified AGEs influence proliferation and migration of pancreatic cancer cells. We assessed changes in cell proliferation

using the Alamar blue assay that measures the metabolic activity of viable cells and is an indirect method of measuring cell proliferation. Thus, in the future, direct cell counting methods could be used: one method consists in counting directly viable cells in a sample, after staining with Trypan blue. Using this more direct method, only viable cells are counted. Dead cells are not counted because they are stained blue. Moreover, we observed that RAGE activation by AGEs further promotes NF-κB activity. Thus, as a part of future studies, it would be interesting to determine NF-κB targeted genes by PCR that could involve in pancreatic cancer progression such as p53 and cyclin D1. p53 is a tumor-suppressor protein that is altered in most cancers and involves in cell-cycle arrest and apoptosis. cyclin D1 is a proto-oncogene that regulates G1 to S phase progression in many cell types and participates in the progression of various cancers. It would also be worthwhile to determine the signaling pathways that would lead to NF-κB activation upon RAGE activation by AGEs. The important signaling pathways involved in the activation of NF-κB are Protein kinase C (PKC), PI3K and AKT that could be investigated in the future by PCR and western blot techniques.

All the above proposed studies would aim for a better understanding of the biology of RAGE in pancreatic cancer and melanoma.

REFERENCES

1. Logsdon, C.D., et al., *RAGE and RAGE ligands in cancer.* Current molecular medicine, 2007. **7**(8): p. 777-789.
2. Kang, R., et al., *RAGE is essential for oncogenic KRAS-mediated hypoxic signaling in pancreatic cancer.* Cell death & disease, 2014. **5**(10): p. e1480-e1480.
3. Neeper, M., et al., *Cloning and expression of a cell surface receptor for advanced glycosylation end products of proteins.* Journal of Biological Chemistry, 1992. **267**(21): p. 14998-15004.
4. Schmidt, A.M., et al., *The multiligand receptor RAGE as a progression factor amplifying immune and inflammatory responses.* The Journal of clinical investigation, 2001. **108**(7): p. 949-955.
5. Medzhitov, R. and C.A. Janeway, *Innate immunity: the virtues of a nonclonal system of recognition.* Cell, 1997. **91**(3): p. 295-298.
6. Taylor, M.E. and K. Drickamer, *Structural requirements for high affinity binding of complex ligands by the macrophage mannose receptor.* Journal of Biological Chemistry, 1993. **268**(1): p. 399-404.
7. Sugaya, K., et al., *Three genes in the human MHC class III region near the junction with the class II: gene for receptor of advanced glycosylation end products, PBX2 homeobox gene and a notch homolog, human counterpart of mouse mammary tumor gene int-3.* Genomics, 1994. **23**(2): p. 408-419.
8. Verweij, C.L., *How RAGE turns in rage.* Genes & Immunity, 2002. **3**(3): p. 117-118.
9. Brett, J., et al., *Survey of the distribution of a newly characterized receptor for advanced glycation end products in tissues.* The American journal of pathology, 1993. **143**(6): p. 1699.
10. Schmidt, A.M., et al., *Regulation of human mononuclear phagocyte migration by cell surface-binding proteins for advanced glycation end products.* The Journal of clinical investigation, 1993. **91**(5): p. 2155-2168.
11. Fehrenbach, H., et al., *Receptor for advanced glycation endproducts (RAGE) exhibits highly differential cellular and subcellular localisation in rat and human lung.* Cell Mol Biol (Noisy-le-grand), 1998. **44**(7): p. 1147-57.
12. Katsuoka, F., et al., *Type II alveolar epithelial cells in lung express receptor for advanced glycation end products (RAGE) gene.* Biochemical and biophysical research communications, 1997. **238**(2): p. 512-516.
13. Rong, L.L., et al., *Antagonism of RAGE suppresses peripheral nerve regeneration.* The FASEB Journal, 2004. **18**(15): p. 1812-1817.
14. Sakatani, S., et al., *Deletion of RAGE causes hyperactivity and increased sensitivity to auditory stimuli in mice.* PloS one, 2009. **4**(12): p. e8309.
15. Zhou, Z., et al., *Regulation of osteoclast function and bone mass by RAGE.* The Journal of experimental medicine, 2006. **203**(4): p. 1067-1080.
16. Sims, G.P., et al., *HMGB1 and RAGE in inflammation and cancer.* Annual review of immunology, 2009. **28**: p. 367-388.
17. Sparvero, L.J., et al., *RAGE (Receptor for Advanced Glycation Endproducts), RAGE ligands, and their role in cancer and inflammation.* Journal of translational medicine, 2009. **7**(1): p. 17.

18. Kang, R., et al., *The expression of the receptor for advanced glycation endproducts (RAGE) is permissive for early pancreatic neoplasia.* Proceedings of the National Academy of Sciences, 2012. **109**(18): p. 7031-7036.
19. Kang, R., et al., *The receptor for advanced glycation end products (RAGE) sustains autophagy and limits apoptosis, promoting pancreatic tumor cell survival.* Cell Death & Differentiation, 2010. **17**(4): p. 666-676.
20. Taguchi, A., et al., *Blockade of RAGE-amphoterin signalling suppresses tumour growth and metastases.* Nature, 2000. **405**(6784): p. 354-60.
21. Gebhardt, C., et al., *RAGE signaling sustains inflammation and promotes tumor development.* The Journal of experimental medicine, 2008. **205**(2): p. 275-285.
22. Heijmans, J., et al., *Rage signalling promotes intestinal tumourigenesis.* Oncogene, 2013. **32**(9): p. 1202-1206.
23. DiNorcia, J., et al., *RAGE gene deletion inhibits the development and progression of ductal neoplasia and prolongs survival in a murine model of pancreatic cancer.* Journal of Gastrointestinal Surgery, 2012. **16**(1): p. 104-112.
24. Tateno, T., et al., *Expression of receptor for advanced glycation end products (RAGE) is related to prognosis in patients with esophageal squamous cell carcinoma.* Annals of surgical oncology, 2009. **16**(2): p. 440-446.
25. Landesberg, R., et al., *The expression of the receptor for glycation endproducts (RAGE) in oral squamous cell carcinomas.* Oral Surgery, Oral Medicine, Oral Pathology, Oral Radiology, and Endodontology, 2008. **105**(5): p. 617-624.
26. Bartling, B., et al., *Proliferative stimulus of lung fibroblasts on lung cancer cells is impaired by the receptor for advanced glycation end-products.* American journal of respiratory cell and molecular biology, 2006. **34**(1): p. 83-91.
27. Takeuchi, A., et al., *Endogenous secretory receptor for advanced glycation endproducts as a novel prognostic marker in chondrosarcoma.* Cancer, 2007. **109**(12): p. 2532-2540.
28. Riuzzi, F., G. Sorci, and R. Donato, *RAGE expression in rhabdomyosarcoma cells results in myogenic differentiation and reduced proliferation, migration, invasiveness, and tumor growth.* The American journal of pathology, 2007. **171**(3): p. 947-961.
29. Bongarzone, S., et al., *Targeting the receptor for advanced glycation endproducts (RAGE): a medicinal chemistry perspective.* Journal of medicinal chemistry, 2017. **60**(17): p. 7213-7232.
30. Ding, Q. and J.N. Keller, *Evaluation of rage isoforms, ligands, and signaling in the brain.* Biochimica et Biophysica Acta (BBA)-Molecular Cell Research, 2005. **1746**(1): p. 18-27.
31. Koch, M., et al., *Structural basis for ligand recognition and activation of RAGE.* Structure, 2010. **18**(10): p. 1342-1352.
32. Xu, D., et al., *Stable RAGE-heparan sulfate complexes are essential for signal transduction.* ACS chemical biology, 2013. **8**(7): p. 1611-1620.
33. Yatime, L. and G.R. Andersen, *Structural insights into the oligomerization mode of the human receptor for advanced glycation end-products.* The FEBS journal, 2013. **280**(24): p. 6556-6568.
34. Mueller, B.K., S. Subramaniam, and A. Senes, *A frequent, GxxxG-mediated, transmembrane association motif is optimized for the formation of interhelical Cα–H hydrogen bonds.* Proceedings of the National Academy of Sciences, 2014. **111**(10): p. E888-E895.

35. Hudson, B.I., et al., *Interaction of the RAGE cytoplasmic domain with diaphanous-1 is required for ligand-stimulated cellular migration through activation of Rac1 and Cdc42.* Journal of Biological Chemistry, 2008. **283**(49): p. 34457-34468.
36. Huttunen, H.J., C. Fages, and H. Rauvala, *Receptor for advanced glycation end products (RAGE)-mediated neurite outgrowth and activation of NF-κB require the cytoplasmic domain of the receptor but different downstream signaling pathways.* Journal of Biological Chemistry, 1999. **274**(28): p. 19919-19924.
37. Sakaguchi, M., et al., *TIRAP, an adaptor protein for TLR2/4, transduces a signal from RAGE phosphorylated upon ligand binding.* PloS one, 2011. **6**(8): p. e23132.
38. Hudson, B.I., et al., *Identification, classification, and expression of RAGE gene splice variants.* The FASEB Journal, 2008. **22**(5): p. 1572-1580.
39. Ostendorp, T., et al., *Expression and purification of the soluble isoform of human receptor for advanced glycation end products (sRAGE) from Pichia pastoris.* Biochemical and biophysical research communications, 2006. **347**(1): p. 4-11.
40. Raucci, A., et al., *A soluble form of the receptor for advanced glycation endproducts (RAGE) is produced by proteolytic cleavage of the membrane-bound form by the sheddase a disintegrin and metalloprotease 10 (ADAM10).* The FASEB Journal, 2008. **22**(10): p. 3716-3727.
41. Takeuchi, A., et al., *Low molecular weight heparin suppresses receptor for advanced glycation end products-mediated expression of malignant phenotype in human fibrosarcoma cells.* Cancer Science, 2013. **104**(6): p. 740-749.
42. Yonekura, H., et al., *Novel splice variants of the receptor for advanced glycation end-products expressed in human vascular endothelial cells and pericytes, and their putative roles in diabetes-induced vascular injury.* Biochemical Journal, 2003. **370**(3): p. 1097-1109.
43. Bierhaus, A., et al., *Understanding RAGE, the receptor for advanced glycation end products.* Journal of molecular medicine, 2005. **83**(11): p. 876-886.
44. Yamagishi, S.-i., et al., *Advanced glycation end products: a molecular target for vascular complications in diabetes.* Molecular Medicine, 2015. **21**(1): p. S32-S40.
45. Wautier, M.-P., et al., *Activation of NADPH oxidase by AGE links oxidant stress to altered gene expression via RAGE.* American Journal of Physiology-Endocrinology and Metabolism, 2001. **280**(5): p. E685-E694.
46. Leclerc, E., et al., *S100B and S100A6 differentially modulate cell survival by interacting with distinct RAGE (receptor for advanced glycation end products) immunoglobulin domains.* Journal of Biological Chemistry, 2007. **282**(43): p. 31317-31331.
47. Hori, O., et al., *The receptor for advanced glycation end products (RAGE) is a cellular binding site for amphoterin: mediation of neurite outgrowth and co-expression of rage and amphoterin in the developing nervous system.* Journal of biological chemistry, 1995. **270**(43): p. 25752-25761.
48. Chen, G.Y. and G. Nuñez, *Sterile inflammation: sensing and reacting to damage.* Nature Reviews Immunology, 2010. **10**(12): p. 826-837.
49. Garlick, R.L., et al., *Nonenzymatic glycation of human lens crystallin. Effect of aging and diabetes mellitus.* The Journal of clinical investigation, 1984. **74**(5): p. 1742-1749.
50. Szewczyk-Golec, K., et al., *Strategies for Modulating Oxidative Stress under Diverse Physiological and Pathological Conditions.* Oxidative Medicine and Cellular Longevity, 2018. **2018**.

51. Ayala, A., M.F. Muñoz, and S. Argüelles, *Lipid peroxidation: production, metabolism, and signaling mechanisms of malondialdehyde and 4-hydroxy-2-nonenal.* Oxidative medicine and cellular longevity, 2014. **2014**.
52. Lee, E.J., J.Y. Kim, and S.H. Oh, *Advanced glycation end products (AGEs) promote melanogenesis through receptor for AGEs.* Scientific reports, 2016. **6**(1): p. 1-11.
53. Ishibashi, Y., et al., *Metformin inhibits advanced glycation end products (AGEs)-induced growth and VEGF expression in MCF-7 breast cancer cells by suppressing AGEs receptor expression via AMP-activated protein kinase.* Hormone and metabolic research, 2013. **45**(05): p. 387-390.
54. Jiao, L., et al., *Dietary consumption of advanced glycation end products and pancreatic cancer in the prospective NIH-AARP Diet and Health Study.* The American journal of clinical nutrition, 2015. **101**(1): p. 126-134.
55. Bao, J.-M., et al., *AGE/RAGE/Akt pathway contributes to prostate cancer cell proliferation by promoting Rb phosphorylation and degradation.* American journal of cancer research, 2015. **5**(5): p. 1741.
56. Lin, L., et al., *Receptor for advanced glycation end products (RAGE) partially mediates HMGB1-ERKs activation in clear cell renal cell carcinoma.* Journal of cancer research and clinical oncology, 2012. **138**(1): p. 11-22.
57. Kim, J.Y., et al., *Advanced glycation end product (AGE)-induced proliferation of HEL cells via receptor for AGE-related signal pathways.* International journal of oncology, 2008. **33**(3): p. 493-501.
58. Abe, R., et al., *Regulation of human melanoma growth and metastasis by AGE–AGE receptor interactions.* Journal of Investigative Dermatology, 2004. **122**(2): p. 461-467.
59. Ko, S.Y., et al., *Cell migration is regulated by AGE-RAGE interaction in human oral cancer cells in vitro.* PLoS One, 2014. **9**(10): p. e110542.
60. Ueda, T., et al., *Acidic C-tail of HMGB1 is required for its target binding to nucleosome linker DNA and transcription stimulation.* Biochemistry, 2004. **43**(30): p. 9901-9908.
61. Thomas, J.O. and A.A. Travers, *HMG1 and 2, and related 'architectural'DNA-binding proteins.* Trends in biochemical sciences, 2001. **26**(3): p. 167-174.
62. Yang, H., et al., *High mobility group box protein 1 (HMGB1): the prototypical endogenous danger molecule.* Molecular medicine, 2015. **21**(1): p. S6-S12.
63. Tang, D., et al., *Endogenous HMGB1 regulates autophagy.* J Cell Biol, 2010. **190**(5): p. 881-92.
64. Völp, K., et al., *Increased expression of high mobility group box 1 (HMGB1) is associated with an elevated level of the antiapoptotic c-IAP2 protein in human colon carcinomas.* Gut, 2006. **55**(2): p. 234-242.
65. Ishiguro, H., et al., *Receptor for advanced glycation end products (RAGE) and its ligand, amphoterin are overexpressed and associated with prostate cancer development.* The Prostate, 2005. **64**(1): p. 92-100.
66. Kuniyasu, H., Y. Chihara, and T. Takahashi, *Co-expression of receptor for advanced glycation end products and the ligand amphoterin associates closely with metastasis of colorectal cancer.* Oncology reports, 2003. **10**(2): p. 445-448.
67. Bresnick, A.R., D.J. Weber, and D.B. Zimmer, *S100 proteins in cancer.* Nature Reviews Cancer, 2015. **15**(2): p. 96-109.

68. Marenholz, I., C.W. Heizmann, and G. Fritz, *S100 proteins in mouse and man: from evolution to function and pathology (including an update of the nomenclature).* Biochemical and biophysical research communications, 2004. **322**(4): p. 1111-1122.
69. Donato, R., *S100: a multigenic family of calcium-modulated proteins of the EF-hand type with intracellular and extracellular functional roles.* The international journal of biochemistry & cell biology, 2001. **33**(7): p. 637-668.
70. Donato, R., et al., *Functions of S100 proteins.* Current molecular medicine, 2013. **13**(1): p. 24-57.
71. Leclerc, E., et al., *Binding of S100 proteins to RAGE: an update.* Biochimica et Biophysica Acta (BBA)-Molecular Cell Research, 2009. **1793**(6): p. 993-1007.
72. Ichikawa, M., et al., *S100A8/A9 activate key genes and pathways in colon tumor progression.* Molecular cancer research, 2011. **9**(2): p. 133-148.
73. Arumugam, T., et al., *S100P stimulates cell proliferation and survival via receptor for activated glycation end products (RAGE).* Journal of Biological Chemistry, 2004. **279**(7): p. 5059-5065.
74. Shubbar, E., et al., *Psoriasin (S100A7) increases the expression of ROS and VEGF and acts through RAGE to promote endothelial cell proliferation.* Breast cancer research and treatment, 2012. **134**(1): p. 71-80.
75. Yin, C., et al., *RAGE-binding S100A8/A9 promotes the migration and invasion of human breast cancer cells through actin polymerization and epithelial–mesenchymal transition.* Breast cancer research and treatment, 2013. **142**(2): p. 297-309.
76. Seguella, L., et al., *S100B Protein Stimulates Proliferation and Angiogenic Mediators Release through RAGE/pAkt/mTOR Pathway in Human Colon Adenocarcinoma Caco-2 Cells.* International journal of molecular sciences, 2019. **20**(13): p. 3240.
77. Penumutchu, S.R., R.-H. Chou, and C. Yu, *Structural insights into calcium-bound S100P and the V domain of the RAGE complex.* PloS one, 2014. **9**(8): p. e103947.
78. Du, M., et al., *Direct interaction of metastasis-inducing S100P protein with tubulin causes enhanced cell migration without changes in cell adhesion.* Biochemical Journal, 2020. **477**(6): p. 1159-1178.
79. Sinha, P., et al., *Proinflammatory S100 proteins regulate the accumulation of myeloid-derived suppressor cells.* The Journal of Immunology, 2008. **181**(7): p. 4666-4675.
80. Ambartsumian, N., et al., *The metastasis-associated Mts1 (S100A4) protein could act as an angiogenic factor.* Oncogene, 2001. **20**(34): p. 4685-4695.
81. Ošlejšková, L., et al., *The metastasis associated protein S100A4: a potential novel link to inflammation and consequent aggressive behaviour of rheumatoid arthritis synovial fibroblasts.* Annals of the rheumatic diseases, 2008. **67**(11): p. 1499-1504.
82. Schmidt-Hansen, B., et al., *Functional significance of metastasis-inducing S100A4 (Mts1) in tumor-stroma interplay.* Journal of Biological Chemistry, 2004. **279**(23): p. 24498-24504.
83. Rosty, C., et al., *Overexpression of S100A4 in pancreatic ductal adenocarcinomas is associated with poor differentiation and DNA hypomethylation.* The American journal of pathology, 2002. **160**(1): p. 45-50.
84. Taylor, S., et al., *S100A4 (p9Ka) protein in colon carcinoma and liver metastases: association with carcinoma cells and T-lymphocytes.* British journal of cancer, 2002. **86**(3): p. 409-416.

85. Kikuchi, N., et al., *Nuclear expression of S100A4 is associated with aggressive behavior of epithelial ovarian carcinoma: an important autocrine/paracrine factor in tumor progression.* Cancer science, 2006. **97**(10): p. 1061-1069.
86. Nakamura, T., et al., *Prognostic significance of S100A4 expression in gallbladder cancer.* International journal of oncology, 2002. **20**(5): p. 937-941.
87. Gongoll, S., et al., *Prognostic significance of calcium-binding protein S100A4 in colorectal cancer.* Gastroenterology, 2002. **123**(5): p. 1478-1484.
88. Dahlmann, M., et al., *RAGE mediates S100A4-induced cell motility via MAPK/ERK and hypoxia signaling and is a prognostic biomarker for human colorectal cancer metastasis.* Oncotarget, 2014. **5**(10): p. 3220.
89. Li, Z., et al., *Increased expression of S100A6 promotes cell proliferation and migration in human hepatocellular carcinoma.* Journal of molecular medicine, 2014. **92**(3): p. 291-303.
90. Maelandsmo, G.M., et al., *Differential expression patterns of S100A2, S100A4 and S100A6 during progression of human malignant melanoma.* International journal of cancer, 1997. **74**(4): p. 464-469.
91. Komatsu, K., et al., *Increased expression of S100A6 (Calcyclin), a calcium-binding protein of the S100 family, in human colorectal adenocarcinomas.* Clinical cancer research, 2000. **6**(1): p. 172-177.
92. Ohuchida, K., et al., *S100A6 is increased in a stepwise manner during pancreatic carcinogenesis: clinical value of expression analysis in 98 pancreatic juice samples.* Cancer Epidemiology and Prevention Biomarkers, 2007. **16**(4): p. 649-654.
93. Wang, X.-H., et al., *S100A6 overexpression is associated with poor prognosis and is epigenetically up-regulated in gastric cancer.* The American journal of pathology, 2010. **177**(2): p. 586-597.
94. Vimalachandran, D., et al., *High nuclear S100A6 (Calcyclin) is significantly associated with poor survival in pancreatic cancer patients.* Cancer research, 2005. **65**(8): p. 3218-3225.
95. Ghavami, S., et al., *S100A8/A9: a Janus-faced molecule in cancer therapy and tumorgenesis.* European journal of pharmacology, 2009. **625**(1-3): p. 73-83.
96. Kerkhoff, C., M. Klempt, and C. Sorg, *Novel insights into structure and function of MRP8 (S100A8) and MRP14 (S100A9).* Biochimica et Biophysica Acta (BBA)-Molecular Cell Research, 1998. **1448**(2): p. 200-211.
97. Ghavami, S., et al., *S100A8/A9 at low concentration promotes tumor cell growth via RAGE ligation and MAP kinase-dependent pathway.* Journal of leukocyte biology, 2008. **83**(6): p. 1484-1492.
98. Hermani, A., et al., *S100A8 and S100A9 activate MAP kinase and NF-κB signaling pathways and trigger translocation of RAGE in human prostate cancer cells.* Experimental cell research, 2006. **312**(2): p. 184-197.
99. Hermani, A., et al., *Calcium-binding proteins S100A8 and S100A9 as novel diagnostic markers in human prostate cancer.* Clinical Cancer Research, 2005. **11**(14): p. 5146-5152.
100. Zhang, L., et al., *Proteins S100A8 and S100A9 are potential biomarkers for renal cell carcinoma in the early stages: results from a proteomic study integrated with bioinformatics analysis.* Molecular medicine reports, 2015. **11**(6): p. 4093-4100.

101. Reeb, A.N., et al., *S100A8 is a novel therapeutic target for anaplastic thyroid carcinoma.* The Journal of Clinical Endocrinology & Metabolism, 2015. **100**(2): p. E232-E242.
102. Stulík, J., et al., *The analysis of S100A9 and S100A8 expression in matched sets of macroscopically normal colon mucosa and colorectal carcinoma: the S100A9 and S100A8 positive cells underlie and invade tumor mass.* ELECTROPHORESIS: An International Journal, 1999. **20**(4-5): p. 1047-1054.
103. Gebhardt, C., et al., *Calgranulins S100A8 and S100A9 are negatively regulated by glucocorticoids in a c-Fos-dependent manner and overexpressed throughout skin carcinogenesis.* Oncogene, 2002. **21**(27): p. 4266-4276.
104. Turovskaya, O., et al., *RAGE, carboxylated glycans and S100A8/A9 play essential roles in colitis-associated carcinogenesis.* Carcinogenesis, 2008. **29**(10): p. 2035-2043.
105. Moskaluk, C.A., et al., *Gastric cancers overexpress S100A calcium-binding proteins.* Cancer research, 2002. **62**(23): p. 6823-6826.
106. Zhu, H., et al., *Profiling protein markers associated with the sensitivity to concurrent chemoradiotherapy in human cervical carcinoma.* Journal of proteome research, 2009. **8**(8): p. 3969-3976.
107. Tan, Y., et al., *Proteomic-based analysis for identification of potential serum biomarkers in gallbladder cancer.* Oncology reports, 2011. **26**(4): p. 853-859.
108. Domoto, T., et al., *Evaluation of S100A10, annexin II and B-FABP expression as markers for renal cell carcinoma.* Cancer science, 2007. **98**(1): p. 77-82.
109. Shang, J., et al., *S100A10 as a novel biomarker in colorectal cancer.* Tumor Biology, 2013. **34**(6): p. 3785-3790.
110. McKiernan, E., et al., *The role of S100 genes in breast cancer progression.* Tumor biology, 2011. **32**(3): p. 441-450.
111. Xiong, T.-f., F.-q. Pan, and D. Li, *Expression and clinical significance of S100 family genes in patients with melanoma.* Melanoma research, 2019. **29**(1): p. 23.
112. Meghnani, V., et al., *The receptor for advanced glycation end products influences the expression of its S100 protein ligands in melanoma tumors.* The international journal of biochemistry & cell biology, 2014. **57**: p. 54-62.
113. Azizan, N., et al., *RAGE maintains high levels of NFκB and oncogenic Kras activity in pancreatic cancer.* Biochemical and biophysical research communications, 2017. **493**(1): p. 592-597.
114. Sharaf, H., et al., *Advanced glycation endproducts increase proliferation, migration and invasion of the breast cancer cell line MDA-MB-231.* Biochimica et Biophysica Acta (BBA)-Molecular Basis of Disease, 2015. **1852**(3): p. 429-441.
115. Li, R., et al., *Downregulation of RAGE Inhibits Cell Proliferation and Induces Apoptosis via Regulation of PI3K/AKT Pathway in Cervical Squamous Cell Carcinoma.* OncoTargets and therapy, 2020. **13**: p. 2385.
116. Thomas, S.J., et al., *The role of JAK/STAT signalling in the pathogenesis, prognosis and treatment of solid tumours.* British journal of cancer, 2015. **113**(3): p. 365-371.
117. Xu, J., et al., *Macrophage endocytosis of high-mobility group box 1 triggers pyroptosis.* Cell Death & Differentiation, 2014. **21**(8): p. 1229-1239.
118. Yang, H., et al., *Inhibition of HMGB1/RAGE-mediated endocytosis by HMGB1 antagonist box A, anti-HMGB1 antibodies, and cholinergic agonists suppresses inflammation.* Molecular Medicine, 2019. **25**(1): p. 1-13.

119. Kang, R., et al., *The HMGB1/RAGE inflammatory pathway promotes pancreatic tumor growth by regulating mitochondrial bioenergetics.* Oncogene, 2014. **33**(5): p. 567-577.
120. Sevillano, N., et al., *Internalization of the receptor for advanced glycation end products (RAGE) is required to mediate intracellular responses.* Journal of biochemistry, 2009. **145**(1): p. 21-30.
121. Perrone, L., G. Peluso, and M.A. Melone, *RAGE recycles at the plasma membrane in S100B secretory vesicles and promotes Schwann cells morphological changes.* Journal of cellular physiology, 2008. **217**(1): p. 60-71.
122. Carreau, A., et al., *Why is the partial oxygen pressure of human tissues a crucial parameter? Small molecules and hypoxia.* Journal of cellular and molecular medicine, 2011. **15**(6): p. 1239-1253.
123. Pouysségur, J., F. Dayan, and N.M. Mazure, *Hypoxia signalling in cancer and approaches to enforce tumour regression.* Nature, 2006. **441**(7092): p. 437-443.
124. Minchinton, A.I. and I.F. Tannock, *Drug penetration in solid tumours.* Nature Reviews Cancer, 2006. **6**(8): p. 583-592.
125. Daly, C.S., et al., *Hypoxia modulates the stem cell population and induces EMT in the MCF-10A breast epithelial cell line.* Oncology reports, 2018. **39**(2): p. 483-490.
126. Semenza, G.L., et al., *Hypoxia-inducible nuclear factors bind to an enhancer element located 3'to the human erythropoietin gene.* Proceedings of the National Academy of Sciences, 1991. **88**(13): p. 5680-5684.
127. Hu, C.-J., et al., *Differential roles of hypoxia-inducible factor 1α (HIF-1α) and HIF-2α in hypoxic gene regulation.* Molecular and cellular biology, 2003. **23**(24): p. 9361-9374.
128. Keith, B., R.S. Johnson, and M.C. Simon, *HIF1α and HIF2α: sibling rivalry in hypoxic tumour growth and progression.* Nature Reviews Cancer, 2012. **12**(1): p. 9-22.
129. Wang, G.L., et al., *Hypoxia-inducible factor 1 is a basic-helix-loop-helix-PAS heterodimer regulated by cellular O2 tension.* Proceedings of the national academy of sciences, 1995. **92**(12): p. 5510-5514.
130. Semenza, G.L., *Oxygen sensing, homeostasis, and disease.* New England Journal of Medicine, 2011. **365**(6): p. 537-547.
131. Kaelin Jr, W.G. and P.J. Ratcliffe, *Oxygen sensing by metazoans: the central role of the HIF hydroxylase pathway.* Molecular cell, 2008. **30**(4): p. 393-402.
132. Cummins, E.P., et al., *The role of HIF in immunity and inflammation.* Molecular aspects of medicine, 2016. **47**: p. 24-34.
133. Tian, H., S.L. McKnight, and D.W. Russell, *Endothelial PAS domain protein 1 (EPAS1), a transcription factor selectively expressed in endothelial cells.* Genes & development, 1997. **11**(1): p. 72-82.
134. Gu, Y.-Z., et al., *Molecular characterization and chromosomal localization of a third α-class hypoxia inducible factor subunit, HIF3α.* Gene Expression The Journal of Liver Research, 1998. **7**(3): p. 205-213.
135. Wiesener, M.S., et al., *Widespread, hypoxia-inducible expression of HIF-2α in distinct cell populations of different organs.* The FASEB Journal, 2003. **17**(2): p. 271-273.
136. Duan, C., *Hypoxia-inducible factor 3 biology: complexities and emerging themes.* American Journal of Physiology-Cell Physiology, 2016. **310**(4): p. C260-C269.
137. Jiang, B.-H., et al., *Dimerization, DNA binding, and transactivation properties of hypoxia-inducible factor 1.* Journal of Biological Chemistry, 1996. **271**(30): p. 17771-17778.

138. Wang, G.L. and G.L. Semenza, *Purification and characterization of hypoxia-inducible factor 1.* Journal of biological chemistry, 1995. **270**(3): p. 1230-1237.
139. Bruick, R.K. and S.L. McKnight, *A conserved family of prolyl-4-hydroxylases that modify HIF.* Science, 2001. **294**(5545): p. 1337-1340.
140. Li, H., H.P. Ko, and J.P. Whitlock, *Induction of Phosphoglycerate Kinase 1 Gene Expression by Hypoxia ROLES OF ARNT AND HIF1α.* Journal of Biological Chemistry, 1996. **271**(35): p. 21262-21267.
141. Ema, M., et al., *A novel bHLH-PAS factor with close sequence similarity to hypoxia-inducible factor 1α regulates the VEGF expression and is potentially involved in lung and vascular development.* Proceedings of the National Academy of Sciences, 1997. **94**(9): p. 4273-4278.
142. Yamashita, K., et al., *Molecular regulation of the endothelin-1 gene by hypoxia contributions of hypoxia-inducible factor-1, activator protein-1, GATA-2, and p300/CBP.* Journal of Biological Chemistry, 2001. **276**(16): p. 12645-12653.
143. Ravenna, L., L. Salvatori, and M.A. Russo, *HIF 3α: the little we know.* The FEBS journal, 2016. **283**(6): p. 993-1003.
144. Webb, J.D., M.L. Coleman, and C.W. Pugh, *Hypoxia, hypoxia-inducible factors (HIF), HIF hydroxylases and oxygen sensing.* Cellular and molecular life sciences, 2009. **66**(22): p. 3539.
145. Koh, M.Y., T.R. Spivak-Kroizman, and G. Powis, *HIF-1 regulation: not so easy come, easy go.* Trends in biochemical sciences, 2008. **33**(11): p. 526-534.
146. Ohh, M., et al., *Ubiquitination of hypoxia-inducible factor requires direct binding to the β-domain of the von Hippel–Lindau protein.* Nature cell biology, 2000. **2**(7): p. 423-427.
147. Maxwell, P.H., C.W. Pugh, and P.J. Ratcliffe, *Activation of the HIF pathway in cancer.* Current opinion in genetics & development, 2001. **11**(3): p. 293-299.
148. Ratcliffe, P.J., *HIF-1 and HIF-2: working alone or together in hypoxia?* The Journal of clinical investigation, 2007. **117**(4): p. 862-865.
149. Luo, W., et al., *Hsp70 and CHIP selectively mediate ubiquitination and degradation of hypoxia-inducible factor (HIF)-1α but not HIF-2α.* Journal of biological chemistry, 2010. **285**(6): p. 3651-3663.
150. Richard, D.E., et al., *p42/p44 mitogen-activated protein kinases phosphorylate hypoxia-inducible factor 1α (HIF-1α) and enhance the transcriptional activity of HIF-1.* Journal of Biological Chemistry, 1999. **274**(46): p. 32631-32637.
151. Sang, N., et al., *MAPK signaling up-regulates the activity of hypoxia-inducible factors by its effects on p300.* Journal of Biological chemistry, 2003. **278**(16): p. 14013-14019.
152. Tang, N., et al., *Loss of HIF-1α in endothelial cells disrupts a hypoxia-driven VEGF autocrine loop necessary for tumorigenesis.* Cancer cell, 2004. **6**(5): p. 485-495.
153. Tsuzuki, Y., et al., *Vascular endothelial growth factor (VEGF) modulation by targeting hypoxia-inducible factor-1α→ hypoxia response element→ VEGF cascade differentially regulates vascular response and growth rate in tumors.* Cancer research, 2000. **60**(22): p. 6248-6252.
154. Jensen, R.L., et al., *Inhibition of hypoxia inducible factor-1α (HIF-1α) decreases vascular endothelial growth factor (VEGF) secretion and tumor growth in malignant gliomas.* Journal of neuro-oncology, 2006. **78**(3): p. 233-247.

155. Maxwell, P.H., et al., *Hypoxia-inducible factor-1 modulates gene expression in solid tumors and influences both angiogenesis and tumor growth.* Proceedings of the National Academy of Sciences, 1997. **94**(15): p. 8104-8109.
156. Ravi, R., et al., *Regulation of tumor angiogenesis by p53-induced degradation of hypoxia-inducible factor 1α.* Genes & development, 2000. **14**(1): p. 34-44.
157. Zhang, W., et al., *HIF-1α promotes epithelial-mesenchymal transition and metastasis through direct regulation of ZEB1 in colorectal cancer.* PloS one, 2015. **10**(6): p. e0129603.
158. Yang, M.-H., et al., *Direct regulation of TWIST by HIF-1α promotes metastasis.* Nature cell biology, 2008. **10**(3): p. 295-305.
159. Kalluri, R. and R.A. Weinberg, *The basics of epithelial-mesenchymal transition.* The Journal of clinical investigation, 2009. **119**(6): p. 1420-1428.
160. Lamouille, S., J. Xu, and R. Derynck, *Molecular mechanisms of epithelial–mesenchymal transition.* Nature reviews Molecular cell biology, 2014. **15**(3): p. 178-196.
161. Stemmler, M.P., et al., *Non-redundant functions of EMT transcription factors.* Nature cell biology, 2019. **21**(1): p. 102-112.
162. Bolós, V., et al., *The transcription factor Slug represses E-cadherin expression and induces epithelial to mesenchymal transitions: a comparison with Snail and E47 repressors.* Journal of cell science, 2003. **116**(3): p. 499-511.
163. Lee, M.-Y., et al., *Epithelial-mesenchymal transition in cervical cancer: correlation with tumor progression, epidermal growth factor receptor overexpression, and snail up-regulation.* Clinical Cancer Research, 2008. **14**(15): p. 4743-4750.
164. Zhang, P., Y. Sun, and L. Ma, *ZEB1: at the crossroads of epithelial-mesenchymal transition, metastasis and therapy resistance.* Cell cycle, 2015. **14**(4): p. 481-487.
165. Weaver, A.M., *Invadopodia: specialized cell structures for cancer invasion.* Clinical & experimental metastasis, 2006. **23**(2): p. 97-105.
166. Hoffmann, C., et al., *Hypoxia promotes breast cancer cell invasion through HIF-1α-mediated up-regulation of the invadopodial actin bundling protein CSRP2.* Scientific reports, 2018. **8**(1): p. 1-14.
167. Hoffmann, C., et al., *CRP2, a new invadopodia actin bundling factor critically promotes breast cancer cell invasion and metastasis.* Oncotarget, 2016. **7**(12): p. 13688.
168. Choi, J.Y., et al., *Overexpression of MMP-9 and HIF-1α in breast cancer cells under hypoxic conditions.* Journal of breast cancer, 2011. **14**(2): p. 88-95.
169. Semenza, G.L., et al., *Transcriptional regulation of genes encoding glycolytic enzymes by hypoxia-inducible factor 1.* Journal of biological chemistry, 1994. **269**(38): p. 23757-23763.
170. Seagroves, T.N., et al., *Transcription factor HIF-1 is a necessary mediator of the pasteur effect in mammalian cells.* Molecular and cellular biology, 2001. **21**(10): p. 3436-3444.
171. Tafani, M., et al., *Hypoxia-increased RAGE and P2X7R expression regulates tumor cell invasion through phosphorylation of Erk1/2 and Akt and nuclear translocation of NF-{kappa}B.* Carcinogenesis, 2011. **32**(8): p. 1167-75.
172. Huber, R., et al., *Tumour hypoxia promotes melanoma growth and metastasis via High Mobility Group Box-1 and M2-like macrophages.* Scientific reports, 2016. **6**: p. 29914.
173. Tang, D., et al., *High-mobility group box 1 and cancer.* Biochimica et Biophysica Acta (BBA)-Gene Regulatory Mechanisms, 2010. **1799**(1-2): p. 131-140.

174. Scaffidi, P., T. Misteli, and M.E. Bianchi, *Release of chromatin protein HMGB1 by necrotic cells triggers inflammation.* Nature, 2002. **418**(6894): p. 191-195.
175. Liu, Y., et al., *Hypoxia induced HMGB1 and mitochondrial DNA interactions mediate tumor growth in hepatocellular carcinoma through Toll-like receptor 9.* Journal of hepatology, 2015. **63**(1): p. 114-121.
176. Jiang, J., et al., *Hypoxia-induced HMGB1 expression of HCC promotes tumor invasiveness and metastasis via regulating macrophage-derived IL-6.* Experimental cell research, 2018. **367**(1): p. 81-88.
177. Cheng, P., et al., *High mobility group box 1 (HMGB1) predicts invasion and poor prognosis of glioblastoma multiforme via activating AKT signaling in an autocrine pathway.* Medical science monitor: international medical journal of experimental and clinical research, 2018. **24**: p. 8916.
178. Pezzolo, A., et al., *Failure of anti tumor-derived endothelial cell immunotherapy depends on augmentation of tumor hypoxia.* Oncotarget, 2014. **5**(21): p. 10368.
179. Mao, X., et al., *Mechanisms through which hypoxia-induced caveolin-1 drives tumorigenesis and metastasis in hepatocellular carcinoma.* Cancer research, 2016. **76**(24): p. 7242-7253.
180. Zhang, R., et al., *Subcellular distribution of S100A4 and its transcriptional regulation under hypoxic conditions in gastric cancer cell line BGC823.* Cancer science, 2010. **101**(5): p. 1141-1146.
181. Horiuchi, A., et al., *Hypoxia upregulates ovarian cancer invasiveness via the binding of HIF-1α to a hypoxia-induced, methylation-free hypoxia response element of S100A4 gene.* International journal of cancer, 2012. **131**(8): p. 1755-1767.
182. Xuan, X., et al., *Increased expression levels of S100A4 associated with hypoxia-induced invasion and metastasis in esophageal squamous cell cancer.* Tumor Biology, 2014. **35**(12): p. 12535-12543.
183. Wu, X.-Y., Z.-X. Fu, and X.-H. Wang, *Effect of hypoxia-inducible factor 1-α on Survivin in colorectal cancer.* Molecular medicine reports, 2010. **3**(3): p. 409-415.
184. Mao, Q., et al., *A tumor hypoxic niche protects human colon cancer stem cells from chemotherapy.* Journal of cancer research and clinical oncology, 2013. **139**(2): p. 211-222.
185. Hongo, K., et al., *Hypoxia enhances colon cancer migration and invasion through promotion of epithelial-mesenchymal transition.* Journal of Surgical Research, 2013. **182**(1): p. 75-84.
186. Grebhardt, S., et al., *Hypoxia and HIF-1 increase S100A8 and S100A9 expression in prostate cancer.* International journal of cancer, 2012. **131**(12): p. 2785-2794.
187. Cokkinides, V., et al., *American cancer society: Cancer facts and figures.* Atlanta: American Cancer Society, 2005.
188. Ruhl, J.L., et al., *Summary stage 2018: codes and coding instructions.* Bethesda, MD: National Cancer Institute, 2018.
189. Orth, M., et al., *Pancreatic ductal adenocarcinoma: Biological hallmarks, current status, and future perspectives of combined modality treatment approaches.* Radiation Oncology, 2019. **14**(1): p. 1-20.
190. Gress, D.M., et al., *Principles of cancer staging.* AJCC cancer staging manual, 2017. **8**: p. 3-30.

191. Caldas, C. and S.E. Kern, *K-ras mutation and pancreatic adenocarcinoma.* International journal of pancreatology, 1995. **18**(1): p. 1-6.
192. Maitra, A. and R.H. Hruban, *Pancreatic cancer.* Annu. Rev. Pathol. Mech. Dis., 2008. **3**: p. 157-188.
193. Logsdon, C.D. and W. Lu, *The significance of Ras activity in pancreatic cancer initiation.* International journal of biological sciences, 2016. **12**(3): p. 338.
194. Hu, Y.-X., et al., *Frequent loss of p16 expression and its correlation with clinicopathological parameters in pancreatic carcinoma.* Clinical cancer research, 1997. **3**(9): p. 1473-1477.
195. Serrano, M., G.J. Hannon, and D. Beach, *A new regulatory motif in cell-cycle control causing specific inhibition of cyclin D/CDK4.* nature, 1993. **366**(6456): p. 704-707.
196. Vogelstein, B. and K.W. Kinzler, *Cancer genes and the pathways they control.* Nature medicine, 2004. **10**(8): p. 789-799.
197. Ahmed, S., et al., *The TGF-β/Smad4 signaling pathway in pancreatic carcinogenesis and its clinical significance.* Journal of clinical medicine, 2017. **6**(1): p. 5.
198. Maitra, A., et al., *Precursors to invasive pancreatic cancer.* Advances in anatomic pathology, 2005. **12**(2): p. 81-91.
199. Hruban, R.H., et al., *Pancreatic intraepithelial neoplasia: a new nomenclature and classification system for pancreatic duct lesions.* The American journal of surgical pathology, 2001. **25**(5): p. 579-586.
200. Hruban, R.H., A. Maitra, and M. Goggins, *Update on pancreatic intraepithelial neoplasia.* International journal of clinical and experimental pathology, 2008. **1**(4): p. 306.
201. Perera, R.M. and N. Bardeesy, *Pancreatic cancer metabolism: breaking it down to build it back up.* Cancer discovery, 2015. **5**(12): p. 1247-1261.
202. Chakraborty, S. and S. Singh, *Surgical resection improves survival in pancreatic cancer patients without vascular invasion-a population based study.* Annals of Gastroenterology: Quarterly Publication of the Hellenic Society of Gastroenterology, 2013. **26**(4): p. 346.
203. Murakami, Y., et al., *Early initiation of adjuvant chemotherapy improves survival of patients with pancreatic carcinoma after surgical resection.* Cancer chemotherapy and pharmacology, 2013. **71**(2): p. 419-429.
204. Loos, M., et al., *Surgical treatment of pancreatic cancer.* Annals of the New York Academy of Sciences, 2008. **1138**(1): p. 169-180.
205. Hua, J., et al., *Duct-to-mucosa versus invagination pancreaticojejunostomy following pancreaticoduodenectomy: a systematic review and meta-analysis.* Journal of Gastrointestinal Surgery, 2015. **19**(10): p. 1900-1909.
206. Cheng, Y., et al., *Pancreaticojejunostomy versus pancreaticogastrostomy reconstruction for the prevention of postoperative pancreatic fistula following pancreaticoduodenectomy.* Cochrane Database of Systematic Reviews, 2017(9).
207. Demir, I.E., et al., *R0 versus R1 resection matters after pancreaticoduodenectomy, and less after distal or total pancreatectomy for pancreatic cancer.* Annals of surgery, 2018. **268**(6): p. 1058-1068.
208. Huang, P., et al., *Action of 2', 2'-difluorodeoxycytidine on DNA synthesis.* Cancer research, 1991. **51**(22): p. 6110-6117.

209. de Sousa Cavalcante, L. and G. Monteiro, *Gemcitabine: metabolism and molecular mechanisms of action, sensitivity and chemoresistance in pancreatic cancer.* European journal of pharmacology, 2014. **741**: p. 8-16.
210. Neoptolemos, J.P., et al., *Adjuvant chemotherapy with fluorouracil plus folinic acid vs gemcitabine following pancreatic cancer resection: a randomized controlled trial.* Jama, 2010. **304**(10): p. 1073-1081.
211. Neoptolemos, J.P., et al., *Comparison of adjuvant gemcitabine and capecitabine with gemcitabine monotherapy in patients with resected pancreatic cancer (ESPAC-4): a multicentre, open-label, randomised, phase 3 trial.* The Lancet, 2017. **389**(10073): p. 1011-1024.
212. Conroy, T., et al., *Unicancer GI PRODIGE 24/CCTG PA. 6 trial: A multicenter international randomized phase III trial of adjuvant mFOLFIRINOX versus gemcitabine (gem) in patients with resected pancreatic ductal adenocarcinomas*. 2018, American Society of Clinical Oncology.
213. Conroy, T., et al., *FOLFIRINOX versus gemcitabine for metastatic pancreatic cancer.* New England Journal of Medicine, 2011. **364**(19): p. 1817-1825.
214. Siegel, R.L., et al., *Cancer Statistics, 2021.* CA: A Cancer Journal for Clinicians, 2021. **71**(1): p. 7-33.
215. Ali, Z., N. Yousaf, and J. Larkin, *Melanoma epidemiology, biology and prognosis.* EJC supplements, 2013. **11**(2): p. 81.
216. McCourt, C., O. Dolan, and G. Gormley, *Malignant melanoma: a pictorial review.* The Ulster medical journal, 2014. **83**(2): p. 103.
217. Oyama, S., et al., *BRAF, KIT and NRAS mutations and expression of c-KIT, phosphorylated extracellular signal-regulated kinase and phosphorylated AKT in Japanese melanoma patients.* The Journal of dermatology, 2015. **42**(5): p. 477-484.
218. Libra, M., et al., *Analysis of BRAF mutation in primary and metastatic melanoma.* Cell Cycle, 2005. **4**(10): p. 1382-1384.
219. Si, L., et al., *Prevalence of BRAF V600E mutation in Chinese melanoma patients: large scale analysis of BRAF and NRAS mutations in a 432-case cohort.* European journal of cancer, 2012. **48**(1): p. 94-100.
220. Colicelli, J., *Human RAS superfamily proteins and related GTPases.* Science's STKE, 2004. **2004**(250): p. re13-re13.
221. Jakob, J.A., et al., *NRAS mutation status is an independent prognostic factor in metastatic melanoma.* Cancer, 2012. **118**(16): p. 4014-4023.
222. Rivera, R.S., et al., *C-kit protein expression correlated with activating mutations in KIT gene in oral mucosal melanoma.* Virchows Archiv, 2008. **452**(1): p. 27-32.
223. Montone, K.T., et al., *Proto-oncogene c-kit expression in malignant melanoma: protein loss with tumor progression.* Modern pathology: an official journal of the United States and Canadian Academy of Pathology, Inc, 1997. **10**(9): p. 939-944.
224. Bertolotto, C., *Melanoma: from melanocyte to genetic alterations and clinical options.* Scientifica, 2013. **2013**.
225. Damsky, W.E., L.E. Rosenbaum, and M. Bosenberg, *Decoding melanoma metastasis.* Cancers, 2011. **3**(1): p. 126-163.
226. Alonso, S.R., et al., *Progression in cutaneous malignant melanoma is associated with distinct expression profiles: a tissue microarray-based study.* The American journal of pathology, 2004. **164**(1): p. 193-203.

227. Damsky, W.E., N. Theodosakis, and M. Bosenberg, *Melanoma metastasis: new concepts and evolving paradigms.* Oncogene, 2014. **33**(19): p. 2413-2422.
228. Wilson, M.A. and L.M. Schuchter, *Chemotherapy for melanoma.* Melanoma, 2016: p. 209-229.
229. Serrone, L., et al., *Dacarbazine-based chemotherapy for metastatic melanoma: thirty-year experience overview.* Journal of experimental & clinical cancer research: CR, 2000. **19**(1): p. 21-34.
230. Sharma, P. and J.P. Allison, *The future of immune checkpoint therapy.* Science, 2015. **348**(6230): p. 56-61.
231. Kirkwood, J.M., et al., *High-dose interferon alfa-2b significantly prolongs relapse-free and overall survival compared with the GM2-KLH/QS-21 vaccine in patients with resected stage IIB-III melanoma: results of intergroup trial E1694/S9512/C509801.* Journal of Clinical Oncology, 2001. **19**(9): p. 2370-2380.
232. Rafique, I., J.M. Kirkwood, and A.A. Tarhini. *Immune checkpoint blockade and interferon-α in melanoma*. Elsevier.
233. Krieg, C., et al., *Improved IL-2 immunotherapy by selective stimulation of IL-2 receptors on lymphocytes and endothelial cells.* Proceedings of the National Academy of Sciences, 2010. **107**(26): p. 11906-11911.
234. Bright, R., et al., *Clinical response rates from interleukin-2 therapy for metastatic melanoma over 30 years' experience: a meta-analysis of 3312 patients.* Journal of Immunotherapy, 2017. **40**(1): p. 21-30.
235. Eggermont, A.M.M., et al., *Adjuvant therapy with pegylated interferon alfa-2b versus observation alone in resected stage III melanoma: final results of EORTC 18991, a randomised phase III trial.* The Lancet, 2008. **372**(9633): p. 117-126.
236. Harris, J.M. and R.B. Chess, *Effect of pegylation on pharmaceuticals.* Nature reviews Drug discovery, 2003. **2**(3): p. 214-221.
237. Bhatia, S., S.S. Tykodi, and J.A. Thompson, *Treatment of metastatic melanoma: an overview.* Oncology (Williston Park, NY), 2009. **23**(6): p. 488.
238. Brunet, J.-F., et al., *A new member of the immunoglobulin superfamily—CTLA-4.* Nature, 1987. **328**(6127): p. 267-270.
239. Brohl, A.S., et al., *A phase IB study of ipilimumab with peginterferon alfa-2b in patients with unresectable melanoma.* Journal for immunotherapy of cancer, 2016. **4**(1): p. 1-8.
240. Raedler, L.A., *Opdivo (nivolumab): second PD-1 inhibitor receives FDA approval for unresectable or metastatic melanoma.* American health & drug benefits, 2015. **8**(Spec Feature): p. 180.
241. Johnson, D.B., C. Peng, and J.A. Sosman, *Nivolumab in melanoma: latest evidence and clinical potential.* Therapeutic advances in medical oncology, 2015. **7**(2): p. 97-106.
242. Franklin, C., et al., *Immunotherapy in melanoma: recent advances and future directions.* European Journal of Surgical Oncology (EJSO), 2017. **43**(3): p. 604-611.
243. Leclerc, E., C.W. Heizmann, and S. Vetter, *RAGE and S100 protein transcription levels are highly variable in human melanoma tumors and cells.* General physiology and biophysics, 2009. **28**(Specia): p. 65-75.
244. Lin, J., et al., *The calcium-binding protein S100B down-regulates p53 and apoptosis in malignant melanoma.* Journal of biological chemistry, 2010. **285**(35): p. 27487-27498.
245. Olaoba, O.T., et al., *RAGE Signaling in Melanoma Tumors.* International Journal of Molecular Sciences, 2020. **21**(23): p. 8989.

246. Wagner, N.B., et al., *Diminished levels of the soluble form of RAGE are related to poor survival in malignant melanoma.* International journal of cancer, 2015. **137**(11): p. 2607-2617.
247. Shain, A.H. and B.C. Bastian, *From melanocytes to melanomas.* nature reviews Cancer, 2016. **16**(6): p. 345.
248. Balch, C.M., et al., *Final version of the American Joint Committee on Cancer staging system for cutaneous melanoma.* Journal of Clinical Oncology, 2001. **19**(16): p. 3635-3648.
249. Meghnani, V., S.W. Vetter, and E. Leclerc, *RAGE overexpression confers a metastatic phenotype to the WM115 human primary melanoma cell line.* Biochimica et Biophysica Acta (BBA)-Molecular Basis of Disease, 2014. **1842**(7): p. 1017-1027.
250. Costa, E.C., et al., *3D tumor spheroids: an overview on the tools and techniques used for their analysis.* Biotechnology advances, 2016. **34**(8): p. 1427-1441.
251. Pampaloni, F., E.G. Reynaud, and E.H.K. Stelzer, *The third dimension bridges the gap between cell culture and live tissue.* Nature reviews Molecular cell biology, 2007. **8**(10): p. 839-845.
252. Ivascu, A. and M. Kubbies, *Rapid generation of single-tumor spheroids for high-throughput cell function and toxicity analysis.* Journal of biomolecular screening, 2006. **11**(8): p. 922-932.
253. De Hoogt, R., et al., *Protocols and characterization data for 2D, 3D, and slice-based tumor models from the PREDECT project.* Scientific data, 2017. **4**(1): p. 1-23.
254. Westermark, B., et al., *Human melanoma cell lines of primary and metastatic origin express the genes encoding the chains of platelet-derived growth factor (PDGF) and produce a PDGF-like growth factor.* Proceedings of the National Academy of Sciences, 1986. **83**(19): p. 7197-7200.
255. Shen, H., et al., *Recent Advances in Three-Dimensional Multicellular Spheroid Culture and Future Development.* Micromachines, 2021. **12**(1): p. 96.
256. Bresciani, G., et al., *Evaluation of spheroid 3D culture methods to study a pancreatic neuroendocrine neoplasm cell line.* Frontiers in endocrinology, 2019. **10**: p. 682.
257. Phung, Y.T., et al., *Rapid generation of in vitro multicellular spheroids for the study of monoclonal antibody therapy.* Journal of Cancer, 2011. **2**: p. 507.
258. Nasatto, P.L., et al., *Methylcellulose, a cellulose derivative with original physical properties and extended applications.* Polymers, 2015. **7**(5): p. 777-803.
259. Kojima, N., S. Takeuchi, and Y. Sakai, *Rapid aggregation of heterogeneous cells and multiple-sized microspheres in methylcellulose medium.* Biomaterials, 2012. **33**(18): p. 4508-4514.
260. Chen, Y.-C., et al., *High-throughput cancer cell sphere formation for characterizing the efficacy of photo dynamic therapy in 3D cell cultures.* Scientific reports, 2015. **5**(1): p. 1-12.
261. Fidler, I.J. and G.L. Nicolson, *Fate of recirculating B16 melanoma metastatic variant cells in parabiotic syngeneic recipients: brief communication.* Journal of the National Cancer Institute, 1977. **58**(6): p. 1867-1872.
262. Fidler, I.J. and M.L. Kripke, *Metastasis results from preexisting variant cells within a malignant tumor.* Science, 1977. **197**(4306): p. 893-895.

263. Ali, S.A. and I. Naaz, *Current challenges in understanding the story of skin pigmentation—Bridging the morpho-anatomical and functional aspects of mammalian melanocytes.* Muscle Cell and Tissue, 2015: p. 262-285.
264. Nakamura, M., D. Ono, and S. Sugita, *Mechanophenotyping of B16 Melanoma Cell Variants for the Assessment of the Efficacy of (-)-Epigallocatechin Gallate Treatment Using a Tapered Microfluidic Device.* Micromachines, 2019. **10**(3): p. 207.
265. Victorelli, S., et al., *Senescent human melanocytes drive skin ageing via paracrine telomere dysfunction.* The EMBO journal, 2019. **38**(23): p. e101982.
266. Chakraborty, A.K., et al., *A spontaneous murine melanoma lung metastasis comprised of host× tumor hybrids.* Cancer research, 2000. **60**(9): p. 2512-2519.
267. Popa, I., E. Ganea, and S.M. Petrescu, *Expression and subcellular localization of RAGE in melanoma cells.* Biochemistry and Cell Biology, 2014. **92**(2): p. 127-136.
268. Saha, A., et al., *Lack of an endogenous anti-inflammatory protein in mice enhances colonization of B16F10 melanoma cells in the lungs.* Journal of Biological Chemistry, 2010. **285**(14): p. 10822-10831.
269. Swami, P., et al., *Inhibition of the Receptor for Advanced Glycation End Products Enhances the Cytotoxic Effect of Gemcitabine in Murine Pancreatic Tumors.* Biomolecules, 2021. **11**(4): p. 526.
270. Levine, B., N. Mizushima, and H.W. Virgin, *Autophagy in immunity and inflammation.* Nature, 2011. **469**(7330): p. 323-35.
271. Levine, B. and G. Kroemer, *Autophagy in the pathogenesis of disease.* Cell, 2008. **132**(1): p. 27-42.
272. Rabinowitz, J.D. and E. White, *Autophagy and metabolism.* Science, 2010. **330**(6009): p. 1344-1348.
273. Liu, E.Y. and K.M. Ryan, *Autophagy and cancer–issues we need to digest.* J Cell Sci, 2012. **125**(10): p. 2349-2358.
274. Bellot, G., et al., *Hypoxia-induced autophagy is mediated through hypoxia-inducible factor induction of BNIP3 and BNIP3L via their BH3 domains.* Molecular and cellular biology, 2009. **29**(10): p. 2570-2581.
275. Daskalaki, I., I. Gkikas, and N. Tavernarakis, *Hypoxia and selective autophagy in cancer development and therapy.* Frontiers in cell and developmental biology, 2018. **6**: p. 104.
276. Rouschop, K.M., et al., *The unfolded protein response protects human tumor cells during hypoxia through regulation of the autophagy genes MAP1LC3B and ATG5.* J Clin Invest, 2010. **120**(1): p. 127-41.
277. Wu, J., et al., *Molecular cloning and characterization of rat LC3A and LC3B--two novel markers of autophagosome.* Biochem Biophys Res Commun, 2006. **339**(1): p. 437-42.
278. Kang, R., et al., *The Beclin 1 network regulates autophagy and apoptosis.* Cell Death Differ, 2011. **18**(4): p. 571-80.
279. Mijaljica, D., M. Prescott, and R.J. Devenish, *The intriguing life of autophagosomes.* International journal of molecular sciences, 2012. **13**(3): p. 3618-3635.
280. Fuentes, M.K., et al., *RAGE activation by S100P in colon cancer stimulates growth, migration, and cell signaling pathways.* Diseases of the colon & rectum, 2007. **50**(8): p. 1230-1240.
281. Chen, R.C., et al., *The role of HMGB1-RAGE axis in migration and invasion of hepatocellular carcinoma cell lines.* Mol Cell Biochem, 2014. **390**(1-2): p. 271-80.

282. Matou-Nasri, S., et al., *Biological impact of advanced glycation endproducts on estrogen receptor-positive MCF-7 breast cancer cells.* Biochimica et Biophysica Acta (BBA)-Molecular Basis of Disease, 2017. **1863**(11): p. 2808-2820.
283. Arumugam, T., et al., *S100P promotes pancreatic cancer growth, survival, and invasion.* Clinical Cancer Research, 2005. **11**(15): p. 5356-5364.
284. Deer, E.L., et al., *Phenotype and genotype of pancreatic cancer cell lines.* Pancreas, 2010. **39**(4): p. 425.
285. Brown, W.S., et al., *Overcoming adaptive resistance to KRAS and MEK inhibitors by co-targeting mTORC1/2 complexes in pancreatic cancer.* Cell Reports Medicine, 2020. **1**(8): p. 100131.
286. Yuan, Y., et al., *Cobalt inhibits the interaction between hypoxia-inducible factor-α and von Hippel-Lindau protein by direct binding to hypoxia-inducible factor-α.* Journal of Biological Chemistry, 2003. **278**(18): p. 15911-15916.
287. Abràmoff, M.D., P.J. Magalhães, and S.J. Ram, *Image processing with ImageJ.* Biophotonics international, 2004. **11**(7): p. 36-42.
288. Shen, C., et al., *RAGE-specific inhibitor FPS-ZM1 attenuates AGEs-induced neuroinflammation and oxidative stress in rat primary microglia.* Neurochemical research, 2017. **42**(10): p. 2902-2911.
289. Deane, R., et al., *A multimodal RAGE-specific inhibitor reduces amyloid β–mediated brain disorder in a mouse model of Alzheimer disease.* The Journal of clinical investigation, 2012. **122**(4): p. 1377-1392.
290. Barceloux, D.G. and D. Barceloux, *Cobalt.* Journal of Toxicology: Clinical Toxicology, 1999. **37**(2): p. 201-216.
291. Maxwell, P. and K. Salnikow, *HIF-1, an oxygen and metal responsive transcription factor.* Cancer biology & therapy, 2004. **3**(1): p. 29-35.
292. Akbar, M., J.M. Brewer, and M.H. Grant, *Effect of chromium and cobalt ions on primary human lymphocytes in vitro.* Journal of immunotoxicology, 2011. **8**(2): p. 140-149.
293. Petit, A., et al., *Induction of protein oxidation by cobalt and chromium ions in human U937 macrophages.* Biomaterials, 2005. **26**(21): p. 4416-4422.
294. Vengellur, A. and J.J. LaPres, *The role of hypoxia inducible factor 1α in cobalt chloride induced cell death in mouse embryonic fibroblasts.* Toxicological Sciences, 2004. **82**(2): p. 638-646.
295. Tripathi, V.K., S.A. Subramaniyan, and I. Hwang, *Molecular and cellular response of co-cultured cells toward cobalt chloride (CoCl2)-induced hypoxia.* ACS omega, 2019. **4**(25): p. 20882-20893.
296. Zhu, H., et al., *Upregulation of autophagy by hypoxia-inducible factor-1α promotes EMT and metastatic ability of CD133+ pancreatic cancer stem-like cells during intermittent hypoxia.* Oncology reports, 2014. **32**(3): p. 935-942.
297. Yang, X., et al., *Hypoxia-induced autophagy promotes gemcitabine resistance in human bladder cancer cells through hypoxia-inducible factor 1α activation.* International journal of oncology, 2018. **53**(1): p. 215-224.
298. Hanna, R.A., et al., *Microtubule-associated protein 1 light chain 3 (LC3) interacts with Bnip3 protein to selectively remove endoplasmic reticulum and mitochondria via autophagy.* Journal of Biological Chemistry, 2012. **287**(23): p. 19094-19104.
299. Yang, S. and A.C. Kimmelman, *A critical role for autophagy in pancreatic cancer.* Autophagy, 2011. **7**(8): p. 912-913.

300. Zhang, M., et al., *Opposite response to hypoxia by breast cancer cells between cell proliferation and cell migration: A clue from microRNA expression profile.* Oncology letters, 2018. **15**(3): p. 2771-2780.
301. Lin, S., et al., *Chemokine C–X–C motif receptor 6 contributes to cell migration during hypoxia.* Cancer letters, 2009. **279**(1): p. 108-117.
302. Zhang, L., et al., *Hypoxia induces epithelial-mesenchymal transition via activation of SNAI1 by hypoxia-inducible factor-1α in hepatocellular carcinoma.* BMC cancer, 2013. **13**(1): p. 1-9.
303. Indurthi, V.S.K., *Interactions of the receptor for advanced glycation end products (RAGE) with advanced glycation end products and S100B.* 2016.
304. Luthra, M. and D. Balasubramanian, *Nonenzymatic glycation alters protein structure and stability. A study of two eye lens crystallins.* Journal of Biological Chemistry, 1993. **268**(24): p. 18119-18127.
305. Ott, C., et al., *Role of advanced glycation end products in cellular signaling.* Redox biology, 2014. **2**: p. 411-429.
306. Wei, Y., et al., *Rapid glycation with D-ribose induces globular amyloid-like aggregations of BSA with high cytotoxicity to SH-SY5Y cells.* BMC cell biology, 2009. **10**(1): p. 1-15.
307. Rondeau, P., et al., *Thermal aggregation of glycated bovine serum albumin.* Biochimica et Biophysica Acta (BBA)-Proteins and Proteomics, 2010. **1804**(4): p. 789-798.
308. Chesne, S., et al., *Effects of oxidative modifications induced by the glycation of bovine serum albumin on its structure and on cultured adipose cells.* Biochimie, 2006. **88**(10): p. 1467-1477.
309. Li, C., et al., *Advanced glycation end products promote the proliferation and migration of primary rat vascular smooth muscle cells via the upregulation of BAG3.* International journal of molecular medicine, 2017. **39**(5): p. 1242-1254.
310. Yamamoto, Y., et al., *Advanced glycation endproducts–receptor interactions stimulate the growth of human pancreatic cancer cells through the induction of platelet-derived growth factor-B.* Biochemical and biophysical research communications, 1996. **222**(3): p. 700-705.
311. Bhawal, U.K., et al., *Association of expression of receptor for advanced glycation end products and invasive activity of oral squamous cell carcinoma.* Oncology, 2005. **69**(3): p. 246-55.
312. Takino, J.-I., S.-I. Yamagishi, and M. Takeuchi, *Cancer malignancy is enhanced by glyceraldehyde-derived advanced glycation end-products.* Journal of oncology, 2010. **2010**.
313. Deng, R., et al., *Glucose-derived AGEs promote migration and invasion of colorectal cancer by up-regulating Sp1 expression.* Biochimica et Biophysica Acta (BBA)-General Subjects, 2017. **1861**(5): p. 1065-1074.
314. Indurthi, V.S.K., E. Leclerc, and S.W. Vetter, *Interaction between glycated serum albumin and AGE-receptors depends on structural changes and the glycation reagent.* Archives of biochemistry and biophysics, 2012. **528**(2): p. 185-196.
315. Ko, S.-Y., et al., *Cell migration is regulated by AGE-RAGE interaction in human oral cancer cells in vitro.* PLoS One, 2014. **9**(10): p. e110542.
316. Swami, P., et al., *RAGE Up-Regulation Differently Affects Cell Proliferation and Migration in Pancreatic Cancer Cells.* International Journal of Molecular Sciences, 2020. **21**(20): p. 7723.

317. Cao, L., et al., *Curcumin inhibits H2O2-induced invasion and migration of human pancreatic cancer via suppression of the ERK/NF-κB pathway.* Oncology reports, 2016. **36**(4): p. 2245-2251.
318. Yan, M., et al., *Correlation of NF-κB signal pathway with tumor metastasis of human head and neck squamous cell carcinoma.* BMC cancer, 2010. **10**(1): p. 1-13.
319. Menini, S., et al., *The advanced glycation end-product N ϵ-carboxymethyllysine promotes progression of pancreatic cancer: implications for diabetes-associated risk and its prevention.* The Journal of pathology, 2018. **245**(2): p. 197-208.